

**Reverse Flow Adsorption
Technology for Homogeneous
Catalyst Recycling**

Promotiecommissie:

Voorzitter	Prof. dr. ing. M. Wessling	Universiteit Twente
Promotor	Prof. dr. ir. A.B. de Haan	Universiteit Twente
Assistent-Promotor	Dr. ir. H. Bosch	Universiteit Twente
Commissieleden	Prof. dr. ir. B. Roffel	Universiteit Twente
	Dr. K. Seshan	Universiteit Twente
	Prof. dr. ir. P.J.A.M. Kerkhof	Universiteit Eindhoven
	Prof. dr. F. Kapteijn	Universiteit Delft
	Dr. D. Bathen	Degussa AG

Reverse Flow Adsorption Technology for Homogeneous Catalyst Recycling
Dunnewijk, J.
Thesis, University of Twente, The Netherlands
ISBN: 90-9021176-4

Copyright © J. Dunnewijk, Enschede, 2006
All rights reserved.
Printed by Gildeprint, Enschede, The Netherlands.

**REVERSE FLOW ADSORPTION TECHNOLOGY FOR HOMOGENEOUS
CATALYST RECYCLING**

PROEFSCHRIFT

ter verkrijging van
de graad van doctor aan de Universiteit Twente,
op gezag van de rector magnificus,
prof. dr. W.H.M. Zijm,
volgens besluit van het College voor Promoties
in het openbaar te verdedigen
op vrijdag 20 oktober 2006 om 13.15 uur

door

Jeroen Dunnewijk

geboren op 16 juli 1972
te de Bilt

Dit proefschrift is goedgekeurd door de promotor

Prof. dr. ir. A.B. de Haan

en de assistent-promotor

Dr. ir. H. Bosch



Voorwoord

Het is gedaan... het onderzoek... het schrijven... het proefschrift...

Allereerst wil ik mijn promotor André de Haan bedanken. Niet alleen voor de mogelijkheid dit promotieonderzoek uit te voeren, maar ook voor de gegeven vrijheid om andere dingen (zoals het volgen van cursussen en bezoeken van conferenties) naast mijn onderzoek te mogen doen. Ook wil ik mijn dagelijks begeleider en assistent-promotor Hans Bosch bedanken voor zijn tomeloze inzet gedurende mijn onderzoek. Voor de grondige (maar plezierige) begeleiding, de discussies en voor de tijd die je genomen hebt om mijn ingeleverde stukken te corrigeren.

Met veel plezier heb ik dit onderzoek mogen doen in de vakgroep Scheidingstechnologie. Eerst met de 'eerste lichting' AIO's: Bart, Boris, Fahong, Johan, José, Karin en Maartje. Gedurende mijn onderzoek groeide de vakgroep zienderogen met persoonlijkheden als: Daleen, Katarina, Lara, Natasja, Maksym, Marjette, Meritxell, Paul, Renze, Tanja en Thijs. Ieder nam zijn of haar tijd voor een sociaal babbeltje of een gesprek van meer technische aard. Ik heb hier altijd zeer veel steun in gevonden; Bedankt allemaal voor jullie betrokkenheid !!!

Vooral Maartje heeft als kamergenoot veel met mij te stellen gehad. Na al onze gesprekken en discussies, de oplossingen die je gaf voor de chemische problemen (waar ik regelmatig mee zat) en de vele gesneuvelde pianostukken kan het ook niet anders dan dat ik jou als paranimf heb gevraagd.

Naast de wisselende samenstelling van de groep AIO's, zorgde de vaste staf voor de ervaring binnen de vakgroep. Jullie stonden altijd met raad en daad klaar: Alfons, Annemiek, Annet, Bert, Henny, Imre, Louis, Norbert, Rita en Wytze. Ook al zal jullie inzet niet direct zichtbaar zijn in dit proefschrift, zonder jullie was het zeker niet mogelijk geweest.

Het werk dat gepresenteerd wordt in dit proefschrift was niet mogelijk zonder de inzet van de volgende studenten. Daarvoor ben ik jullie allemaal zeer dankbaar. Tonny heeft de basis gelegd voor de selectie van adsorbents (wat niet zo eenvoudig bleek te zijn als verwacht).

Voorwoord

Anita heeft een grote bijdrage geleverd aan de vele metingen die vermeld staan in hoofdstukken 2 en 3. Tanja werkte aan de kinetiek metingen zoals deze vermeld staan in hoofdstuk 4. Prachi heeft de opzet gemaakt tot de simulatie van een Reverse Flow Adsorptie process zoals beschreven in hoofdstuk 5.

Pa en ma, bedankt voor jullie steun gedurende al die jaren. Helaas zit de tijd van het eeuwige student zijn er nu op.

Mijn vrouw Anita heeft veel geduld moeten oefenen de afgelopen jaren. Elke dag was anders en iedere keer kwam er weer wat nieuws op haar pad. Bedankt voor je geduld en ondersteuning.

De jongste telg in het geslacht Dunnewijk – Joaquin – heeft enkel de laatste maanden van het proces meegemaakt. In deze korte maar krachtige tijd heb jij ervoor gezorgd dat de laatste loodjes zeer draagbaar werden.

Jeroen



Contents

Voorwoord	i
Contents	iii
Summary	vii
1 Introduction	1
1.1 Homogeneous versus heterogeneous catalysis	1
1.2 Common homogeneous catalyst recovery methods	3
1.2.1 Decomposition and Precipitation	3
1.2.2 Distillation	4
1.2.3 Extraction	5
1.2.4 Membranes	7
1.2.5 Immobilization	7
1.2.5.1 Silica carriers and polymeric resins	7
1.2.5.2 Polymer Aided (filtration, precipitation)	8
1.2.5.3 dendrimers	8
1.2.5.4 Supported Liquid Phase	8
1.2.6 In Conclusion	9
1.3 Reverse Flow Adsorption	9
1.4 Approach	11
1.4.1 Adsorbents	11
1.4.2 kinetics	13
1.4.3 Simulation	14
1.5 References	14
2 Selection of Suitable Adsorbents for the Reversible Recovery of Co(II)Cl₂	23
2.1 Introduction	23
2.2 Exploitable Adsorptive Interactions	24
2.2.1 Ion Exchange	24
2.2.2 σ/π -interactions	24

2.3 Experimental	28
2.3.1 Solutions	28
2.3.2 Adsorbents	28
2.3.2.1 Ion exchange resins	28
2.3.2.2 σ/π -interaction based adsorbents	28
2.3.3 Adsorption and desorption measurements	30
2.4 Experimental Results	30
2.4.1 Ion exchange resins	30
2.4.2 σ/π -interaction based adsorbents	32
2.4.3 Influence of the $\text{PPh}_3/\text{CoCl}_2$ ratio	33
2.5 Discussion	34
2.5.1 Ion exchange resins	34
2.5.2 σ/π -interaction based adsorbents	36
2.5.3 Influence of the $\text{PPh}_3/\text{CoCl}_2$ ratio	37
2.5.3.1 Co(II) adsorption from the uncomplexed solution	37
2.5.3.2 Co(II) adsorption from the complex solution	38
2.6 Conclusion	40
2.7 References	41
3 Selection of Suitable Adsorbents for the Reversible Recovery of PPh_3	43
3.1 Introduction	43
3.2 Exploitable Adsorption mechanisms	44
3.2.1 Acid/Base interactions	44
3.2.2 σ/π interactions	45
3.3 Experimental	46
3.3.1 Solutions	46
3.3.2 Adsorbent preparation	46
3.3.2.1 Polystyrene/divinylbenzene carrier	46
3.3.2.2 Siliceous carrier	47
3.3.3 Adsorption and desorption measurements	48
3.4 Experimental results	48
3.4.1 Acid/base interaction	48
3.4.2 σ/π interactions	48
3.4.2.1 Soft acid	48
3.4.2.2 Transition Metals	49

3.4.2.3 Hard acids	50
3.4.3 Influence carrier	50
3.5 Discussion	51
3.5.1 Acid/base interactions	51
3.5.2 σ/π interaction	52
3.5.2.1 Soft acid	52
3.5.2.2 Transition metals	52
3.5.2.3 Hard acids	53
3.5.3 Carrier influence	53
3.6 Conclusion	54
3.7 References	55
4 Study of Adsorption Kinetics of CoCl_2 and PPh_3 over Macroreticular and Gel Type Adsorbents by a Generalized ZLC method	57
4.1 Introduction	57
4.2 Theory	59
4.2.1 Geometry	59
4.2.2 Kinetic model for macroreticular adsorbent	60
4.2.3 Kinetic model for gel type adsorbent	64
4.3 Experimental	65
4.3.1 Solutions	65
4.3.2 Adsorbents	65
4.3.3 Experimental set-up	66
4.3.4 Calibration of the set-up	68
4.3.5 Adsorption experiments	69
4.4 Experimental Results	70
4.4.1 Adsorption of CoCl_2 over macroreticular resins	70
4.4.2 Adsorption of PPh_3 over macroreticular resins	73
4.4.3 Adsorption of CoCl_2 over gel type resin: polymerbound PPh_3	76
4.5 Discussion	78
4.5.1 Influence of the liquid flow rate	78
4.5.2 Adsorption rate parameters	79
4.5.3 Comparison with ZLC method	81
4.6 Conclusion	81
4.7 Symbols	82

4.8 References	83
5 Simulation of Reverse Flow Adsorption	87
5.1 Introduction	87
5.2 Dynamic model for concentration gradients in adsorption beds	89
5.3 Simulation Results and Discussion	93
5.3.1 Process Stability	93
5.3.2 Influence Adsorbent Parameters	96
5.3.3 Influence Process Parameters	98
5.3.4. OXO-synthesis process	100
5.4 Conclusion	102
5.5 Symbols	102
5.6 References	104
6 Conclusions and Recommendations	107
6.1 Conclusions	107
6.1.1 Adsorbents	107
6.1.2 Kinetics	108
6.1.3 Simulation	109
6.1.4 Implementation into an OXO-synthesis process	109
6.1.5 Overall conclusion	109
6.2 Recommendations	110
6.3 References	111



Summary

Catalysis is a very important process from an industrial point of view as the production of most industrially important chemicals involves catalysis. Two types of catalysis are generally distinguished: heterogeneous – or heterogenized – catalysts and homogeneous catalysts. From these two, the heterogeneous type of catalyst is the major one in today's chemistry. With the increasing demands for more complex chemicals in the fine chemical industry, the selectivity becomes more and more important. In these new evolving fields of catalysis, homogeneous catalysts become of a more and more increasing popularity. In spite of the advantages, homogeneous catalysis is still not as common utilized as heterogeneous catalysis due to important draw-backs of the standard recovery methods, among which: decomposition during distillation, need for additional solvents during extraction or leaching of catalyst compounds in membrane filtration.

To avoid the drawbacks of the various methods for catalyst recovery, we have suggested an alternative recovery of the homogenous catalyst: Reverse Flow Adsorption. By using a selective adsorbent, the homogeneous catalyst can be retained in an adsorption bed while the product flow continues to the product purification. Just before breakthrough of the homogenous catalyst from the adsorption bed, the saturated adsorption bed is regenerated by the reversal of the flow provided that the adsorption is reversible. During this regeneration process, the homogeneous catalyst is recycled to the reactor and a semi-continuous recovery and recycling process is gained. In actual homogeneous catalyzed processes, a homogeneous transition-metal catalyst is at equilibrium with its free transition-metal center and ligands. Therefore, to apply Reverse Flow Adsorption, a combination of two adsorbents has to be used to reversibly adsorb: the transition-metal center and its ligands.

In chapter 2, the exploitability of ion exchange and σ -donation/ π back donation for recovery of the transition-metal center has been evaluated for two series of pre-selected adsorbents. The first series of adsorbents – ion exchange resins – have been tested on their ability to reversibly adsorb the Co(II)Cl_2 transition metal center of a homogeneous model catalyst: $(\text{PPh}_3)_2\text{Co(II)Cl}_2$. The second series of adsorbents have been characterized on their ability to undergo a reversible σ/π interaction with Co(II)Cl_2 by a suitable ligand that is immobilized onto the adsorbent. In the latter case, pre-selection was done on basis of the Hard and Soft

Acids and Bases theory which predicts the strength – a measure for the adsorption capacity – of the interaction between the transition metal and the immobilized ligand. The adsorption capacities of the various adsorbents have been determined by means of classical batch adsorption experiments in 1-butanol. The reversibility of the adsorption was investigated by desorbing Co(II) from the loaded adsorbents by contacting them with lean 1-butanol. The results demonstrated that the transition metal center – Co(II)Cl₂ – can be recovered by ion exchange or σ/π interactions. From the experimental results it could be concluded that:

- Ion exchange over the higher group I functionalized Amberlyst 15 adsorbents was found to reversibly adsorb Co(II) from 1-butanol according to: $\text{Cs}^+ \approx \text{Rb}^+ > \text{K}^+ > \text{Na}^+$.
- Reversible adsorption has been observed for the polymeric adsorbents that were functionalized with groups which can undergo σ donation/ π back donation for the recovery of Co(II). The observed trend was: Group IV (N and P) > Group V (O and S) > Group IV (Cl and Br)

To investigate the exploitability of an acid/base equilibrium and σ/π -interactions for ligand adsorption, in chapter 3 a series of modified ion exchange resins have been tested. For recovery by an acid/base reaction, an acidic resin has been tested on its capability to reversibly adsorb the PPh₃ ligands of a homogeneous model catalyst: (PPh₃)₂Co(II)Cl₂. The second series of adsorbents that have been selected are functionalized with a transition metal that is immobilized onto the adsorbent and are expected to form a reversible σ/π interaction with the PPh₃ ligands. In the latter case, pre-selection was done on basis of the Hard and Soft Acids and Bases theory which predicts the strength of the interaction between the immobilized transition metal – which act as an adsorption site – and the PPh₃ ligands. The adsorption capacities of the various adsorbents have been obtained by means of classical batch adsorption experiments in 1-butanol. The reversibility of the adsorption was demonstrated by desorbing PPh₃ from the loaded adsorbents by contacting them to lean 1-butanol. The results showed that the ligands can be recovered both by an acid/base equilibrium as well as σ/π interactions. From the experimental results it could be concluded that:

- Adsorption of the PPh₃ ligands by an acid/base equilibrium was found to be reversible over H⁺ functionalized Amberlyst 15.

- PPh_3 prefers Ag^+ functionalized Amberlyst 15 above the other types of selected metals. The trend in the adsorption capacity for the recovery by σ/π interactions follows: $\text{Ag}^+ \gg \text{Ni}^{2+} \approx \text{Co}^{2+} > \text{Fe}^{2+} > \text{Mn}^{2+} > \text{Na}^+ \approx \text{K}^+ \approx \text{Rb}^+ \approx \text{Cs}^+$

In practice, the feasibility of the Reverse Flow Adsorption concept is not purely given by the capacity of these adsorbents, but also strongly depends on the complications that occur due to internal and external mass transfer limitations and dispersion effects. These effects cause the concentration fronts in adsorption beds to widen which in its turn leads to a faster breakthrough out of the adsorption bed. In chapter 4, the internal diffusivity constants for the adsorption kinetics of CoCl_2 into Amberlyst A21 and polymerbound PPh_3 and the adsorption of PPh_3 into Ag^+ functionalized Amberlyst 15 have been determined by fitting a generalized Zero Length model to experimentally determined concentration changes as a function of time. The model appeared to be applicable to non-linear isotherms without neglecting the adsorption of the sorbate in and at the macropore walls. It was obtained that:

- Although CoCl_2 diffuses both into the macro- and micropores of the macroreticular Amberlyst A21, the main adsorption capacity is located in the microparticles.
- CoCl_2 is adsorbed into the gel matrix of polymerbound PPh_3 at a faster diffusion rate compared to the gel type microparticles of Amberlyst A21 due to the lower degree of crosslinking.

In chapter 5 a model is presented that describes the concentration profiles in the adsorption beds during adsorption and desorption. Reverse Flow Adsorption was modeled for a CSTR with an adsorption bed upstream and another downstream the reactor. We used this model to demonstrate the feasibility of the Reverse Flow Adsorption concept by studying the influence of following process parameters: strength of the adsorption (initial slope of adsorption isotherm), adsorption capacity, effective internal diffusion, velocity of the liquid phase and the dimensionless cycle time. The model parameters concerning the adsorption isotherm and kinetics were taken from chapters 2, 3 and 4. It was demonstrated that the concentration fronts after adsorption and desorption eventually reach a fixed position, even if internal mass transfer is a limiting factor: no leaching of catalyst will occur. From the discussion on the adsorbent specific parameters, it was concluded that the required adsorption bed volumes can be minimized if the adsorbents – to be used in Reverse Flow Adsorption – have:

Summary

- A low adsorption strength.
- A high adsorption capacity.
- Fast effective diffusivity from inside the particles to the liquid phase.

Implementation of the Reverse Flow Adsorption process in an OXO-synthesis process is possible with adsorption beds with a relative volume less than 16 [%] of the reactor volume. The total pressure drop is then approximately 5 [%] of the process pressure. Although these results indicate that Reverse Flow Adsorption may become technically feasible for homogeneously catalyzed processes such as the OXO-synthesis, considerably more research has to be done before Reverse Flow Adsorption can be introduced in industry. First of all a more detailed study on the optimization strategy for the selection of adsorbents and process parameters has to be undertaken in order to obtain improved adsorbents. In such a study the effects of solvents and type of homogeneous catalysts on adsorbent efficiency should be investigated. For application of Reverse Flow Adsorption in real industrial processes, this study should be extended to include the effects of reactants and products on the adsorption equilibrium and demonstrate the reusability and activity preservation of the homogeneous catalyst for different systems.

1.1 Homogeneous versus heterogeneous catalysis

Catalysis is a very important process from an industrial point of view [Farkas, 1986] as the production of most industrially important chemicals involves catalysis [Leach, 1983; Hagen, 1999; Armor, 2001]. Research into catalysis is a major field in applied science [Ertl et al., 1997; Wöhrle and Pomogailo, 2003; Leeuwen, 2004], and involves many fields of chemistry and physics.

Catalysts accelerate the chemical reaction by providing a lower energy pathway between the reactants and the products. This usually involves the formation of an intermediate which cannot be formed without the catalyst. The formation of this intermediate and the subsequent reaction generally has a much lower activation energy barrier than is required for the direct reaction of reactants to products.

Two types of catalysis are generally distinguished: heterogeneous – or heterogenized – catalysts and homogeneous catalysts [Leach, 1983; Mortreux and Petit, 1988; Hagen, 1999; Cornils and Herrmann, 2000; Bhaduri and Mukesh, 2001]. From these two, the heterogeneous type of catalyst is the major one in today's chemistry. It is approximated that 80 [%] of all catalyzed reactions is performed by using the heterogeneous catalysts [Mortreux and Petit, 1988; Hagen, 1999; Bhaduri, 2001]. Its main application is in the bulk industry for basic chemicals, where no important requirements have to be fulfilled in terms of selectivity and therefore this type of catalysts is the one of choice.

But with the increasing demands for more complex chemicals in the fine chemical industry [Leach, 1983; Kragl and Dwars, 2001; Leeuwen, 2004], the selectivity becomes more and more important. In these new evolving fields of catalysis, homogeneous catalysts become of a more and more increasing popularity. Homogeneous transition-metal catalysts offer a number of advantages when one compares them to the heterogeneous class of catalysts: high activity and selectivity [Leach, 1983; Parshall and Ittel, 1993; Herrmann and Cornils, 1997; Hagen, 1999; Bhaduri, 2001].

In heterogeneous catalysts, the catalytic active transition-metal center is immobilized onto a solid carrier [Leach, 1983; Herrmann and Cornils, 1997; Hagen, 1999; Cornils and Herrmann, 2000]. These solid matrices negatively affect the activity and selectivity of a reaction due to: the slow transport of reactants and products [Leach, 1983; Herrmann and Cornils, 1997; Wijngaarden et al., 1998; Hagen, 1999, Cornils and Herrmann, 2000], the

distortion of the electronic properties of the catalytic active transition-metal center and the undefined environment in which the reaction takes place [Hagen, 1999].

In heterogeneous catalysis, activity is affected by diffusion because reactants from the liquid bulk phase to the catalytic active sites that are located in the solid phase. Subsequently, the formed products are then to be transported backwards from the solid to liquid phase. On top of this influence of the transport rates of reactants and products on the activity of transition-metal based catalysts, the activity can also be negatively affected by the presence of a carrier acting as a secondary ligand. The solid carrier forms a secondary ligand which influences the electronic properties of the catalytic active transition-metal.

Although high selectivities have also been obtained with heterogeneous catalysts, this is not inherent to the heterogeneous system [Herrmann and Cornils, 1997]. First, the undefined structure of the matrix will affect the steric environment of the reaction and thereby affecting the selectivity. Secondly, the selectivity is affected as the degrees of freedom to attach a selectivity regulating ligand into the coordination sphere are reduced. This, because one of bonding sites has to be sacrificed for the immobilization.

In homogeneous catalyzed reactions, mass transfer resistances are negligible because all compounds – such as reactants, products and homogeneous catalyst – are located in one single reaction phase [Leach, 1983; Mortreux and Petit, 1988; Parshall, 1993; Herrmann and Cornils, 1997; Hagen, 1999; Cornils and Herrmann, 2000; Bhaduri, 2001; Leeuwen, 2004]. Therefore, the activity of a homogeneously catalyzed reaction is primarily given by the kinetics of the reaction that is imposed by the combination of the selected homogeneous catalyst and its reactants. In homogeneous transition-metal based catalysts the influence of a carrier is omitted since these secondary ligands are not present. As a consequence, an evident increment in the activity of the homogeneous catalysts can be achieved under milder reaction conditions compared to the heterogeneous catalysts.

The molecular structures of a transition-metal based homogeneous catalyst are relatively better understood and more easily to predict in comparison to the steric nature of the carrier matrices used for heterogeneous catalysts. Therefore, homogeneous catalysis is a better base for engineering catalysts to achieve the high selectivities – as desired – with well-understood ligands and their following steric environment.

In spite of the advantages, homogeneous catalysis is still not as common utilized as heterogeneous catalysis due to important draw-backs of the standard recovery methods [Hagen, 1999; Cornils and Herrmann, 2000; Bhaduri, 2001] such as: decomposition, additional solvents, requirement of recovery agents and underrating the effect of the equilibrium between the ligands and catalytic active transition metal center.

It is clear that recovery methods that can overcome these draw-backs will give rise to the utilization of homogeneous catalysts and open new evolving fields in the application of the latter. In our opinion, a suitable candidate for the recovery of homogeneous catalysts is an adsorptive separation method which is combined with the reverse flow technology.

1.2 Common homogeneous catalyst recovery methods

Easy separation of the catalyst from the reaction phase is desirable not only because of its reuse but also avoids problems in the downstream processing and trace metal removal. In the past, various separation routes have been proposed and researched (figure 1.1) [Herrmann and Cornils, 1997; Behr, 1998; Hagen, 1999; Bhaduri, 2001; Kragl and Dwars, 2001; Cole-Hamilton, 2003].

In this paragraph, a short overview of technologies – in use or on laboratory sale – will be given to show their usability in chemistry. The advantages and drawbacks of the various methods will be discussed as these limit their use in bulk chemistry.

1.2.1 Decomposition and Precipitation

Separation of homogeneous catalysts by precipitation is one of the earliest forms of homogeneous catalysts recovery [Hagen, 1999]. It is a straight forward method in which a complete recovery of the homogeneous catalyst can be achieved. In this method, the homogeneous catalyst is prevented to continue down-stream the process by formation of an insoluble compound that can be filtered from the liquid product flow [Balmat and Square, 1979; Quick, 1982; Bodurow, 1990; Jeffery and Whiston, 1998; Buysch et al., 1999]. In general, two methods are used: 1) formation of insoluble salts by reaction and 2) electrochemical decomposition to the elementary metallic form of the catalytic active metal center [Silva et al., 1993].

Although this method well established, two main draw-backs limit the use of precipitation. This method mainly focuses on the recovery of the precious metal but eventual ligands are not dealt with. Therefore, this method has to be preferably used for simple homogeneous catalysts with simple and inexpensive ligands. The ligands have to be separated in a later stage down-stream the process [Leeuwen, 2001].

The second draw-back of this method is given by the fact that the precipitated form of the catalytic active metal center has to be worked-up to a catalytic active homogeneous catalyst before it can be recycled to the process.

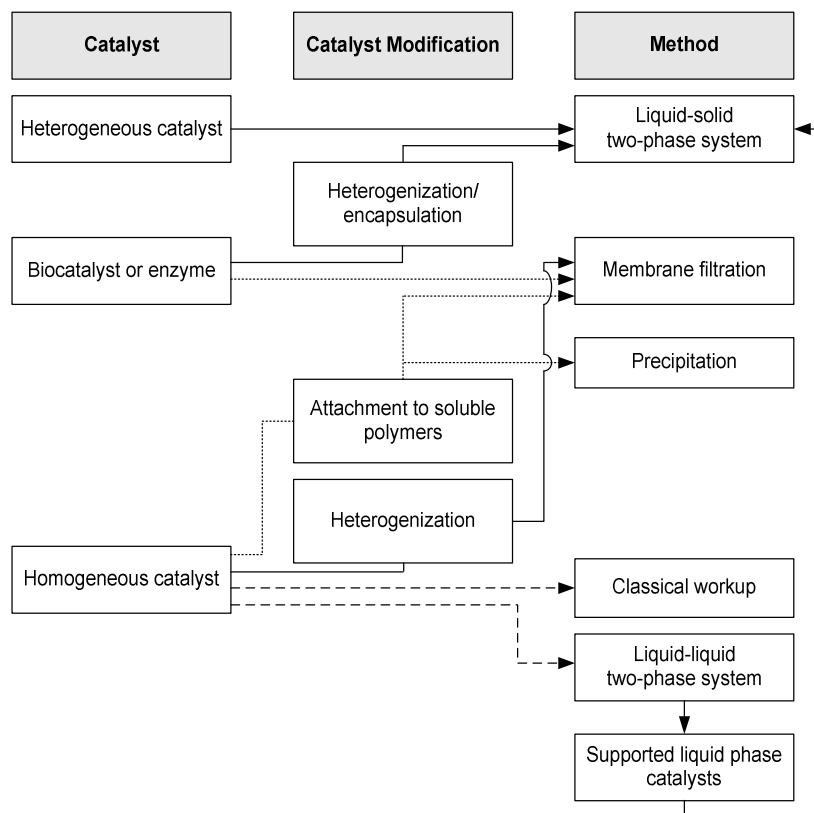


Figure 1.1. Methods for the recycling of homogeneous catalysts (derived from Kragl and Dwars [2001]).

Recently, researchers at the U.S. Department of Energy's Brookhaven National Laboratory [Dioumaev and Bullock, 2000; Bullock and Dioumaev, 2003] have developed an elegant way to overcome these draw-backs. In their method, the homogenous catalyst is soluble in a liquid phase due to the presence of the reactants but insoluble in the products. During the reaction, the catalyst will precipitate due to the decreasing amounts of reactants. At the end of the reaction, all homogeneous catalyst will be precipitated and can be filtered and re-used in the next reaction. Unfortunately the catalyst that was used had to be specially designed for this purpose and the equilibrium is a rather delicate one.

1.2.2 Distillation

Distillation is a well documented method [Perry and Green, 1998; Khoury, 2005] to separate high boiling from low boiling components. For example in the Monsanto process this

separation technique is used in the Rhodium catalyzed carbonylation of methanol [Bhaduri, 2001] to produce acetic acid.

This simple separation method is used nowadays for the recovery of homogeneous catalysts [Hagen, 1999] in two forms: 1) flash distillation to instantly recover the product during the reaction [Zehner et al., 1987; Sunley, 2000] and 2) distillation external from the reaction to evaporate the reactants, products and solvent to form a concentrated homogeneous catalyst solution [Kummer et al., 1977; Kummer et al., 1978].

In flash distillation, the reaction is done at elevated temperatures to continuously evaporate the products while the homogeneous catalyst remains in solution. No recycling of the homogeneous catalyst will be needed, as it will always remain in the reactor. The reactants that may eventually evaporate with the products can be easily re-used by recycling to the reactor.

Application of distillation externally from the reactor is focused on a more efficient separation of the products and concentrating the homogeneous catalyst liquid phase. A part of the solvent is evaporated together with the reactants and products, while the high boiling homogeneous catalyst is recycled via the bottom section of the distillation column.

A very important draw-back of distillation is encountered daily in real processes: decomposition of the homogeneous catalyst at elevated temperatures [Leeuwen, 2001]. The maximal temperature of both the flash and external distillation will therefore be limited by the temperature at which the homogeneous catalyst decomposes. Thus only a select number of reactions can be performed by using distillation as the boiling points of the formed products may not exceed the decomposition temperature.

A special case in distillation is the use of ionic liquids as solvent [Wasserscheid and Keim, 2000; Gordon, 2001; Olivier-Bourbigou and Magna, 2002]. Ionic liquids are salts that remain in their liquid state due to the large steric environment. These liquids have a negligible vapor pressure and therefore will not boil. Thus, products and reactants can be distilled without loss of solvent as the liquid does not evaporate. Besides the non-volatile behavior of ionic liquids, another advantage of the latter is that they can stabilize the homogeneous transition metal catalysts [Wasserscheid and Keim, 2000]. Therefore, higher temperatures can be applied before the transition metal complexes start to decompose.

1.2.3 Extraction

Next to distillation, extraction is one of the most simple and well-documented separation methods [Lo et al., 1983; Perry, 1998; Khoury, 2005]. In extraction, the differences in solubilities of various compounds – present in the reaction phase – are exploited. Recovery

of homogeneous catalysts by extraction [Hagen, 1999] can be done by focusing on two compounds in the reaction mixture [Behr, 1998]: 1) extraction of the products from a (temperature regulated) bi-phasic reactor and 2) recovery of the homogeneous catalyst by changing the polarity of the complex [Hashizume, 2000].

Non-polar organic and aqueous phases do not mix. This effect can be exploited as the products and reactants prefer the organic phase above an aqueous [Joó, 1998] or fluorous phase. By removing, only the organic phase from the reactor, the aqueous or fluorous phase remains inside.

When the homogeneous catalyst preferably remains in the aqueous phase, the catalyst will be kept inside the reactor. For example in the Ruhrchemie/Rhône-Poulenc process – hydroformylation of propylene –, this is achieved by incorporation ionogenic SO_3^- groups in the ligands of the catalysts [Joó, 1998; Hanson, 1999; Kohlpaintner et al., 2001; Bhaduri, 2001]. The ionogenic groups make that the ligands preferably remain in the aqueous phase, which in their turn immobilize the metal. But, in this method mass transfer limitations can occur as the reactants from the organic phase have to be transported to the aqueous phase. Exploiting a fluorous phase in the extractive separation of the reaction products goes analog to the separation of an aqueous phase. This difference ensures that the catalyst remains in an highly halogenated solvent which often give bilayers with organic solvents [Rutherford, 1998]. The preference of the catalyst to the fluorous phase is hereby regulated by the substitution of hydrogen by fluor in the ligands of the catalyst complex [Cavazini et al., 1999].

A very nice solution to this mass transfer problem in the above mentioned method is the temperature regulated phase transfer [Behr and Fängewisch, 2001; Behr and Fängewisch, 2002; Behr and Fängewisch, 2002]. Here, a combination of polar, non-polar and intermediate solvents forms one phase at elevated temperatures. At lower temperatures, a phase split occurs. By fine-tuning of the solvent system, one can regulate the preference of the catalyst for one phase and products for the second phase. Again, leach of the metal can occur and still forms a problem for the recovery of the precious catalytic active metals.

Extraction of the homogeneous catalyst after reaction in a non-polar reaction phase can be done by transforming the complex from a non-polar to a polar compound. In pH controlled extraction [Hashizume, 2000], the catalyst can be brought to its acidic form by reacting with H^+ . The latter is soluble in an aqueous phase, while the products and reactants remain in the organic solution. Addition of an fresh organic phase while neutralizing the acidic catalyst recovers the latter for the reaction.

The draw-back of the extraction method is the required addition of solvent and the leaching of the transition metal center, that is – without ligands – soluble in water.

1.2.4 Membranes

Recovery of homogeneous catalysts by means of membrane filtration [Marcano, 2002] can be done externally [Smet, 2001; Gallego, 2004] from the reactor as well inside [Kim and Datta, 1991; Dwar et al., 2001; Luthra et al., 2002] a so-called membrane reactor. The principle of both forms is the same: separation of the homogeneous catalyst from the products by means of differences in size [Desrocher and Rezac, 2001]. While the large transition-metal complexes are retained by the membranes, the smaller product molecules can continue to the product purification. There should be considerable difference in the ratio of the sizes of the homogeneous catalyst compared to the products as this gives the limitation of this technique. Especially for metal complexes that contain macro molecular ligands, this method can establish a high degree of separation.

One of the draw-backs of this method is that a transition-metal complex is always in equilibrium with its free ligands and transition-metal center. This enables the small transition-metal center to leach [Dwar et al., 2001; Luthra et al., 2002; Scarpello et al., 2002] through the membrane and continues down-stream the process. Although, the leaching of precious metal can be highly influenced by the choice of solvent, a complete retaining of the transition-metal can not ever be guaranteed.

Another problem of the use of membranes is that the required membrane area is determined by the size of the product stream and not the catalyst concentration.

1.2.5 Immobilization

In this paragraph, immobilization refers to the art of keeping the homogeneous catalyst inside the reactor during the time of the operational process [De Vos, 2000]. This can be achieved by 'anchoring' the homogeneous catalyst to a solid or solving in a second liquid phase [Choplin and Quignard, 1998; Hanson, 1999; Park et al., 2000] that is kept inside the reactor. Most of these methods use membranes or solid carriers to reject the catalyst – and its immobilization phase – from leaving the reactor.

1.2.5.1 Silica carriers and polymeric resins

The homogeneous catalyst can be anchored to a solid such as a siliceous [Brunel et al., 1998; Merckle, 2001] or a polymeric [Leadbeater and Scott, 2000; Leadbeater, 2001] matrix.

This makes the catalyst immobilized inside the reactor and no additional separation methods are required. Although this method is – even today – in extensive progress, it is nothing but heterogenization of the homogeneous catalyst. As a result, all negative characteristics of heterogeneous catalyst apply to this type of separation.

1.2.5.2 Polymer Aided (filtration, precipitation)

If – at least – one of the ligands of the homogeneous catalyst is formed by a longer polymer chain, one can use the differences in size to keep the catalyst inside the system [Bergreiter, 2000] in combination with a membrane recovery. Or a biphasic system [Bergreiter, 2001] can be exploited if the polymer is soluble at higher temperatures, but precipitates at lower temperatures.

This method will influence the selectivity of the reaction and most likely the activity of the catalyst. This because of one of the selectivity regulating ligands is replaced by a polymer chain [Bergreiter, 1998] which in its turn affects the selectivity and electronic characteristics of the transition metal center.

1.2.5.3 dendrimers

A more sophisticated method for the polymer aided recovery of homogeneous catalysts is to incorporate the metal into a larger system [Gorman, 1998; Stoddart and Welton, 1999; Hecht and Fréchet, 2001]. By placing the metal onto the outside of the surface or in the center of a so-called dendrimer, the transition metal will be entangled by the various strains that keep it in its place.

The formed homogeneous catalyst is a large sphere of very large dimensions. These molecules are rejected from exiting the reactor when a membrane is present at its exit. Leaching of the transition metal is not that large when compared to standard polymeric aided recovery because the transition metal is incorporated into the large system of the dendrimer [Wilkinson et al., 2005]

1.2.5.4 Supported Liquid Phase

A possible solution to overcome the problems of selectivity loss in heterogeneous catalysts is to keep all possible bonding sites on the transition metal free for their interaction with the ligands [Choplin and Quignard, 1998]. This can be achieved by impregnating a resin with a solvent. When a homogeneous catalyst is dissolved into this secondary phase, it will remain

in its original state, enclosed by the selectivity regulating ligands. The selectivity of the reaction will remain unaltered, compared to the reaction in one reaction phase.

Two possible problems can occur from this approach. First is that the mass transfer limitation [Rony, 1969] will still be present as the reactants and products have to be transferred from the resin to the bulk phase. But the largest problem and therefore more important, the secondary liquid phase can leach out of the resin with the bulk phase [Beckmann and Keil, 2003].

1.2.6 In Conclusion

All methods used for the recovery and recycling of homogeneous catalysts have their advantages and draw-backs, such as the influence on the stability of the catalyst. The use of additional solvents, leaching of the precious catalytic active transition metal center and even precipitation due to high temperatures should be taken into account when designing a process.

In this thesis another approach to the recovery and recycling of homogeneous catalysts is taken. By exploiting the dissociation of the homogeneous catalysts, the homogeneous catalysts can be recovered by adsorption – without decomposition – and recycled by desorption only by concentration differences as the driving force. This approach is expected to address most of the draw-backs of the existing recovery techniques:

- No additional solvents or recovery agents will be needed.
- Decomposition of the homogeneous catalyst can be avoided if the separation is done at temperatures below the point of decomposition.
- The quantity of adsorbent is pre-determined by the amount of homogeneous catalyst in the system and not by the volume of the process flow.

1.3 Reverse Flow Adsorption

To avoid the drawbacks of the various methods for catalyst recovery, we have suggested [Dunnewijk, 2001] an alternative recovery of the homogenous catalyst: Reverse Flow Adsorption. By using a selective adsorption, the homogeneous catalyst can be retained in an adsorption bed while the product flow continues to the product purification. Just before breakthrough of the homogenous catalyst from the adsorption bed, the saturated adsorption bed can be regenerated by the reversal of the flow if the adsorption is reversible. This technique is well established in the field of process technology and in use in Reverse Flow

Reactors for the entrapment of heat and Pressure Swing Adsorption for the recovery of matter. During this regeneration process, the homogeneous catalyst can be recycled to the reactor and a semi-continuous recovery and recycling process is gained.

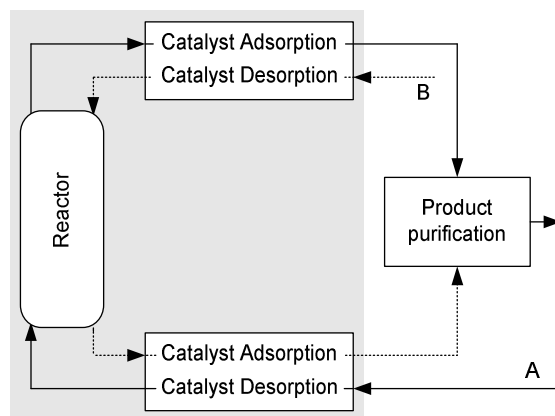


Figure 1.2. Homogeneous catalyst recycling by Reverse Flow Adsorption (feed alternates between A and B).

In Reverse Flow Adsorption, the flow at the feed and exit of the reactor alternately change direction (figure 1.2). The catalyst is separated from the reaction mixture by adsorption downstream the reactor. Then, in the subsequent step, it is recycled by desorption from the saturated adsorbent due to reversal of the process flow.

The adsorption bed at the bottom (bed 1) of figure 1.2 is initially saturated with the homogeneous catalyst and the adsorption bed at the top (bed 2) is in its regenerated state. When bed 1 is fed with fresh solvent, the homogeneous catalyst will desorb into the solvent and fed to the reactor. The concentration of the homogeneous catalyst inside the reactor is at its required level for the reaction and constant over time. The homogeneous catalyst leaving the reactor will be adsorbed in bed 2. The concentration front of the homogeneous catalyst moves through the adsorption bed at a velocity that is lower as the solvent velocity. Before breakthrough of the concentration front at the exit of bed 2, the feed and product flows are interchanged. Hereby, the adsorption and desorption functions of beds 1 and 2 are interchanged and the process as mentioned above is reversed until a semi-initial situation is reached. Again, the feed and product flows are interchanged and the Reverse Flow Adsorption continues as a semi-continuous process.

1.4 Approach

To make the Reverse Flow Adsorption concept technically feasible, the availability of adsorbents that can selectively and reversibly recover the homogeneous catalyst from the product flow is crucial. The dimensions of the adsorption beds are then determined by the adsorbent capacity combined with the mass transfer kinetics of the homogeneous catalyst to and from the adsorbent. As a result, the feasibility of integrating the recovery and recycling by Reverse Flow Adsorption can be shown by combining these adsorption capacities and kinetics into a theoretical simulation model of the Reverse Flow Adsorption concept.

1.4.1 Adsorbents

In homogeneous catalysis, the catalytic active transition metal center forms a metal-ligand bond with the available ligands. This metal-ligand bond can be described by the sharing of electrons between the ligand and transition metal [Kettle, 1996; Cotton, 1988]. The first step of this sharing is taken by the ability of the ligands to donate a pair of electrons – σ -donation – to an empty d-orbital that is located on the transition metal. This makes the transition metal more electron rich and in order to compensate for the increased electron density, the metal may relieve itself by donating electrons back – π -backdonation – to an empty ligand orbital in a successive step.

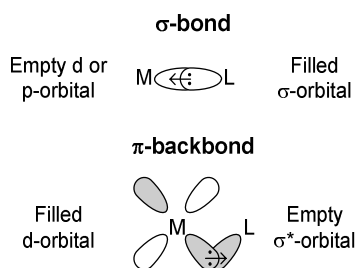
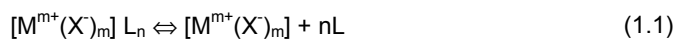


Figure 1.3. σ -bond and π -backbond between a transition metal (M) and ligand (L).

The σ -bond/ π -backbond principle as shown in figure 1.3 can also occur between the solvent and the free transition metal. In this view, homogeneous catalyst complexes are always in equilibrium with their free transition metal center and its free ligands. In a simplified form, this equilibrium can be rewritten for a halogenated transition metal according to:



Herein, M, X, L and m stand respectively for the transition metal, a halogen, the ligand of the complex and the valence of the metal.

In the case that this equilibrium is located completely on the left side, one can recover the homogeneous catalyst as a whole. But, given the fact that transition metal complexes are always – more or less – dissociated, both the ligands and metal centers are available in both complex and free forms. This equilibrium can be used to separately recover the transition metal center and its ligands.

In chapter 2, the focus will be placed on the separate recovery of the transition metal. A strategy will be put forward to select adsorbents that are potential suitable for their use in Reverse Flow Adsorption. A pre-selection has been done on basis of the possible interactions that can occur between the transition metal and the adsorbents. The strengths of these interactions – and thus the adsorption capacities – have been qualitatively predicted by the Hard and Soft Acids and Bases Theory.

The pre-selected adsorbents have been characterized on their capacity for the adsorption of transition metals. From the most promising adsorbent, the influence of the presence of ligands on the adsorption will be shown.

Once the transition metal has been recovered, the remaining ligands have to be recovered in a second adsorption bed. Therefore, in Reverse Flow Adsorption, a two extra adsorption beds will be required as shown in figure 1.4.

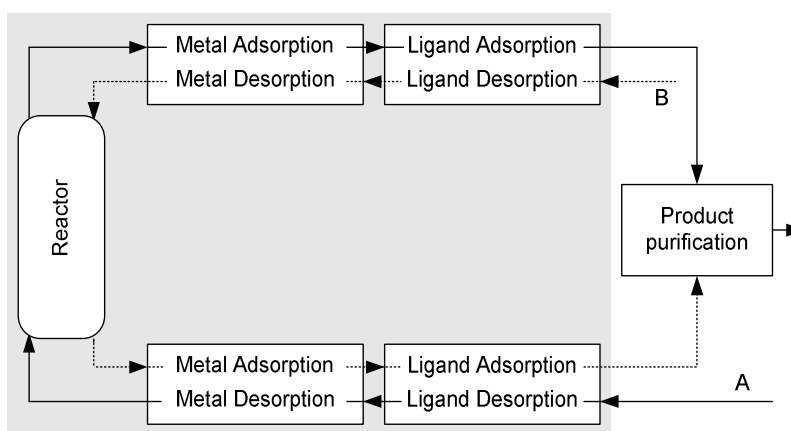


Figure 1.4. Homogeneous catalyst recycling by Reverse Flow Adsorption (feed alternates between A and B).

The adsorption bed for the ligand recovery requires an adsorbent that can reversibly recover the ligands from the liquid phase. In chapter 3 it will be demonstrated, that using a similar

strategy – compared to the transition metal recovery -, leads to the selection of adsorbents that can reversibly adsorb the ligands of the homogeneous catalyst.

It will be shown that a pre-selection can be made on basis of some the HSAB theory. The selected adsorbents have been characterized on their capacity to adsorb the ligands by a classical batch adsorption experiment.

The most promising adsorbents will be used to derive the influence of the composition of the carrier matrix.

1.4.2 kinetics

Suitable adsorbents should not only be able to reversibly adsorb the various parts of the homogeneous catalyst – at a high enough capacity –, but also be capable of adsorbing at a sufficiently fast rate. Therefore, adsorption kinetics are of large importance in Reverse Flow Adsorption. This because of the fact that in adsorptive processes, such as the Reverse Flow Adsorption concept mass transfer of the catalyst to and from the adsorbents cause dispersion of the concentration fronts in the adsorption beds.

The adsorption kinetics influences two aspects of the Reverse Flow Adsorption concept. First, the volumes of the adsorption beds that have to be used, not only depend on the capacity of the adsorption but also on the broadening of the concentration fronts in the adsorption beds. This broadening is due to the dispersive behavior of the fronts.

Secondly, and much more important, the mass transfer influences the cycle times of the Reverse Flow Adsorption. As large dispersion gives rise to an earlier breakthrough of the catalyst, the cycle times have to be chosen shorter. A large amount of catalyst will then remain in the adsorption bed without being returned to the reactor.

In order to determine the adsorption kinetics, chapter 4 will discuss a technique to measure the various parameters of the mass transfer inside the adsorbents. This method – Zero Length Column with recycle – will be used to determine the mass transfer kinetics over the adsorbents that have been found to be most promising for their use in Reverse Flow Adsorption. The experimental adsorption kinetics will be determined on basis of the mentioned theories and from the experimental data of the adsorption rates over the selected adsorbents as discussed in chapters 2 and 3.

The experimental data will be analyzed on basis of a simulation model that describes the experimental set up. From this model, that gives predictions for the experimental data, the diffusion coefficients of respectively the transition metal or ligands in the adsorbents will be determined.

1.4.3 Simulation

In chapter 5, all experimental data from chapter 2, 3 and 4 will be combined to show the feasibility of the Reverse Flow Adsorption concept. For this purpose a mathematical model has been developed to describe the concentration fronts in the adsorption beds.

It should be noted that for reasons of complexity, chemical reactions will be omitted in the simulation of the Reverse Flow Adsorption concept carried out for this thesis. Although the presence of reactants and products can influence the adsorption of the homogeneous catalyst, these effects are out of scope at this stage of the research.

The experimental data derived from chapters 2 and 3 are used in this model to calculate the capacities of the adsorption beds. For the calculations on the influence of the adsorption rates on the broadening of the concentration fronts, the experimental data from chapter 4 has been used. All the data of the adsorption capacities, reversibility and adsorption kinetics will be integrated into the simulation model to describe the Reverse Flow Adsorption as realistic as possible.

The dimensions of the adsorption beds and timescales of the cycle times in Reverse Flow Adsorption will be evaluated. In conclusion, the feasibility of the Reverse Flow Adsorption concept will be shown for the selected homogeneous model catalyst, when Reverse Flow Adsorption is theoretically implemented into an OXO-synthesis process.

1.5 References

Armor, J. N., New Catalytic Technology Commercialized in the USA During the 1990s, Appl. Cat. A: General, 222, 407, 2001

Balmat, J. L. and Square, K., Rhodium Recovery from Hydroformylation Still Heel with Triaryl Phosphite Ligand, US 4,135,911, 1979

Beckmann, A. and Keil, F. J., Increasing Yield and Operating Time of SLP-Catalyst Processes by Flow Reversal and Instationary Operation, Chem. Eng. Sci., 58, 841, 2003

Behr, A., Technische Konzepte zum Recycling von Homogenkatalysatoren, Chemie Ingenieur Technik, 70(6), 685, 1998

Behr, A. and Fängewisch, C., Temperatur-gesteuerte Lösungsmittelsysteme – Ein alternatives Konzept zum Recycling homogener Übergangsmetallkatalysatoren, Chem. Ing. Techn., 73, 874, 2001

Behr, A. and Fängewisch, C., Temperature-Dependent Multicomponent Solvent Systems – An Alternative Concept for Recycling Homogeneous Catalysts, Chem. Eng. Technol., 25, 143, 2002

Behr, A. and Fängewisch, C., Rhodium-Catalysed Synthesis of Branched Fatty Compounds in Temperature-Dependent Solvent Systems, Jour. Mol. Cat. A: Chem., 3899, 1, 2002

Bhaduri, S., Mukesh, D., Homogeneous Catalysis; Mechanisms and Industrial Applications, Wiley-Interscience, 2001

Bergbreiter, D. E., The Use of Soluble Polymers to Effect Homogeneous Catalyst Separation and Reuse, Catalysis Today, 42, 389, 1998

Bergbreiter, D. E., Polymer-Facilitated Biphasic Catalysis, in: Green Chemical Syntheses and Processes, Edited by Anastas, P. T., Heine, L. G. and Williamson, T. C., ACS Symposium series, 2000

Bergbreiter, D. E., Using Polymers to Control Substrate, Ligand or Catalyst Solubility, Journal of Polymer Science Part A: Polymer Chemistry, 39(14), 2351, 2001

Bodurow, C.C, Process for Catalyst Recovery, US 4,950,629, 1990

Brunel, D., Bellocq, N., Sutra, P., Caucel, A., Lasperas, M., Moreau, P., Di Renzo, F., Galarneau, A. and Fajula, F., Transition-Metal Ligands Bound onto the Micelle-Templated Silica Surface, Coord. Chem. Rev., 178-180, 1085, 1998

Bullock and Dioumaev, A Self-Separating, Reusable Catalyst. Catalyst Precipitates at End of Reaction, Ready for Another Round of Activity, C&EN, 81(31), 6, 2003

Buyusch, H.J., Hesse, C., Rechner, J. and Wirges, H.P., Recovery of Catalyst Systems from Diaryl Carbonate-Containing Reaction Solutions by Suspension Crystallization, US 5,965,472, 1999

Cavazinni, M., Montanari, F., Pozzi, G. and Quici, S., Perfluorocarbon-Soluble Catalysts and Reagents and the Application of FBS (Fluorous Biphasic System) to Organic Synthesis, 94, 183, 1999

Choplin, A. and Quignard, F., From Supported Homogeneous Catalysts to Heterogeneous Molecular Catalysts, *Coord. Chem. Rev.*, 178, 1679, 1998

Cole-Hamilton, D. J., Homogeneous Catalysis – New Approaches to Catalyst Separation, Recovery and Recycling, *Science*, 299, 1702, 2003

Cornils, B. and Herrmann, W. A., Applied Homogeneous Catalysis with Organometallic Compounds, Wiley-Interscience, 2000

Cotton F.A., et. al., Advanced inorganic chemistry, Wiley-Interscience, 1988

De Smet, K., Aerts, S., Ceulemans, E., Vankelecom, I.F.J. and Jacobs, P.A., Nanofiltration-coupled Catalysis to Combine the Advantages of Homogeneous and Heterogeneous Catalysis, *Chem. Comm.*, 597, 2001

De Vos, D.E., Vankelecom, I.F.J. and Jacobs, P.A., Chiral Catalyst Immobilization and Recycling, Wiley, 2000

Desrocher, D. J. and Rezac, M. E., Membranes for the Recovery of a Homogeneous Catalyst in an Organic Synthesis, *AIChE.org*, 2003

Dioumaev, V. K. and Bullock, R.M., A Recyclable Catalyst that Precipitates at the End of the Reaction, *Nature*, 424, 530, 2000

Dunnewijk, J., Bosch, H. and de Haan, A. b., "Reverse Flow Adsorption Concept for the Recovery of Homogeneous Catalysts: A Technical Feasibility Study", *AIChE Meeting*, Reno, NV, 2001

Dwars, T., Haberland, J., Grassert, I., Oehme, G. and Kragl, U., Asymmetric Hydrogenation in a Membrane Reactor: Recycling of the Chiral Catalyst by Using a Retainable Micellar System, *J. Mol. Cat. A: Chemical*, 168, 81, 2001

Ertl, G., Knözinger, H. and Weitkamp, J., *Handbook of heterogeneous Catalysis*, Wiley, 1997

Farkas, A., *Ullmann's Encyclopedia of Industrial Chemistry*, Volume A5, Page 313, VCH Verlagsgesellschaft, 1986

Gállego, I, et al, Selective Separation of Homogeneous Catalysts Using Silicate Membranes, *Inorg. Chim. Acta*, article in press, 2004

Gordon, C. M., New Developments in Catalysis Using Ionic Liquids, *Appl. Cat. A: general*, 222, 101, 2001

Gorman, C., Metallo dendrimers: Structural Diversity and Functional Behavior, *Adv. Mat.*, 10, 295, 1998

Hagen, J., *Industrial Catalysis, A Practical Approach*, Wiley-VCH, New York, 1999

Hanson, B.E., New Directions in Water Soluble Homogeneous Catalysis, *Coord. Chem. Rev.*, 185-186, 795, 1999

Hashizume, T., Yonehara, K., Ohe, K. and Uemura, S., A Novel Amphiphilic Chiral Ligand Derived from D-Glucosamine, Application to Palladium-Catalyzed Asymmetric Allylic Substitution Reaction in an Aqueous or an Organic Medium, Allowing for Catalyst Recycling, *J. Org. Chem.*, 65, 5197, 2000

Hecht, S. and Fréchet, J.M.J, Dendritisch Eingeslossene Aktive Zentren: Anwendung des Isolationsprinzips der Natur in Biomimetik und den Materialwissenschaften, *Angew. Chem.*, 113, 76, 2001

Herrmann, W. A. and Cornils, B., Organometallic Homogeneous Catalysis – Quo Vadis?, *Angew. Chem. Int. Ed. Engl.*, 36, 1048, 1997

Jeffery, I.C. and Whiston, K., Catalyst Recovery, WO 98/08605, 1998

Joó, F., Papp, É. and Kathó, Á, Molecular Catalysis in Liquid Multiphase Systems, *Topics in Catalysis*, 5, 113, 1998

Kettle S.F.A., Physical inorganic chemistry; a coordination chemistry approach, Spektrum Academic publishers, 1996

Khoury, F.M., Multistage Separation Processes, CRC-press, 2005

Kim, J. S. And Datta, R., Supported Liquid Phase Catalytic Membrane Reactor-Separator for Homogeneous Catalysis, *AIChE Journal*, 37(11), 1657, 1991

Kohlpaintner, C.W., Fischer, R.W. and Cornils, B., Aqueous Biphasic Catalysis: Ruhrchemie/Rhône-Poulenc OXO process, *Appl. Cat. A: Gen.*, 221, 219, 2001

Kragl, U. and Dwars, T, The Development of New Methods for the Recycling of Chiral Catalysts, *Trends in Biotechnology*, 19(11), 442, 2001

Kummer, R., Schwirten, K. and Schindler, H.D., Regeneration and Separation of Rhodium-Containing or Iridium-Containing Catalysts from Distillation Residues Following Hydroformylation, US 4,021,463, 1977

Kummer, R., Schneider, H.W. and Schwirten, K, Isolation and Regeneration of Rhodium-Containing Catalysts from Distillation Residues of Hydroformylation Reactions, US 4,113,754, 1978

Leach, B. E., Applied Industrial Catalysis, Volume I, Academic Press, New York, 1983

Leach, B. E., Applied Industrial Catalysis, Volume 2, Academic Press, New York, 1983

Leadbeater, N.E. and Scott, K.A., Preparation of a Resin-Bound Cobalt Phosphine Complex and Assessment of Its Use in Catalytic Oxidation and Acid Anhydride Synthesis, *J. Org. Chem.*, 65, 4470, 2000

Leadbeater, N.E., Preparation of a Resin-Bound Ruthenium Phosphine Complex and Assessment of Its Use in Transfer Hydrogenation and Hydrocarbon Oxidation, *J. Org. Chem.*, 66, 2168, 2001

Leeuwen, P. W. N. M., Decomposition Pathways of Homogeneous Catalysts, *Appl. Cat. A: Gen.*, 212, 61, 2001

Leeuwen, P. W. N. M., *Homogeneous Catalysis. Understanding the Art*, Kluwer Academic Publishers, Dordrecht, 2004

Lo, T.C., Baird, M.H.I. and Hanson, C. *Handbook of Solvent Extraction*, Wiley, 1983

Luthra, S.S., Yang, X., Freitas dos Santos, L.M., White L.S. and Livingston, A.G., Homogeneous Phase Transfer Catalyst Recovery and Re-Use Using Solvent Resistant Membranes, *Journ. Memb. Sci.*, 201, 65, 2002

Marcano, J.G.S. and Tsotsis T.T., *Catalytic Membranes and Membrane Reactors*, Wiley, 2002

Merckle, C., Haubrich, S. and Blumel, J., Immobilized Rhodium Hydrogenation Catalysts, *Journ. Organomet. Chem.*, 627, 44, 2001

Mortreux, A. and Petit, F, *Industrial Applications of Homogeneous Catalysis*, Kluwer Academic Publishers, 1988

Olivier-Bourbigou, H. and Magna, L., Ionic Liquids: Perspectives for Organic and Catalytic Reactions, *Journ. Mol. Cat. A: Chem.*, 182, 419, 2002

Park, E.D., Lee, K.H. and Lee, J.S., Easily Separable Molecular Catalysis, *Cat. Today*, 63, 147, 2000

Parshall, G. W. and Ittel, S. D., Homogeneous Catalysis, The Applications and Chemistry of Catalysis by Soluble Transition Metal Complexes, Wiley-Interscience, New York, 1993

Perry, R.H. and Green, D.W., Perry's Chemical Engineers' Handbook, McGrawHill, 1998

Quick, M.H., Recovery of Catalysts, US 4,312,779, 1982

Rony, P.R., Diffusion Kinetics within Supported Liquid-Phase Catalysts, Journ. Cat., 14, 142, 1969

Rutherford, D., Juliette, J.J.J., Rocaboy, C., Horváth, I. and Gladysz, J.A., Transition Metal Catalysis in Fluorous Media: Application of a New Immobilization Principle to Rhodium-Catalyzed Hydrogenation of Alkenes, Cat. Today, 42, 381, 1998

Scarpello, J.T., Nair, D., Freitas dos Santos, L.M., White, L.S. and Livingston, A.G., The Separation of Homogeneous Organometallic Catalysts Using Solvent Resistant Nanofiltration, Journ. Membr. Sci., 5180, 1, 2002

Silva, L., Bray, L. A. and Watson, D. W., Catalyzed Electrochemical Dissolution for Spent Catalyst Recovery, Ind. Eng. Chem. Res., 32, 2485, 1993

Stoddart, F.J. and Welton, T., Metal-Containing Dendritic Polymers, Polyhedron, 18, 3575, 1999

Sunley, G.J. and Watson, D.J., High Productivity Methanol Carbonylation Catalysis Using Iridium The Cativa™ Process for the Manufacture of Acetic Acid, Cat. Today, 58, 293, 2000

Wijngaarden, R.J., Kronberg, A. And Westerterp, K.R., Industrial Catalysis, Wiley 1998

Wilkinson, M. J., van Leeuwen, P. W. N. M. and Reek, J. N. H., New directions in supramolecular transition metal catalysis, Org. Bio. Chem. , 3, 2371, 2005

Wasserscheid, P. and Keim, W., Ionic Liquids – New “solutions” for Transition Metal Catalysis, Angew. Chem. Int. Ed., 39, 3772, 2000

Wöhrlé, D. And Pomogailo, A.D., Metal Complexes and Metals in Macromolecules: Synthesis, Structure and Properties, Wiley, 2003

Zechner, P., Hoffmann, H., Richter, W., Steuzer, D., Strohmeyer, M., Walz, H. and Weippert, E., Verfahren zur kontinuierlichen Hydroformylierung olefinisch ungesättigter Verbindungen, EP 0 254 180 A2, 1987

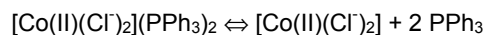
2

Selection of Suitable Adsorbents for the Reversible Recovery of Co(II)Cl₂

2.1 Introduction

Cobalt and PPh₃ ligands are commonly encountered in processes that make use of homogeneous catalysis. Therefore, Co(II) – in complex with PPh₃ and as its individual species – has been selected as a model compound for a catalytic active transition metal center to be recovered.

As stated in chapter 1, in homogeneous catalysis, the catalytic active transition metal center forms a σ/π bond with the available ligands [Kettle, 1996]. This σ -bond/ π -backbond is also formed when Co(II) is contacted with its PPh₃ ligands. In a liquid phase, the homogeneous catalyst complex is always partly dissociated and in equilibrium with its free transition metal – Co(II) – and ligands. In a simplified form, this equilibrium reads:



Due to this equilibrium, all three species will be present in the liquid phase during the recovery of the transition metal complex. It is clear that, if one does not take account for the dissociation of the complex and tries to recover it as a whole, leaching of Co(II) and/or its PPh₃ ligands will occur.

The solution to avoid leaching of the transition metal and ligands, is to separately recover both components from the reaction phase. In this chapter, the separate recovery of the Co(II) has been selected to avoid possible leaching of the transition metal. In this view, suitable adsorbents to be used in Reverse Flow Adsorption should be able to undergo a selective and reversible interaction with the transition metal – Co(II) – with a high enough capacity. Interactions that are possibly exploitable are:

1. Electrostatic forces – for example van der Waals attractions – can undergo interactions with Co(II), but also with all other species that are present in the liquid phase. Therefore, this type of interaction will not be considered.

2. Ion exchange is of interest because it is a well known topic in the selective recovery of transition metals. As Co(II) is expected to be the only ionic species in the reaction mixture, it will be the only species that can be exchanged.
3. σ -donation/ π backdonation can be exploited as it always forms an equilibrium between the transition metal and a suitable ligand that is immobilized to a solid carrier. The transition metal is the only compound in the liquid phase that accepts electrons. Thus, it can be selectively separated from the reaction mixture.

To test the exploitability of ion exchange and σ -donation/ π backdonation, two series of adsorbents have been pre-selected for characterization. The first series of adsorbents – ion exchange resins – have been tested on their ability to reversibly adsorb Co(II). Here, precipitation is used to ensure the reversibility (see paragraph 2.1 for a more detailed explanation) of the Co(II) adsorption.

The second series of adsorbents that have been characterized are expected to form a reversible σ/π interaction of Co(II) with a suitable ligand that is immobilized onto the adsorbent. In this case, pre-selection was done on basis of the Hard and Soft Acids and Bases theory which predicts the strength – a measure for the adsorption capacity – of the interaction between the transition metal and the immobilized ligand.

The adsorption capacities of the various adsorbents have been tested by means of classical batch adsorption experiments over the pre-selected adsorbents in 1-butanol. The reversibility of the adsorption will then be demonstrated by desorbing Co(II) from the loaded adsorbents by contacting them with lean 1-butanol.

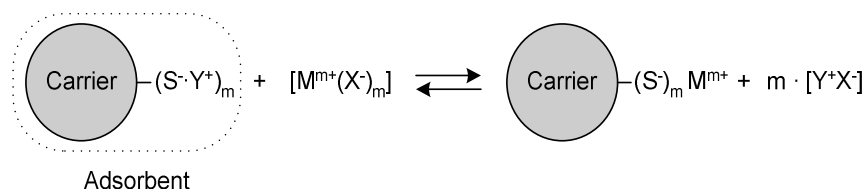
In addition to these adsorption experiments, the most promising adsorbent has been selected to examine the influence on the adsorption capacity of the presence of ligands in the liquid bulk phase. By addition of PPh₃, the influence of the presence of ligands will be shown.

2.2 Exploitable Adsorptive Interactions

2.2.1 Ion Exchange

Metal recovery by ion exchange is a well-documented topic [Dorfner, 1991; Helfferich, 1995]. It is based on the exchange of an immobilized cation – in case of metal recovery – for a metal cation that is in solution. The catalytic active center in a transition metal based homogeneous catalyst is formed by a salt of a halogenated transition metal ($M^{m+}(X^-)_m$) in

equation 2). When contacted with an ion exchange resin, the transition metal of the homogenous catalyst will exchange with the immobilized cation of the resin by:



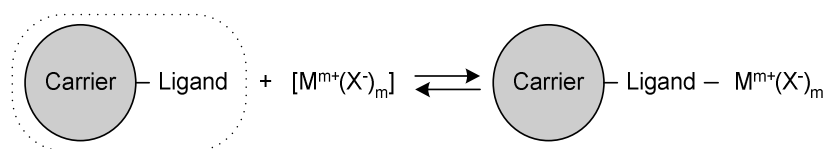
In this equation, the anionic group (S) is covalently immobilized onto the ion exchange resin. The cation (Y⁺) is replaced by the transition metal (M^{m+}) of the homogeneous catalyst. As a result of this exchange, the transition metal will remain immobilized onto the adsorbent. The capacity of the ion exchange resin for the transition metal is directly related to the charge of the immobilized cation [Dorfner, 1991; Helfferich, 1995; Perry, 1998]. A lower positive charge of the immobilized cation increases the capacity for the transition metal. Therefore, ion exchange resins that have been functionalized with a group I element – such as Na⁺ – are preferred above ions from group II – such as Mg²⁺ – when capacity forms the main selection criterion. The latter are more difficult to exchange due to their higher formal charge, leading to a lower exchange of the transition metal.

Recovery of the transition metal can be achieved by the introduction of recovery agents – counter ions – that have to be added to the liquid phase during the recovery. Here, one can think of halide salts that contain the former immobilized cation – such as Na⁺ –.

In conclusion, it can be stated that the preferred ion exchange resins have to be functionalized with a group I element – low formal charge for a higher capacity for the most efficient recovery.

2.2.2 σ/π interactions

In the coordination sphere of transition-metal based homogeneous catalysts, its ligands are always at equilibrium with their free transition-metal centers. This equilibrium – σ -bond/ π -backbond – is also expected between the free transition-metal and its immobilized counterpart if one of the components is bound to a solid carrier:



The adsorption capacities of these adsorbents are directly connected with the strength of the bond that is being formed between the adsorbate and its immobilized counterpart. The order of magnitude of the interaction strength can be estimated by theories such as the Hard and Soft Acids and Bases (HSAB) theory [Pearson, 1987]. The HSAB theory provides a classification of acids (metals) and bases (ligands) for a first order prediction on the stability of certain ligands towards the catalytic active transition metal center. In table 2.1 the most frequently used metals and ligands have been summarized.

Table 2.1. Classification of some selected species as hard, borderline and soft acids and bases.

Hard acids	Borderline acids	Soft acids
H^+, Li^+, Na^+, K^+ $Be^{2+}, Mg^{2+}, Ca^{2+}, Mn^{2+}$ $Al^{3+}, Fe^{3+}, Co^{3+}, Cr^{3+}$ $Si^{4+}, Ti^{4+}, Zr^{4+}, Th^{4+}$	$Fe^{2+}, \underline{Co}^{2+}, Ni^{2+}, Cu^{2+}, Zn^{2+},$ Sn^{2+}	M^0 Cu^+, Ag^+, Au^+, Hg^+ $Pd^{2+}, Cd^{2+}, Pt^{2+}, Hg^{2+}$
Hard bases	Borderline bases	Soft bases
$H_2O, \underline{ROH}, NH_3, RNH_2, OH^-,$ OR^-	$(C_6H_5)NH_2, (CH_3)_3N, SO_3^-,$ $\underline{Cl}^-, \underline{Br}^-, NO_2^-$	$\underline{R_2S}, RSH, \underline{R_3P}, R_3As,$ I^-, SCN^-, CN^-

According to the HSAB theory, a base is defined as an electron pair donor – such as the ligands in homogeneous catalysts – and an acid – the transition metal – as an electron pair acceptor. Acids and bases can be classified – based on the ease of sharing electrons – into three types: hard, soft and borderline. Hard acids are characterized by a low electronegativity and a relatively small size. Hard bases are characterized by a very high electronegativity of a small sized donor atom. Soft acids are characterized by an acceptor atom of an intermediate to high electronegativity and a large size. Soft bases are characterized by a donor atom of intermediate to high electronegativity and a large size also leading to polarizability. From table 2.1 it is seen however that Co^{2+} is a borderline acid that is intermediate between hard and soft acids. They tend to have lower charge and somewhat

larger size than hard acids. Similarly borderline bases are intermediate between hard and soft bases. They tend to be larger and less electronegative than hard bases, smaller and more electronegative than soft bases. Since Co^{2+} is a borderline acid it is more difficult to predict in advance which interaction will be preferential to be exploited. In a first instance it might seem the most logical to use a borderline base such as chlorine or bromide. However, from the electronegativity of the elements, it can be concluded that the ease of sharing electrons by σ -donation and π -back-donation decrease according to the periodic table of elements, as follows:



Thus, group IV elements like nitrogen and phosphorus form stronger non-ionic bonds with transition metals as the group V – oxygen and sulfur – elements. Furthermore oxygen and sulfur will undergo a more stable interaction than the chloride and bromide – group VI – would do with a soft acid. Based on these considerations we decided to select adsorbents functionalized with a hard base (ROH), a borderline base (Cl^- , Br^- or R_3N) and a soft base (R_2S or R_3P) for further experimental evaluation.

Additionally the influence of the side groups has been taken into account when selecting functionalized adsorbents. It is known that the ability of the central atom (N or P) to interact with hydrogen and thus its ability to give off its electrons, decrease when electron pulling groups (for example: aromatics like phenyl (Ph) groups) are connected to the central atom. On the other hand, when electron pushing groups (such as alkyl groups) are introduced, the stability of the bonds increases.

In conclusion it can be stated, that the most preferable adsorbents contain functional groups that are composed of electron pushing groups (such as alkyls) connected to an element originating from group IV from the periodic table of elements. In contrast to this conclusion, we have selected a triphenylphosphine as functional group to determine the exploitability of phosphorus because alkyl phosphines are highly sensitive to oxygen.

For reasons of comparison to the ion exchange resins, all selected adsorbents (see table 2.4) were based on a polystyrene/divinylbenzene carrier.

2.3 Experimental

2.3.1 Solutions

CoCl₂ (anhydrous, Fluka) and dichlorobis(triphenylphosphine)cobalt(II) (98 [%], Sigma-Aldrich) solutions of $1 \pm 4 \cdot 10^{-3}$, $2 \pm 5 \cdot 10^{-3}$, $4 \pm 7 \cdot 10^{-3}$ and $8 \pm 1 \cdot 10^{-2}$ [mM] of Co(II) in a organic liquid phase were prepared with either 1-butanol (p.a., Merck) or 1-Octanol (99 [%], Sigma-Aldrich). Preliminary experiments showed that from these two solvents, adsorbents in combination with 1-butanol had a capacity for CoCl₂ at least twice of that from 1-octanol.

2.3.2 Adsorbents

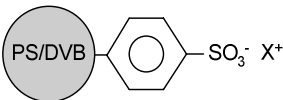
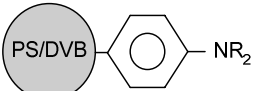
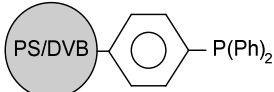
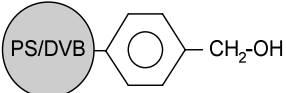
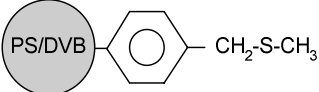
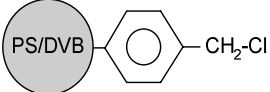
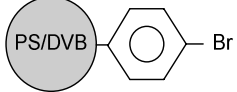
2.3.2.1 Ion exchange resins

Because of its use in a wide variety of non-aqueous applications, Amberlyst 15 (4.7 [mmol H/g dry], Sigma-Aldrich) has been selected as a carrier for the group I elements. The Amberlyst 15 was firstly washed with de-ionized water (Millipore) in a column. The functionalization of the Amberlyst 15 was done by contacting the resin with 0.1 [mM] aqueous solutions of the selected group I elements (see table 2.2). During the ion exchange, the hydrogen of the Amberlyst 15 was exchanged for the transition metal. The exchange was continued until a constant concentration was reached in the effluent. Then the adsorbents were rinsed with de-ionized water and the remaining water was rinsed out of the resin with methanol (p.a., Merck). The remaining methanol was rinsed with 1-butanol (p.a., Merck). The adsorbents thus prepared were taken from the column and used in the batch adsorption experiments.

2.3.2.2 σ/π -interaction based adsorbents

These selected adsorbents (see table 2.2) were commercially available and needed only to be rinsed from possible impurities that remained in the resins after its synthesis. All functionalized adsorbents were pre-rinsed with de-ionized water over a filter. Then, the remaining water was rinsed out of the adsorbents with methanol (p.a., Merck). The remaining methanol was rinsed with 1-butanol (p.a., Merck). The adsorbent materials thus prepared were used in the batch adsorption experiments.

Table 2.2. Overview of the selected adsorbents

Adsorbent type	Notes	Aqueous salt used	Adsorbent	Q [mmol sites /g dry]
Group I element				
H+ loaded Amberlyst 15	Macroreticular Sigma-Aldrich			4.7
Li+ loaded Amberlyst 15	Macroreticular Sigma-Aldrich	1.0 [M] LiOH		4.6
Na+ loaded Amberlyst 15	Macroreticular Sigma-Aldrich	1.0 [M] NaOH		4.3
K+ loaded Amberlyst 15	Macroreticular Sigma-Aldrich	1.0 [M] KOH		4.0
Rb+ loaded Amberlyst 15	Macroreticular Sigma-Aldrich	1.0 [M] RbOH		3.4
Cs+ loaded Amberlyst 15	Macroreticular Sigma-Aldrich	1.0 [M] CsOH		2.9
Group IV				
Amberlyst A21	Macroreticular Sigma-Aldrich (R=C ₂ H ₅)			4.7
Polymer bound PPh ₃	Gel Sigma-Aldrich			3.0
Group V				
Polymer bound benzyl alcohol	Gel Polymerlabs			1.1
Polymer bound methylsulfanylmethyl	Gel Sigma-Aldrich			3.0
Group VI				
PL-CMS Resin	Gel Polymerlabs			2.0
PL-PBS Resin	Gel Polymerlabs			2.0

2.3.3 Adsorption and desorption measurements

The adsorption of Co(II) and PPh₃ onto the various adsorbents were measured in batch adsorption experiments. A series of the selected functionalized adsorbents ($m_{\text{ads}} \approx 0.3 \pm 1 \cdot 10^{-4}$ [g]) were contacted in erlenmeyer flasks with 10 ± 0.01 [ml] the selected solution. The Erlenmeyer flasks were then equilibrated at 90 [°C] in a thermostated shaking water bath for 15-16 [hr] (approximately 5 times the time required for equilibrium). The liquid phases were decanted and the Co(II) concentrations ($\pm 1 \cdot 10^{-4}$ [mM]) were analyzed by AAS (Varian Spectraa 110). After adsorption, all equilibrated samples were contacted with 10 ± 0.01 [ml] of fresh 1-butanol for 15-16 [hr] at 90 [°C] to investigate the desorption. The equilibrium concentrations ($\pm 1 \cdot 10^{-4}$ [mM]) after desorption of the relevant components were also measured by AAS. The amounts of adsorbed Co(II) were calculated from the differences in initial and equilibrium amounts. The loading of the adsorbents after adsorption (with a maximal error of ± 1.4 [%]) and desorption (maximal error ± 1.8 [%]) are expressed with respect to the number of functional sites in the adsorbents. Note that the total available number of selective groups (Q) is given in table 2.2, as these differ due to the differences in molar masses of the various elements.

The reproducibility of the adsorption and desorption measurements have been tested by repeating the experiments. The experimental results were within the error margins of the adsorption experiments.

The presence of group I elements was determined by AAS. To check for the possible loss of aromatic groups from the carrier and adsorption of the PPh₃ ligands, also UV/Vis spectra were recorded from the liquid phases. Chlorine in the liquid phase after adsorption was determined by XRF analysis.

2.4 Experimental Results

2.4.1 Ion exchange resins

Figures 2.1 through 2.6 (see next page) respectively show the loadings of the H⁺, Li⁺, Na⁺, K⁺, Rb⁺ and Cs⁺ functionalized Amberlyst 15 from 1-butanol at 90 [°C]. In these figures, the capacity to adsorb Co(II) is shown at equilibrium as a function of its concentration which remained in the liquid phase after the adsorption. In addition to these, also the loading of Co(II) that remained in the solid phase after the desorption experiments is shown against the equilibrium concentrations in the liquid phase.

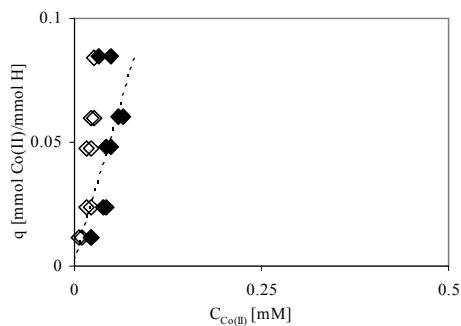


Figure 2.1. Co(II) adsorption (closed symbols) and desorption (open symbols) over H^+ loaded Amberlyst 15 from 1-butanol at 90 [°C]

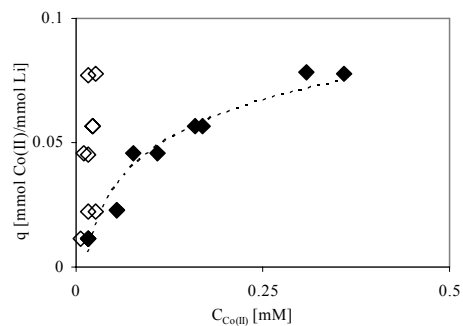


Figure 2.2. Co(II) adsorption (closed symbols) and desorption (open symbols) over Li^+ loaded Amberlyst 15 from 1-butanol at 90 [°C]

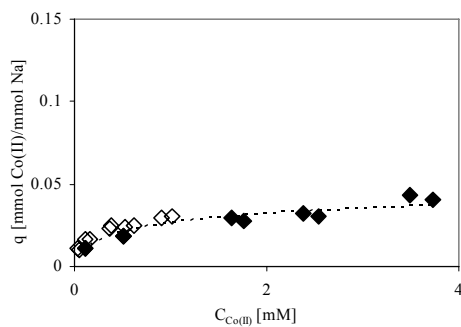


Figure 2.3. Co(II) adsorption (closed symbols) and desorption (open symbols) over Na^+ loaded Amberlyst 15 from 1-butanol at 90 [°C]

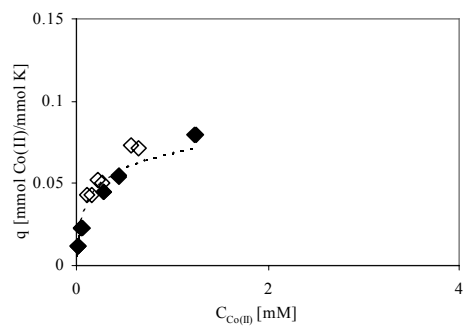


Figure 2.4. Co(II) adsorption (closed symbols) and desorption (open symbols) over K^+ loaded Amberlyst 15 from 1-butanol at 90 [°C]

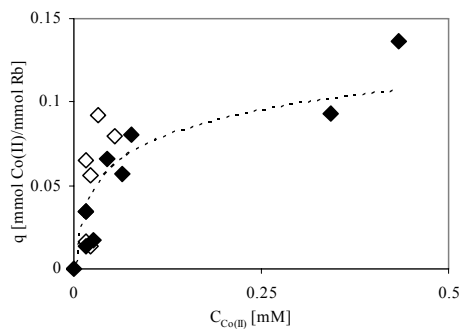


Figure 2.5. Co(II) adsorption (closed symbols) and desorption (open symbols) over Rb^+ loaded Amberlyst 15 from 1-butanol at 90 [°C]

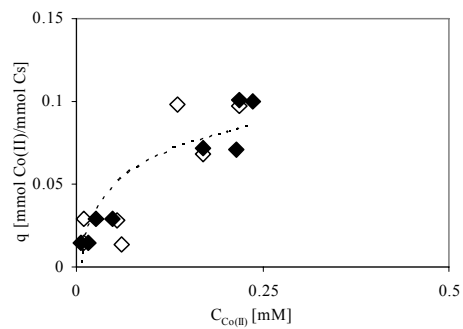


Figure 2.6. Co(II) adsorption (closed symbols) and desorption (open symbols) over Cs^+ loaded Amberlyst 15 from 1-butanol at 90 [°C]

It is clear from these figures, that the strongest Co(II)Cl₂ adsorption is observed for the H⁺, Li⁺, Rb⁺ and Cs⁺ functionalized Amberlyst 15 resins. The Na⁺ and K⁺ functionalized resins, show only a relatively mild interaction with the catalytic transition metal center.

For the lower group I elements of the periodic table of elements, it is shown that the desorption results – except for the Li⁺ functionalized Amberlyst 15 – are in reasonable agreement with the adsorption experiments. Therefore, it can be concluded that the adsorption of Co(II) is reversible by replacement of the mother liquor used during the adsorption experiments with clean 1-butanol.

The adsorption and desorption results do not show a complete overlap due to leaching of group I elements from the adsorbents during decanting the liquid phase before the desorption experiments. This leads to less counter ions that can be used to recover the immobilized Co(II) from the adsorbents.

2.4.2 σ/π -interaction based adsorbents

We measured the adsorption of Co(II) over nitrogen, phosphor, sulfur, oxygen, chloride and bromide functionalized polystyrenic resins. The adsorption and desorption of Co(II) over these functionalized resins are shown in figures 2.7 to 2.10 (next page) as a function of its equilibrium concentration in the liquid phase after adsorption and desorption at 90 [°C] from 1-butanol.

The chloride and bromide functionalized adsorbents have not been included as they have only a very small capacity for Co(II). This made these latter two adsorbents unimportant for our purpose.

Again, the desorption results are in reasonable agreement with the adsorption experiments. Thus, the adsorption of Co(II)Cl₂ onto these types of resins is reversible by replacing the liquid phase with clean 1-butanol.

Note that the desorption results in figures 4.9 and 4.10 are measured at a very low concentration. The adsorption of Co(II) onto the sulfur and oxygen functionalized polystyrenic resins is very low, which results in very low Co(II) concentrations after desorption.

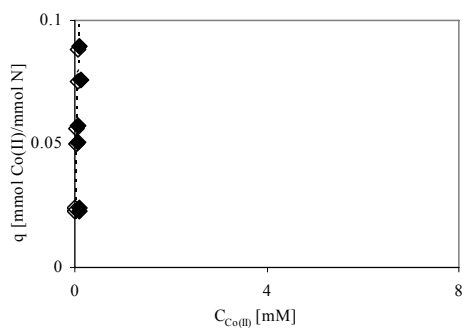


Figure 2.7. Co(II) adsorption (closed symbols) and desorption (open symbols) over nitrogen functionalized Amberlyst A21 from 1-butanol at 90 [°C]

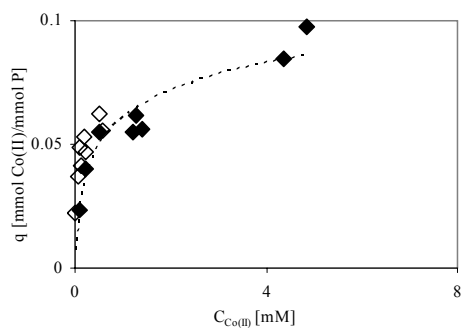


Figure 2.8. Co(II) adsorption (closed symbols) and desorption (open symbols) over polymer bound PPh₃ from 1-butanol at 90 [°C]

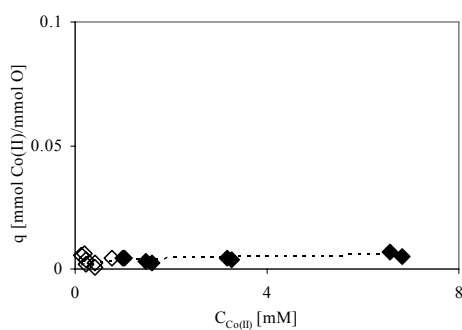


Figure 2.9. Co(II) adsorption (closed symbols) and desorption (open symbols) over polymer bound benzyl alcohol from 1-butanol at 90 [°C]

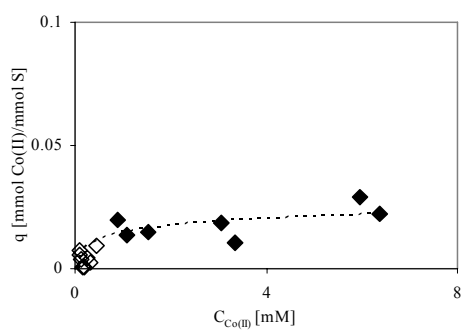


Figure 2.10. Co(II) adsorption (closed symbols) and desorption (open symbols) over polymer bound methylsulfanylmethyl from 1-butanol at 90 [°C]

2.4.3 Influence of the PPh₃/CoCl₂ ratio

In figure 2.11, the loading of the initially complexed Co(II) – containing PPh₃ in a ratio of 2 compared to CoCl₂ – onto polymer bound triphenylphosphine is compared to the adsorption of initially free Co(II) from 1-butanol at 90 [°C].

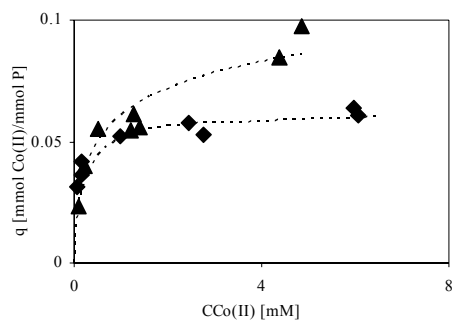


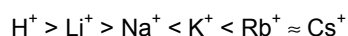
Figure 2.11. Comparison of Co(II) desorption over polymer bound PPh₃ from 1-butanol at 90 [°C] in presence of PPh₃ ligands (closed diamonds; PPh₃/Co ratio = 2) and without PPh₃ (closed triangles).

The influence of PPh₃ on the adsorption of Co(II) is clearly visible when compared to the free Co(II), as the adsorption isotherm for the complex form of Co(II) shows a lower capacity for adsorption. The interactions that the PPh₃ ligands undergo with the Co(II) in the liquid phase, influence the amount of free Co(II) which leads to a lower adsorption capacity of Co(II).

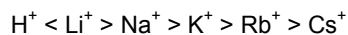
2.5 Discussion

2.5.1 Ion exchange resins

The observed ion exchange capacities for the group I elements are known to differ [Helferich, 1995] with the choice of the counter ion. The capacities – as represented in figures 2.1 through 2.6 – increase down the periodic table of elements for the heavier group I elements:



This trend depends on the polarity of the solvent that is used. For the highly polar solvent water, this trend namely reads:



which is in reversed order when one compares this trend to the observed one for the slightly polar 1-butanol solvent.

The irreversibility of the Co(II) adsorption over Li⁺ functionalized Amberlyst 15 is clearly reflected in figure 2.2. The adsorption and desorption results for the Co(II) capacities do not follow each other. After desorption, a large amount of the adsorbed Co(II) remains immobilized on the Li⁺ loaded Amberlyst 15.

During the adsorption of Co(II) from the 1-butanol phase, Co(II) exchanges with the Li⁺ under formation of its chloride salt (LiCl). This salt is highly soluble in 1-butanol as is shown for indicative reasons at 25 [°C] in table 2.5.

Due to the high solubility of the formed salts in 1-butanol at 90 [°C] [Stephen, 1963] no precipitation occurs and all will remain in solution. The formed salt is transferred to the bulk of the solution. Due to the large solubility of LiCl in 1-butanol [Stephen, 1963], all of the formed chloride salt is removed with the 1-butanol when decanting the liquid phase from the loaded resin after adsorption. Thus, LiCl will be completely removed and can not be used for to exchange with the immobilized Co(II) from the loaded resin after contacting it with pure 1-butanol. Contacting the loaded resin with pure solvent – 1-butanol – will have no effect as no counter ions are present to exchange with the immobilized Co(II). The loading of Co(II) will remain unaltered after desorption. To recover the immobilized Co(II) from the Li⁺ loaded Amberlyst 15, recovery agents have to be introduced – such as LiCl – to exchange the Co(II).

Table 2.3. Solubilities of group I element chlorides in butanol [Stephen, 1963].

Group I chloride	Solubility in Butanol at 25 [°C] [weight-%]
HCl	28.92
LiCl	11.49
NaCl	0.014
KCl	-
RbCl	0.010 ^{a)}
CsCl	0.621

^{a)} Estimated from the RbCl solubilities in methanol, ethanol, propanol and pentanol.

Although not clearly shown in figure 2.1, this mechanism was also confirmed by XRF analysis for the H⁺ functionalized Amberlyst 15; when most of the Co(II) had been immobilized, chloride was found back in the liquid phase. The only explanation for this can

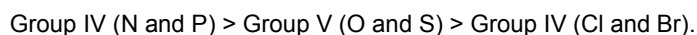
be the formation of HCl that dissolved into the liquid phase after H⁺ has been exchanged for Co(II).

The solubilities of the chloride salts of the heavier group I elements into 1-butanol are known to be low [Stephen, 1963]. The heavier group I elements have been exchanged for Co(II) during the adsorption and the related chloride salts precipitated in the pores of the resin. When contacted with pure 1-butanol during the desorption experiments, a trace of the respective chloride salt dissolves into the liquid phase and exchanges with the immobilized Co(II). The phenomenon is clearly shown as the recovered amounts of Co(II) after contacting the loaded adsorbents with pure solvent are in line with the adsorption results.

Qualitative AAS measurements showed the presence of traces of group I elements in the liquid phase, both after adsorption and desorption. Although their solubilities are low, the group I elements leached out of the resin. Therefore, the reversibility of the Co(II) adsorption is only partly reversible without the addition of recovery agents. When used in Reverse Flow Adsorption, these types of adsorbents will give rise to a limited number of adsorption and desorption cycles for the recovery of the catalytic active transition metal center.

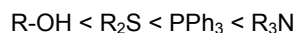
2.5.2 σ/π -interaction based adsorbents

It is clear from figures 2.7 through 2.10 that the adsorption capacities of the various adsorbents decrease in the order of increasing electronegativity of the immobilized ligand:



As predicted by the HSAB theory, this effect is caused by the fact that highly electronegative elements are less able to share electrons with Co(II) compared to elements of medium electronegativity.

The trends inside one group are more difficult to explain from the central atom as already mentioned in the theory. But the trend that is observed is as given by the ligand field theory:



Side groups that are connected to the central atom strongly influence the ease of sharing electrons and thus effect the adsorption of the borderline acid Co(II). The adsorbents functionalized with the group V elements showed the trend for oxygen and sulfur to be: O < S. Sulfur has two alkyl groups connected – electron pushing – which makes it softer and easier to share electrons.

The effects of electron pushing or pulling groups are clearly shown for the nitrogen and phosphorous functionalized adsorbents. The aromatic groups on the phosphor make the phosphor harder, while the alkyl groups make the nitrogen softer. In this extreme case, the capacities are interchanged.

From the desorption results in figures 2.7 through 2.10 it can be concluded that the adsorption is reversible as the desorption results are in reasonable agreement with the adsorption isotherms. The initial loading at the start of the desorption experiments is located at the y-axis – initially no Co(II) present – and the level of the amount Co(II) that remained on the adsorbent after decanting. The reversibility of the adsorption is noe reflected in both a horizontal – decrease in loading – and a vertical shift – increase in Co(II) concentration – from the initial loading after the desorption.

The adsorbed amounts of Co(II) can be recovered from the resins by introducing fresh 1-butanol, without addition of a recovering agent. Therefore it is not expected that the adsorption and desorption cycles will be limited by leaching of any component out of the resin.

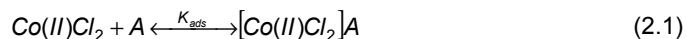
In terms of capacity and reversibility of the Co(II) adsorption, the most promising adsorbent is the polymerbound triphenylphosphine.

2.5.3 Influence of the $\text{PPh}_3/\text{CoCl}_2$ ratio

The lower adsorption capacity for the complexed Co(II) can be explained by the fact that besides the immobilized adsorption sites, the PPh_3 ligands compete to interact with Co(II).

2.5.3.1 Co(II) adsorption from the uncomplexed solution

The adsorption of the free – uncomplexed – Co(II)Cl_2 is purely given by the interaction of Co(II) with the adsorption sites:



Wherein, K_{ads} and A respectively represent the adsorption constant and the adsorption sites for this equilibrium. As the immobilized ligands are situated at the inner-surface of the adsorbent, it may be assumed that a monolayer coverage is formed at lower Co(II) concentrations. The adsorption equilibrium for the uncomplexed solution of Co(II) can be rewritten in the form of a Langmuir isotherm [Atkins, 1992]:

$$q = \frac{q_m \cdot K_{ads} \cdot C_{Co(II),free}}{1 + K_{ads} \cdot C_{Co(II),free}} \quad (2.2)$$

Wherein, q , q_m and $C_{Co(II),free}$ respectively stand for the equilibrium loading, the maximal monolayer coverage and the free Co(II) concentration at equilibrium. The Langmuir isotherm can be rewritten into a linear form according to:

$$\frac{C_{Co(II),free}}{q} = \left(\frac{1}{q_m} \right) C_{Co(II),free} + \left(\frac{1}{K_{ads} \cdot q_m} \right) \quad (2.3)$$

Thus, the maximal monolayer coverage ($q_m = 0.10$ [mol Co(II)/mol sites]) for the uncomplexed solution of Co(II) is given by the slope of the linearized Langmuir isotherm – dotted line in figure 2.12 – and the adsorption equilibrium ($K_{ads} = 1.59$ [m³/mol Co(II)]) constant can be derived from its intercept.

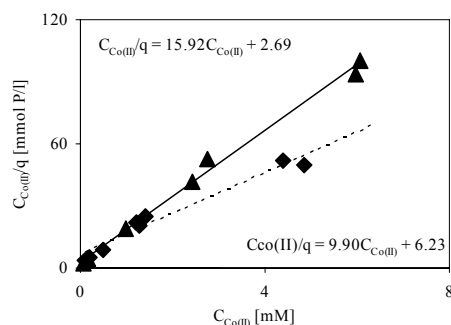
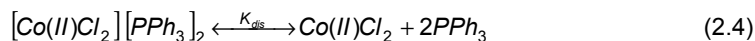


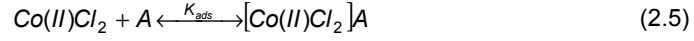
Figure 2.12. Linearized Langmuir isotherms for Co(II) adsorption over polymer bound PPh₃ from 1-butanol at 90 [°C] in presence of PPh₃ ligands (closed triangles; PPh₃/Co ratio = 2) and without PPh₃ (closed diamonds).

2.5.3.2 Co(II) adsorption from the complex solution

The lower apparent adsorption capacity for the complexed Co(II) can be explained by the fact that besides the immobilized adsorption sites, the PPh₃ ligands compete to interact with Co(II). In the complex solution, Co(II) undergoes an interaction with the PPh₃ ligands and forms a dissociation equilibrium according to:



Wherein, K_{dis} represents the dissociation constant for this equilibrium. Due to the interaction of the PPh_3 ligands with $Co(II)$, the concentration of free $Co(II)$ in the complex solution will be lower as that for the solution without addition of PPh_3 . The free $Co(II)$ will be adsorbed in its turn as mentioned above:



Again, assuming monolayer coverage of the immobilized adsorption sites, we can derive a Langmuir type isotherm according to:

$$q = \frac{q_m \cdot K_{ov} \cdot C_{Co(II),total}}{(1 + K_{ov} \cdot C_{Co(II),total})} \quad (2.6)$$

Wherein, K_{ov} and $C_{Co(II),total}$ respectively represent the overall equilibrium constant and the total – in complex as well as in free form – $Co(II)$ concentration in the solution. Thus, the found equilibrium constant ($K_{ov} = 6.92 [m^3/mol Co(II)]$) found from this linearized Langmuir isotherm (solid line in figure 2.12), is the overall equilibrium constant of the complex solution system. And the found $q_m (= 0.06 [mmol Co(II)/mmol sites])$ is an apparant value.

Assuming that the adsorption equilibrium of the complexed solution equals that of the uncomplexed solution, one can calculate the free $Co(II)$ in the complexed solution via equation (2.6). The complexed amount – $Co(II)Cl_2(PPh_3)_2$ is then given by the mass balance:

$$C_{Co(II),total} - C_{Co(II),free} = C_{Co(II),complexed} \quad (2.7)$$

Wherein, $C_{Co(II),complexed}$ represents the concentration of $Co(II)Cl_2$ in complex with two PPh_3 ligands. Now the total concentration of complexed $Co(II)Cl_2$ can be calculated and represented as a function of the free $Co(II)$ as in figure 2.14.

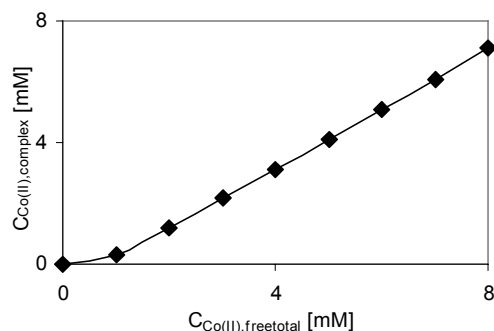


Figure 2.14. Concentration complexed Co(II)Cl₂ versus free Co(II)Cl₂ in complex solution.

From figure 2.14 it is clear that with increasing starting concentration of Co(II)-complex, – as also the PPh₃ concentration increases – the ration of complexed Co(II) versus its free form increases rapidly. This gives rise to the lower apparent maximal loading of the adsorbent. The ratio between these two is given by the discossiation constant as follows:

$$\frac{C_{Co(II),complexed}}{C_{Co(II),free}} = \frac{C_{PPh_3}}{K_{dis}} \quad (2.8)$$

The influence of the PPh₃ ligands on the equilibrium that is being formed during the adsorotion of the complexed Co(II) leads to less free Co(II)Cl₂ that can penetrate the matrix of the polymerbound triphenylphosphine. This, in its turn leads to a decreased capacity of the adsorbent.

2.6 Conclusion

The capacity and reversibility of Co(II) adsorption by ion exchange and sharing of electrons by the σ -donation and π -back-donation principle has been characterized in this chapter:

- Reversible adsorption has been observed for the adsorbents that use σ -donation and π -back-donation for the recovery of Co(II). As leaching of the functional groups is not expected for these types of adsorbents, the σ/π interaction is the most preferred mechanism for the recovery of transition metals.
- Higher group I elements – Na⁺, K⁺, Rb⁺ and Cs⁺ – were found to reversibly adsorb Co(II) from 1-butanol. Due to the precipitation of the newly formed salt inside the pores of the adsorbents, a small amount became available for desorption when contacted with

lean solvent. A small amount of salt remained in solution and leached from the resin. The number of adsorption and desorption cycles will therefore be limited.

- Irreversible adsorption has been observed when using H^+ and Li^+ loaded Amberlyst 15. The adsorbed $Co(II)$ can only be recovered by addition of recovering agents such as HCl or $LiCl$.

Especially the polymerbound triphenylphosphine is of large interest, as its capacity is relatively high – compared to the groups V and VI elements – and the reversibility of the $Co(II)$ adsorption is assured without addition of recovery agents.

The influence of the presence of PPh_3 ligands was found to influence the maximal $Co(II)$ loading onto the polymerbound triphenylphosphine. It decreased the amount of free $Co(II)$ which lead to a decrease in capacity of the $Co(II)Cl_2$ adsorption.

2.7 References

Alfarra, A., Frackowiak, E. and Béguin, F., The HSAB Concept as a Means to Interpret the Adsorption of Metal Ions onto Activated Carbons, *Appl. Surf. Sci.*, 228, 84, 2004

Atkins, P.W., *Physical Chemistry*, Oxford University Press, 1992

Bhaduri S., et. al., *Homogeneous catalysis; mechanisms and industrial applications*, Wiley-Interscience, 2000

Cotton F.A., Faut, O.D., Goodgame, M.L. and Holm, R.H., Magnetic Investigations of Spin-free Cobaltous Complexes. VI. Complexes Containing Phosphines and the Position of Phosphines in the Spectrochemical Series, *J. Am. Chem. Soc.*, 83, 1780, 1961

Cotton F.A., et. al., *Advanced inorganic chemistry*, Wiley-Interscience, 1988

Dorfner K., *Ion Exchangers*, Walter de Gruyter, 1991

Fifield F.W., Kealey D., *Analytical Chemistry*, Blackie A&P, 1992

Helferich F., *Ion Exchange*, Dover Publications Inc., 1995

Kettle S.F.A., Physical inorganic chemistry; a coordination chemistry approach, Spektrum Academic publishers, 1996

Pearson R.G., Benchmark papers in inorganic chemistry: Hard and soft acids and bases, Wiley, 1973

Pearson, R. G., Recent Advantages in the Concept of Hard and Soft Acids and Bases, Journ. Chem. Ed., 64(7), 561, 1987

Pearson R.G., Absolute Electronegativity and Hardness: Application to Inorganic Chemistry, Inorg. Chem., 27, 734, 1988

Perry, R.H. and Green, D.W., Perry's Chemical Engineers' Handbook, McGrawHill, 1998

Stephen H., Stephen T., Solubilities of organic and inorganic compounds, Pergamon press, 1963

3

Selection of Suitable Adsorbents for the Reversible Recovery of PPh₃

3.1 Introduction

The strategy – chosen in chapter 2 – to recover the homogenous catalyst is to use its dissociation to firstly recover the transition metal separately from its ligands. Then, in a second step, the ligands need to be recovered from the reaction phase by a second type of adsorbent.

Co(II) and triphenylphosphine – PPh₃ – are commonly encountered in homogeneously catalyzed processes [Bhaduri, 2000]. Therefore, PPh₃ has been selected as a model ligand, both in complexed – as (PPh₃)₂CoCl₂ – and as individual species.

In this chapter, the emphasis will be put on the recovery of the remaining PPh₃ ligands from a liquid phase that remain in solution after the removal of the transition metal center. Analog to the transition metal recovery, the selection of potential suitable adsorbents for the selective recovery of the ligands will be focused on:

1. Ion exchange; although the ligand will be neutral in charge, it can accept hydrogen – Brønsted acid/base interaction – which will distort the electronic configuration around the central atom and raising its charge. It will be the only charged species in solution that can be exchanged.
2. σ -donation/ π backdonation; as the ligands are able to donate electrons, they can be selectively separated from the reaction mixture by correctly selected electron accepting functional group.

To test the exploitability of ion exchange and σ/π -interactions, a series of modified ion exchange resins have been selected. For recovery by ion exchange, an acidic resin will be tested on its capability to reversible adsorb the PPh₃ ligands. The remaining adsorbents that have been selected are functionalized with a transition metal that is immobilized onto the adsorbent and are expected to form a reversible σ/π interaction with PPh₃. In the latter case, pre-selection was done on basis of the Hard and Soft Acids and Bases theory which predicts

the strength of the interaction between the immobilized transition metal – which act as an adsorption site – and the PPh₃ ligands.

The adsorption capacities of the various adsorbents have been tested by means of classical batch adsorption experiments over the pre-selected adsorbents in 1-butanol. The reversibility of the adsorption will then be demonstrated by desorbing PPh₃ from the loaded adsorbents by contacting them to lean 1-butanol.

In addition to these adsorption experiments, two adsorbents that reversibly adsorb PPh₃ with the highest capacity have been selected to demonstrate the effects of the matrix material of which the solid carrier is composed

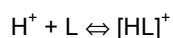
By using a different carrier and replacement of 1-butanol for 1-octanol, the influence of the presence of matrix material and the choice of solvent on the adsorption capacities will be shown.

3.2 Exploitable Adsorption mechanisms

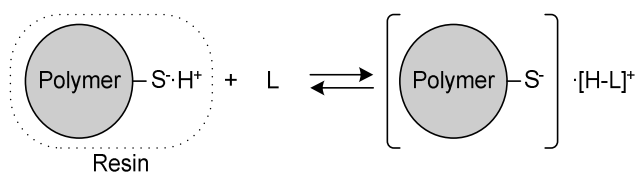
In chapter 2 we already discussed the selection of adsorbents that are capable to reversibly adsorb the transition metal of the homogeneous catalyst. Here we will limit the discussion to the selection of adsorbents that are expected to reversibly adsorb the ligands of the homogeneous catalyst.

3.2.1 Acid/Base interactions

Although many of the used ligands in the homogeneous catalyzed reactions are commonly in a neutral charged state, the ligands that contain atoms of groups IV – nitrogen and phosphorous – and V – sulfur and oxygen – of the periodic table of elements accept hydrogen [Sowa, 1991] via Brønsted acid/base reactions:



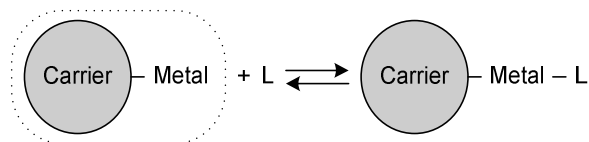
Wherein H⁺ and L respectively represent hydrogen or ligand. Thus, when contacted with – for example – a strong acidic resin, the charged species can now be readily adsorbed by ion exchange. The ligand is then adsorbed to an immobilized anionic group:



As Brønsted acid/base reactions are of the equilibrium type, the adsorption will be reversible so that the ligands can be recovered by inversion of the equilibrium. This is achieved by means of concentration differences between the solid and liquid phases.

3.2.2 σ/π interactions

In the coordination sphere of transition-metal complex, its ligands are always at equilibrium with their free transition-metal [Kettle, 1996]. This equilibrium – σ -bond/ π -backbond – is also expected between the free transition metal – or ligand – and its immobilized counterpart if one of the components is bound to a solid carrier (equation 3.1).



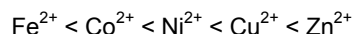
This is demonstrated by the studies on the adsorption of benzene over Ag^+ functionalized adsorbents [Yang, 1995], Olefin/Paraffin separations [Padin, 1999] and desulfurization of fuels [Hernández-Maldonado, 2003] over Cu(I) zeolites show that both solid and immobilized transition metals are able to share electrons with electron rich ligands.

The Hard and Soft Acids and Bases (HSAB) theory [Pearson, 1987] provides empirical rules – based on the classification of Lewis acids – for a first order prediction on the selectivity and stability of the bonds that may be formed between various – transition – metals and ligands (see chapter 2).

The HSAB theory states that a soft base, such as PPh_3 prefers to interact with soft acids – such as Ag^+ – above hard acids – such as Na^+ –. On the other hand we know that PPh_3 interacts with Co^{2+} , indicating that borderline acids might also be of interest. On basis of these considerations we selected Ag^+ (soft acid), Fe^{2+} , Co^{2+} , Ni^{2+} , Cu^{2+} , Zn^{2+} (borderline acid) and Mn^{2+} , Na^+ (hard acids) for functionalization of the ion exchange resins. It is expected that that the capacity of the adsorbents follows the trend:

soft acids (Ag⁺) > borderline acids (Fe²⁺, Co²⁺, Ni²⁺, Cu²⁺, Zn²⁺) > hard acids (Mn²⁺, Na⁺)

Within the borderline acids group the general stability sequence of the metal complexes, indicating the adsorbent capacity to be expected, is given by the ease of replacing a water molecule by other ligand, is given by the Irving-William series [Cotton, 1988; Kettle, 1996]:



3.3 Experimental

3.3.1 Solutions

PPh₃ (99 [%], Sigma-Aldrich) and (PPh₃)₂CoCl (98 [%], Sigma-Aldrich) solution were prepared in a series that contained $2 \pm 1 \cdot 10^{-2}$, $4 \pm 1 \cdot 10^{-2}$, $8 \pm 2 \cdot 10^{-2}$ and $16 \pm 2 \cdot 10^{-2}$ [mM] of PPh₃. For the liquid organic phase, two solvents have been used to determine the effects of polarity on the adsorption of the PPh₃: 1-Butanol (p.a., Sigma-Aldrich) and 1-Octanol (99 [%], Sigma-Aldrich). All solvents were treated with Ar (5.0, Hoekloos) prior to their use to remove oxygen. Preliminary experiments showed that for these two solvents, the adsorbents had a capacity for PPh₃ which was at the same order of magnitude.

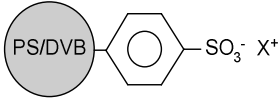
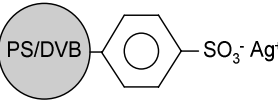
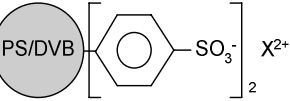
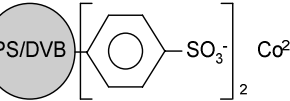
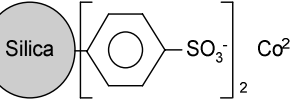
3.3.2 Adsorbent preparation

3.3.2.1 Polystyrene/divinylbenzene carrier

The selected carrier for the metals elements was Amberlyst 15 (4.7 [mmol H/g dry], Sigma-Aldrich). The Amberlyst 15 was firstly washed with de-ionized water (Millipore) in a column. The functionalization of DOWEX 50W-X4 and Amberlyst 15 was done by contacting the resin with 0.1 [mM] aqueous solutions of the selected metals (see table 3.1). During the ion-exchange, the hydrogen of the resins was exchanged for the metal. The exchange was done until maximum loading was reached. All adsorbents were pre-rinsed with de-ionized water. Then, the remaining water was rinsed out of the resin with methanol (p.a., Merck). The remaining methanol was rinsed with 1-butanol (p.a., Merck). The adsorbents thus prepared were taken from the column and used in the adsorption experiments.

The number of adsorption sites (Q) is given in table 3.1. These differ per adsorbent as these depend of the synthesis procedure of the adsorbents.

Table 3.1. Overview of the selected adsorbents

Adsorbent type	Note	Aqueous salt used	Adsorbent	Q [mmol sites/g dry]
Group I element				
H ⁺ loaded Amberlyst 15	Macroreticular Sigma-Aldrich			4.7
Na ⁺ loaded Amberlyst 15	Macroreticular Sigma-Aldrich	1.0 [M] LiOH		4.3
Transition metals				
Ag ⁺ loaded Amberlyst 15	Macroreticular Sigma-Aldrich	1.0 [M] AgNO ₃		3.1
Mn ²⁺ loaded Amberlyst 15	Macroreticular Sigma-Aldrich	1.0 [M] MnCl ₂		4.2
Fe ²⁺ loaded Amberlyst 15	Macroreticular Sigma-Aldrich	1.0 [M] FeCl ₂		4.2
Co ²⁺ loaded Amberlyst 15	Macroreticular Sigma-Aldrich	1.0 [M] CoCl ₂		4.2
Ni ²⁺ loaded Amberlyst 15	Macroreticular Sigma-Aldrich	1.0 [M] NiCl ₂		4.2
Co²⁺ on DOWEX				
Co ²⁺ loaded DOWEX 50W-X4	Gel-Type Sigma-Aldrich	1.0 [M] CoCl ₂		
Co²⁺ on silica				
Co ²⁺ loaded SCX silica	Alltech	1.0 [M] CoCl ₂		

3.3.2.2 Siliceous carrier

Strong acidic silica (SCX) was commercially available from Alltech. The SCX functionalized adsorbents were pre-rinsed with de-ionized water over a filter to remove possible impurities that remained in the resins after its synthesis. Then, the remaining water was rinsed out of the adsorbents with methanol (p.a., Merck). The remaining methanol was rinsed with 1-butanol (p.a., Merck). The siliceous adsorbent thus prepared was taken from the filter and used in the adsorption experiments.

3.3.3 Adsorption and desorption measurements

The adsorption capacities of the various adsorbents were measured via batch adsorption experiments – as described chapter 2 – at 90 [°C] under Argon. The samples of the PPh₃ concentrations after the adsorption and desorption experiments had to be diluted 50 times before being analyzed by a UV method (Cary 300). The amounts adsorbed were calculated from the differences in initial and equilibrium amounts. The loading of the adsorbents after adsorption and desorption are expressed with respect to the number of functional sites in the adsorbents.

3.4 Experimental results

3.4.1 Acid/base interaction

In figure 3.1 the loadings of PPh₃ are shown as a function of the equilibrium concentrations respectively after adsorption and desorption experiments over H⁺ loaded Amberlyst 15 at 90 [°C] from 1-butanol.

Besides a relative large interaction with PPh₃, it is shown that the adsorption is reversible: the desorption results are in line with the adsorption.

3.4.2 σ/π interactions

3.4.2.1 *Soft acid*

Figure 3.2 represent the loadings of PPh₃ as a function of the equilibrium concentrations – respectively, after adsorption and desorption experiments – over Ag⁺ loaded Amberlyst 15 at 90 [°C] from 1-butanol.

The adsorption capacity of the Ag⁺ loaded Amberlyst 15 is relatively high. It can also be seen that this interaction is reversible. In figure 3.2, it is shown that after addition of fresh 1-butanol – over a period of 10 to 12 hours – the concentration of PPh₃ in the liquid phase has increased. This increase is in line with the adsorption isotherm as shown as the solid points in figure 3.2. Thus, a new PPh₃ equilibrium is being set between the adsorbent and the liquid phase, by releasing the adsorbed PPh₃ from the adsorbent.

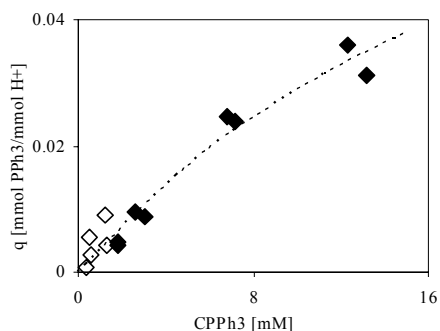


Figure 3.1. PPh₃ adsorption and desorption over H⁺ loaded Amberlyst 15 from 1-butanol at 90 [°C]

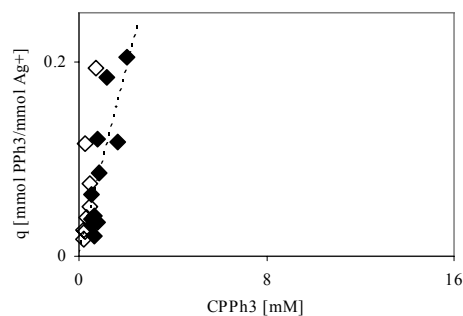


Figure 3.2. PPh₃ adsorption and desorption over Ag⁺ loaded Amberlyst 15 from 1-butanol at 90 [°C]

3.4.2.2 Transition Metals

In figures 3.3 through 3.6, the loadings of PPh₃ over the transition metal – respectively, Mn²⁺, Fe²⁺, Co²⁺ and Ni²⁺ – loaded Amberlyst 15 are shown as a function of the equilibrium PPh₃ concentrations after adsorption or desorption at 90 [°C] from 1-butanol.

The adsorption capacities of PPh₃ onto the transition metal loaded Amberlyst 15 resins indicate that the interactions between the borderline acids – transition metals – and the soft base PPh₃ are relatively weak, when compared to the Ag⁺ loaded Amberlyst 15.

Note that the errors encountered in the desorption experiments are relatively large, due to the fact that the errors that occurred during the adsorption experiments have to be included. Therefore, the results of the desorption experiments cannot be taken quantitatively. Although a small amount of PPh₃ – that was not adsorbed – remained in the pores of the transition metal functionalized adsorbents, the increase in the PPh₃ concentration – not clearly visible on these axes – after the desorption experiments was larger as may be expected from the dilution.

Lets assume that in case of no adsorption 16 [mM] of PPh₃ remained in the pores of the functionalized Amberlyst 15. With a pore porosity of 32 [%] and a total dry mass of approximately 0.13 [g] of adsorbent, a total of 0.05 [ml] remain in the pores. After addition 10 [ml] of fresh 1-butanol the PPh₃ can maximal range up to a concentration of 0.08 [mM] PPh₃. This is a factor 5 lower as the minimal concentration of PPh₃ that has been recovered during the desorption – maximal 0.4 [mM] – as shown in figures 3.3 through 3.6. Concluding in can be stated that the PPh₃ can be recovered by a concentration difference between the liquid and solid phases.

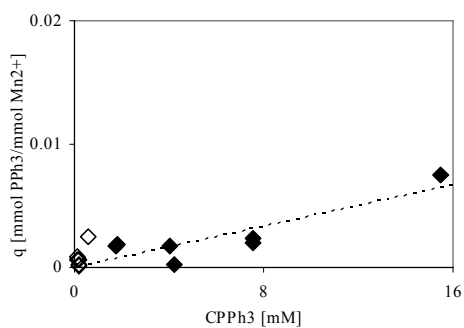


Figure 3.3. PPh₃ adsorption over Mn²⁺ loaded Amberlyst 15 from 1-butanol at 90 [°C]

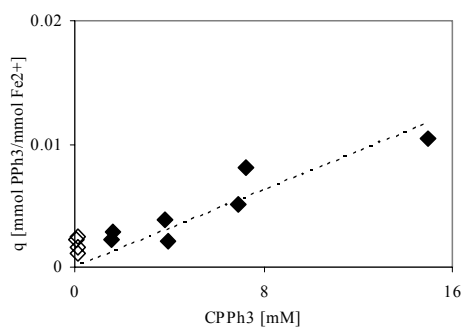


Figure 3.4. PPh₃ adsorption over Fe²⁺ loaded Amberlyst 15 from 1-butanol at 90 [°C]

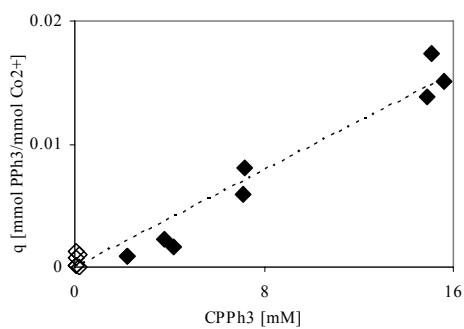


Figure 3.5. PPh₃ adsorption over Co²⁺ loaded Amberlyst 15 from 1-butanol at 90 [°C]

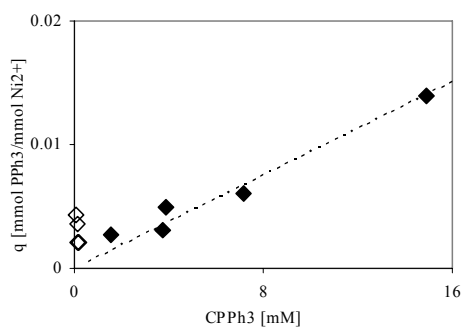


Figure 3.6. PPh₃ adsorption over Ni²⁺ loaded Amberlyst 15 from 1-butanol at 90 [°C]

3.4.2.3 Hard acids

Adsorption experiments of PPh₃ over Na⁺ and Mn⁺ loaded Amberlyst 15 in 1-butanol at 90 [°C] showed no change in concentration of PPh₃. From the adsorption experiments, it became clear that the initial PPh₃ concentrations remained unaltered after contacting with a hard acid such as Na⁺ and Mn⁺.

3.4.3 Influence carrier

Figure 3.7 represent the loadings of PPh₃ as a function of the equilibrium concentrations after adsorption experiments over Co²⁺ loaded silica at 90 [°C] from 1-butanol.

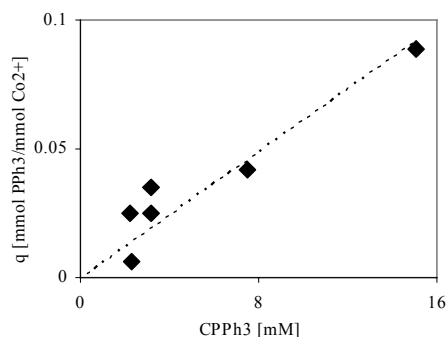


Figure 3.7. PPh₃ adsorption over Co²⁺ loaded silica from 1-butanol at 90 [°C].

These batch desorption experiments are difficult, because a large amount of adsorbent will be lost during decanting – and even filtering – of the liquid phase. Therefore, desorption experiments have been done by testing the release of PPh₃ in a qualitative way. The recovered PPh₃ concentrations were found to be above the concentration that could be expected from dilution alone. Therefore it may be concluded that the adsorption is reversible.

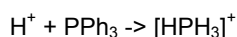
Adsorption experiments of PPh₃ over Co²⁺ loaded DOWEX 50W-X4 in 1-butanol at 90 [°C] showed no change in concentration of PPh₃. From the adsorption experiments, it became clear that the initial PPh₃ concentrations remained unaltered.

3.5 Discussion

3.5.1 Acid/base interactions

The HSAB theory predicts a hard acid, such as H⁺ to have a low preference to a soft base such as PPh₃. The relatively large capacity – compared to the transition metal functionalized Amberlyst 15 – of the H⁺ loaded Amberlyst 15 for the PPh₃ ligand is therefore out of line with the HSAB theory.

In comparison to the borderline acids, it was expected that the transition metals would have a larger preference to interact with a soft base above the H⁺ loaded Amberlyst 15. While the remaining hard acids – such as Na⁺ – have almost no affinity towards the PPh₃ ligand, H⁺ does. A possible mechanism that prefers H⁺ above the other hard acids can then be found in the fact that H⁺ has the ability to protonate the hydroxyl groups of 1-butanol. The free H⁺, then can transfer [Russell, 1988] its positive charge, by accepting electrons from PPh₃ according to:



The positive charged complex can then be adsorbed to the SO₃⁻ according to:

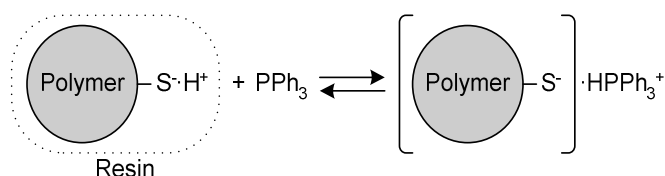


Figure 3.8. Proposed mechanism for PPh₃ adsorption by H⁺ loaded Amberlyst 15.

Where, S and H stand respectively for the anionic counter group of the ion exchange resin and its immobilized acidic hydrogen. The other group I elements have a lower electronegativity and therefore have a lower ability to accept electrons. Therefore, PPh₃ complexes with those group I elements are much more unlikely to be formed.

3.5.2 σ/π interaction

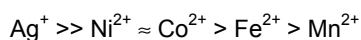
3.5.2.1 *Soft acid*

The adsorption capacity of the Ag⁺ loaded Amberlyst 15 is relatively high. This is caused by a strong interaction between the soft acid Ag⁺ and soft base PPh₃. This has been predicted by the HSAB theory; the soft base PPh₃ easily shares its lone pair electrons with the soft acid Ag⁺.

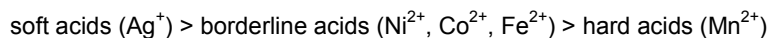
It can also be seen that this interaction is reversible. In figure 3.2, it is shown that after addition of fresh 1-butanol – over a period of 10 to 12 hours – the concentration of PPh₃ in the liquid phase increases. This increase follows the adsorption isotherm as shown as the solid line in figure 3.1. Thus, a new PPh₃ equilibrium is being set between the adsorbent and the liquid phase, by releasing the adsorbed PPh₃ from the adsorbent.

3.5.2.2 *Transition metals*

Within the group of the selected transition metal loaded Amberlyst 15 resins, the trend of adsorption capacities follow the Irving-Williams series: Mn²⁺ < Fe²⁺ < Co²⁺ < Ni²⁺. The trends of the PPh₃ adsorption capacities that have been found and shown in figures 3.2 through 3.6 are:



This is in line with the HSAB theory that states that the stability of bonds formed between soft bases and various acid classes decrease according to:



Besides the effect of electron sharing – which gives the overall trends as observed –, the steric hindrance posed on the PPh₃ ligands during the adsorption also contributes to a large decrease in the adsorption capacity. The immobilized transition metal is located at two SO₃⁻ groups that sterically interact with the bulky aromatic phenyl groups located in the triphenylphosphine. This makes the immobilized transition metal it less attractive for adsorption.

It has been shown in literature [Kettle, 1996; Cotton, 1988] that the complexation stability of transition metals by phosphine ligands largely depend on the steric effects caused by the relative bulky phosphines. In the transition metal loaded Amberlyst 15 resins, the PPh₃ are strongly hindered to adsorb due to the steric environment of the two sulfonic groups connected to one transition metal atom. In the H⁺ loaded Amberlyst 15, the steric hindrance is much smaller as only one SO₃⁻ forms a steric effect.

Concluding it can be stated that the steric effects, imposed by the relative bulky ligands have to be taken into account when selecting adsorbents.

3.5.2.3 Hard acids

From the adsorption experiments, it became clear that the initial PPh₃ concentrations remained unaltered after contacting with Na⁺ loaded Amberlyst 15 in 1-butanol at 90 [°C]. As expected from the HSAB theory, the hard acids – Na⁺ – have only a small preference to interact with the soft base PPh₃. Due to the fact that the initial PPh₃ concentrations remain unaltered when contacted with one of the adsorbents that has been functionalized with one of the hard acids, it may be concluded that no interaction occurs between the hard acids and the soft base PPh₃.

3.5.3 Carrier influence

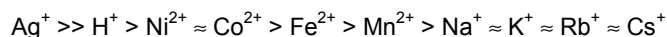
The adsorption capacity of PPh₃ onto Co²⁺ functionalized silica is larger, compared to the polystyrenic counterpart. This effect is caused by the fact that siliceous carriers have better

properties for non-aqueous media due to the polarity of the siliceous matrix. This effect is clearly shown with the increase of capacity.

From the adsorption experiments, it became clear that the initial PPh₃ concentrations remained unaltered after contacting with Co²⁺ loaded DOWEX 50W-X4 in 1-butanol at 90 [°C]. It has been shown for the other adsorbents that Co²⁺ can undergo an interaction with PPh₃. The reason that no adsorption of PPh₃ is observed can be found in the fact that the relative large PPh₃ molecule can not enter the microporous structure of the gel type DOWEX 50W-X4.

3.6 Conclusion

The HSAB theory gives a qualitative predicting on the stability of various hard and soft acids and bases combinations. To test this hypothesis, triphenylphosphine – PPh₃ – has been contacted with various adsorbents that were functionalized with elements of the three – hard, soft and borderline – types of acids. The observed trends in the adsorption capacity was:



This trend is explained by the facts that:

- Soft PPh₃ prefers soft Ag⁺ above the other types of metals
- A sharp decrease in adsorption capacity for the transition metal functionalized due to steric effects of 2 sulfonic groups with the PPh₃ instead of one sulfonic groups as in the Ag⁺ loaded Amberlyst 15.
- The trend for the borderline acids is according to the Irving-Williams series.
- The hard acids – Na⁺ and down – do not show any affinity towards the PPh₃ ligands. These types of metals do not like to share any electrons from the PPh₃ ligands.

From all tested adsorbents, both the H⁺ and Ag⁺ loaded Amberlyst 15 proved to be the most suitable adsorbents in Reverse Flow Adsorption in terms of adsorption capacity and reversibility. Selection of these latter two implies that the catalytic active transition metal center has to be recovered before adsorption of the ligands. The transition metal can – chapter 2 – undergo an ion exchange with the H⁺ or Ag⁺ and become immobilized.

3.7 References

Bhaduri S., et. al., Homogeneous catalysis; mechanisms and industrial applications, Wiley-Interscience, 2000

Cotton F.A., et. al., Advanced inorganic chemistry, Wiley-Interscience, 1988

Hernandez-Maldonado, A.J., Yang, R.T. and Cannella, W., Desulfurization of Commercial Jet Fuel by Adsorption via π -Complexation with Vapor Phase Exchanged (VPIE) Cu(I)-Y Zeolites, Ind. Eng. Chem. Res., 43, 6142, 2004

Kettle S.F.A., Physical inorganic chemistry; a coordination chemistry approach, Spektrum Academic publishers, 1996

Padin, J., Yang, R.T. and Munson, C.L., New Sorbents for Olefin-Paraffin Separations and Olefin Purification for C4 Hydrocarbons, Ind. Eng. Chem. Res., 38, 3614, 1999

Pearson R.G., Benchmark papers in inorganic chemistry: Hard and soft acids and bases, Wiley, 1973

Pearson R.G., Absolute Electronegativity and Hardness: Application to Inorganic Chemistry, Inorg. Chem., 27, 734, 1988

Russell C.B. and Angelici R.J., Phosphine Basicities As Determined by Enthalpies of Protonation, Inorg. Chem. 1988, 27, 681-686

Sowa J.R. and Angelici R.J., Bidentate Phosphine Basicities As Determined by Enthalpies of Protonation, Inorg. Chem., 30, 3534, 1991

Yang, R.T. and Kikkinides, E.S. , New Sorbents for Olefin-Paraffin Separations by Adsorption via π -Complexation, AIChE Journal, 41, 3, 509, 1995

4

Study of Adsorption Kinetics of CoCl_2 and PPh_3 over Macroreticular and Gel Type Adsorbents by a Generalized ZLC method

4.1 Introduction

Adsorbents that reversibly interact with transition metals and/or ligands at a sufficiently high capacity are able to separate and recycle the individual components of a selected homogeneous model catalyst – $(\text{PPh}_3)_2\text{Co(II)Cl}_2$ – from a liquid phase. Recently, we have found [Dunnewijk, 2005] two suitable adsorbents for the recovery of CoCl_2 : macroreticular Amberlyst A21 and the gel type polymerbound triphenylphosphine. For the PPh_3 ligand recovery, macroreticular Ag^+ functionalized Amberlyst 15 can be used [Dunnewijk, 2005].

In practice, the feasibility of the Reverse Flow Adsorption concept is not purely given by the capacity of these adsorbents, but also strongly depends on the complications that occur due to internal and external mass transfer limitations and dispersion effects. These effects cause the concentration fronts in adsorption beds to widen [Sajonz, 1996; Sajonz, 1997; Shalliker, 2003] which in its turn leads to a faster breakthrough out of the adsorption bed. As a consequence, the length of the adsorption bed has to be increased to retain the same amount of homogeneous catalyst when compared to a system where mass transfer resistances and dispersion do not affect the adsorption [Dunnewijk, 2004].

This lower column efficiency emphasizes the importance to identify and quantify the rate determining parameters of the adsorption for an optimal process design. Internal mass transfer can be measured accurately in a set-up, minimizing external mass transfer and dispersion. Dispersion [Westerterp, 1995] and external mass transfer [Perry, 1998] can be quantified for the adsorption beds by exploiting the empirical rules that result from the extensive studies in this area.

A suitable method to measure internal mass transfer rates is the Zero Length Column (ZLC) technique. The ZLC method has been developed by Eic and Ruthven in 1988 [Eic, 1988] for gas-zeolite systems. They measured mass transfer rates over a differential or 'zero length' bed of porous particles which was first saturated with the sorbate. Desorption is started by switching to a pure carrier gas passing the ZLC. Due to the shallow dimensions of the ZLC –

to minimize the effect of dispersion – only a small pressure drop will be present over the column. Therefore, relatively high flow rates can be applied to minimize the effects external mass transfer limitations. By monitoring desorption of the sorbate over time, one can derive the mass transfer coefficients that affect the adsorption rates.

Since its first appearance, the ZLC technique has been used to investigate the diffusivity in a large number of zeolite-gas systems [for example: Silva, 1997; Cavalcante, 1995; Hufton, 1993; Shavit, 1992; Voogd, 1991]. Ruthven and Stapleton [Ruthven, 1993] were the first to investigate liquid systems with this technique. Not only diffusion in zeolite liquid systems [Brandani, 1995] have been studied, the use the ZLC method was also extended to ion diffusion in gel-type – in structure similar to polymerbound PPh_3 – ion-exchange system [Valverde, 2004; Rodriguez, 1998].

The rate of adsorption in bi-dispersed adsorbents – such as the macroreticular Amberlyst A21 and Ag^+ functionalized Amberlyst 15 – was first modeled by Ruckenstein in 1971 [Ruckenstein, 1971]. Ruckenstein derived an analytical solution for the infinite bath case for a step change in sorbate concentration. This solution was later extended for the finite bath case by Lee [Lee, 1978] and in 1996 adapted for its use in the ZLC method by Brandary and Silva [Brandani, 1996; Silva, 1996]. Due to the complexity to derive the analytical solution, they had to make the following assumptions: no external mass-transfer limitations, holdup due to adsorption in the macropores is neglected [Silva, 1996], linear adsorption isotherms [Brandani, 1998], the ZLC cell is equivalent to a continuous stirred tank adsorber [Ruthven, 1993] and a smart data reduction is used to limit computation time [Loos, 2000].

In this chapter, we propose an alternative approach to the ZLC method by exploiting the practical advantages of the ZLC method in combination with the advantages of a more generalized dynamic model over the column. The resulting set of partial differential equations is then to be solved by a standard modeling, simulation and optimization tool such as g-PROMS.

Analog to the ZLC method, we use a thin layer of adsorbent. At sufficiently high liquid flow rates, axial dispersion and external mass transfer effects can be neglected and only internal mass transfer effects influence the uptake rate of the sorbate. The adsorption kinetics is modeled by a mathematical model for a both mono- and bi-dispersed particles. In this model, adsorption of the sorbate onto the walls will be incorporated into the mass balance over the macropores. The adsorption isotherms may or may not be taken linear. Contrary to the general ZLC method, the concentration profile of the sorbate over the thin layer of adsorbent is accounted for by extending the mass balance over the ZLC cell to a plug flow model over a packed bed.

In this chapter, the diffusivity of CoCl_2 into macroreticular Amberlyst A21 and gel-type polymerbound PPh_3 and of PPh_3 in macroreticular Ag^+ functionalized Amberlyst 15 will be determined. By fitting the theoretical model to the experimental data at sufficient high flow rates, the diffusion coefficients of metal and ligand are determined.

4.2 Theory

4.2.1 Geometry

For practical reasons, mentioned in the introduction, the adsorption kinetics of the individual compounds of a transition metal complex have been determined over a thin layer of adsorbent particles.

The adsorbent particles are contacted with a solution of the sorbate at a sufficiently high flow rate. In this special case, the adsorption rate of the sorbate is completely controlled by the internal mass transfer rate. For the shallow dimensions of the adsorption bed, we can neglect the effects of

axial dispersion and due to the high flow rates the dimensions of the stagnant liquid layer around the adsorbent particles becomes sufficiently small to neglect its effect on the adsorption kinetics. However, the axial concentration gradient, likely to be very small, will be taken into account.

The matrices of the adsorbents, as used in this research, are composed of polystyrene – crosslinked by divinylbenzene – and have a gel or macroreticular structure (figure 4.2). To enhance their adsorption capacity, these materials have been functionalized with active groups as will be discussed in the experimental section.

The *gel* type resins – right hand side in figure 4.2 – are made up of a very loose structure of long polystyrene chains – crosslinked by divinylbenzene – that form particles [Corain, 2001] of sizes $R_p = 0.024$ [mm]. The morphology of these types of particles is often described as being of a continuous phase in which the functional groups are homogeneously distributed. The time depended uptake of a sorbate in the continuous phase can thus be given in terms of an overall diffusivity constant – D_i [cm^2/s] – which describes the internal mass transfer rate.

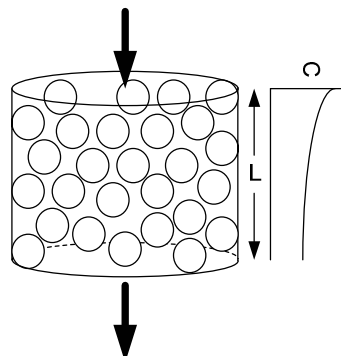


Figure 4.1. A liquid flow contacted with a layer of adsorbent.

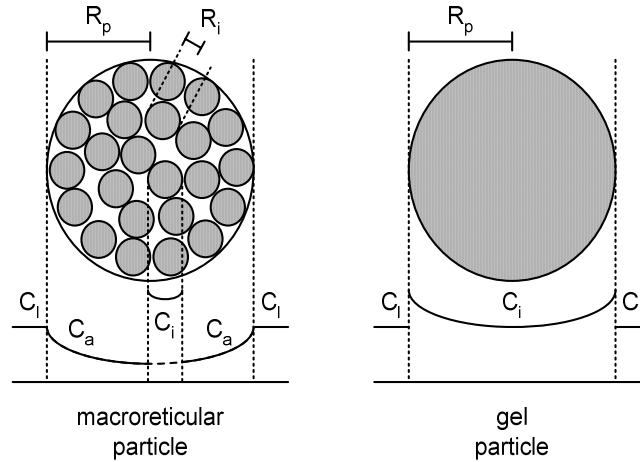


Figure 4.2. Schematic representation of the structures, boundary conditions between the various phases and resulting concentration profiles in macroreticular [Ruckenstein, 1971] or gel [Corain, 2001] particles.

The *macroreticular* particles of size $R_p \approx 0.25$ [mm] – left hand side in figure 4.2 –, are composed of smaller – R_i [m] – gel type microparticles [Ruckenstein, 1971; Corain, 2001] that are crosslinked into a larger network that forms the macroporous matrix. The internal mass transfer rates of the sorbate inside the macroreticular particles, is given by two processes that occur in series; macropore and micropore diffusion. While the transport of the sorbate inside the macroporous structure – around the microparticles – can be given in terms of an overall macropore diffusivity – D_a [cm^2/s] –, the uptake of the sorbate by the microparticles is, similarly to the gel type particles, characterized with an overall micropore diffusivity of D_i [cm^2/s].

4.2.2 Kinetic model for *macroreticular* adsorbent

Mass balance over the adsorbent layer

In contrast to the standard ZLC model [Rodríguez, 1984], we account for the sorbate accumulation in the interparticle void fraction by writing the mass balance over the column as a plug flow model for packed beds. Neglecting the influence of axial dispersion and external mass transport in the liquid phase and assuming that Fick's 2nd law for diffusion is valid for diffusion into the macroreticular matrix, the mass balance reads:

$$\varepsilon_b \frac{\partial C_l}{\partial t} = -u \varepsilon_b \frac{\partial C_l}{\partial z} - \delta_b D_a \frac{\partial C_a}{\partial r_p} \Big|_{r_p=R_p} \quad (4.1)$$

The term on the left hand side in equation 4.1 gives the accumulation of the sorbate in the liquid between the adsorbent particles, the first term on the right hand side represents the convective flow and the remaining term describes the flux of sorbate that is transferred into the adsorbent particles.

Mass balance over the macroreticular particle

In the ZLC method, accumulation of sorbate on the internal macropore surface area is usually neglected [Silva, 1996]. This assumption may not be applicable in adsorption from liquids. Following Ruckenstein's considerations on bi-dispersed adsorbents [Ruckenstein, 1971], accumulation by the adsorbed amount onto the macropore walls is accounted for. In all our kinetic experiments, the maximal contribution of the accumulation in the macropore liquid appeared to be less than 2 [%] of the total take-up; therefore, we neglected the term $\frac{\partial C_a}{\partial t}$. Assuming that Fick's 2nd law for diffusion is valid for both micro- and macropore diffusion, the concentration profile over the radial distance in the macroreticular particle is given by:

$$\delta_a \frac{\partial C_{sa}}{\partial t} = \frac{\varepsilon_a D_a}{r_p^2} \frac{\partial}{\partial r_p} \left(r_p^2 \frac{\partial C_a}{\partial r_p} \right) - \delta_a D_i \frac{\partial C_i}{\partial r_i} \Big|_{r_i=R_i} \quad (4.2)$$

In equation 4.2, the first and second terms on the left hand side, respectively describe the accumulation in the macropore volume and on the macropore surface. The first term on the right hand side represents the diffusional flux in the macropores and the remaining term represents the transfer of the sorbate from the macropores into the microparticles.

Mass balance over the microparticles

The sorbate that entered the sphere of the microparticles is considered to be adsorbed in a continuous state. The concentration profile inside the gel type microparticles is given by [Ruthven, 1993]:

$$\frac{\partial C_i}{\partial t} = \frac{D_i}{r_i^2} \frac{\partial}{\partial r_i} \left(r_i^2 \frac{\partial C_i}{\partial r_i} \right) \quad (4.3)$$

Note that the mass balances over a gel type particle will be given by equations 4.1 and 4.3 only, as the macroporous structure is absent in this type of adsorbent.

Parameter estimation for macroreticular particles

Equations 4.1 through 4.3 describe the adsorption of a sorbate into a bi-dispersed adsorbent. We introduce two reciprocal time constants to respectively characterize the macro- and micro diffusivities:

$$\alpha = \frac{D_a}{R_p^2} \quad (4.4) \quad \beta = \frac{D_i}{R_i^2} \quad (4.5)$$

Also, we introduce the respective dimensionless variables for the radial distances inside the macro- and microparticles:

$$\gamma = \frac{r_p}{R_p} \quad (4.6) \quad \eta = \frac{r_i}{R_i} \quad (4.7)$$

Substitution of α , β , γ and η into equations 4.1 to 4.3, gives the mass balances of the sorbate in terms of α and β at linear isotherm conditions:

$$\frac{\partial C_b}{\partial t} = u \frac{\partial C_b}{\partial z} - \frac{3(1-\varepsilon_b)}{\varepsilon_b} \alpha \frac{\partial C_a}{\partial \gamma} \Big|_{\gamma=1} \quad (4.8)$$

$$\frac{\delta_a K_a}{\varepsilon_a} \frac{\partial f(C_a)}{\partial t} = \alpha \frac{1}{\gamma^2} \frac{\partial}{\partial \gamma} \left(\gamma^2 \frac{\partial C_a}{\partial \gamma} \right) - \frac{3(1-\varepsilon_a)}{\varepsilon_a} \beta \frac{\partial C_i}{\partial \eta} \Big|_{\eta=1} \quad (4.9)$$

$$\frac{\partial C_i}{\partial t} = \beta \frac{1}{\eta^2} \frac{\partial}{\partial \eta} \left(\eta^2 \frac{\partial C_i}{\partial \eta} \right) \quad (4.10)$$

If, at $t = 0$ [s], the adsorbent is equilibrated with lean solvent, the initial conditions are given by:

$$C_b(0, z) = 0$$

$$C_a(0, z, \gamma) = 0$$

$$C_i(0, z, \gamma, \eta) = 0$$

From $t = 0$ [s], a change in sorbate concentration is applied in the feed of the adsorbent layer and boundary conditions (see figure 4.2) are given by:

$$C_b(t, 0) = C_{feed}$$

$$C_a(t, z, 1) = C_b(t, z)$$

$$C_i(t, z, \gamma, 1) = K_i f(C_a(t, z, \gamma))$$

$$\frac{\partial C_a}{\partial \gamma}(t, z, 0) = 0$$

$$\frac{\partial C_i}{\partial \eta}(t, z, \gamma, 0) = 0$$

The adsorption isotherms, $K_a f(C_a)$ and $K_i f(C_a)$ are expressed in the experimental adsorption isotherm – $K_{exp} f(C_a)$ – as presented in chapters 2 and 3. If we assume that the adsorption isotherms are of a same shape, then:

$$K_{exp} f(C) = \delta_a K_a f(C) + (1 - \varepsilon_a) K_i f(C) \quad (4.11)$$

The functional groups inside the macroreticular adsorbents are homogeneously distributed inside the microparticles but are also immobilized onto the walls of the macropores.

Assuming a constant ratio $\theta = \frac{n_{sa}}{n_{sa} + n_i}$ of amounts adsorbed at the macropore walls and

inside the microparticles [Ruckenstein, 1971], K_a and K_i can be expressed in K_{exp} as:

$$\delta_a K_a = \theta K_{exp} \quad (4.12)$$

$$K_i = (1 - \theta)(1 - \varepsilon_a) K_{exp} \quad (4.13)$$

Fitting procedure

The mathematical model of the bi-dispersed particles has been implemented in a g-PROMS model of the complete experimental set-up. By varying the values for α , β and θ , the simulation of the sorbate concentration in the liquid phase have been fitted to the experimental data. The values of the two diffusion constants – D_a and D_i – can then be estimated from α and β by using the dimensions of the macro and microparticles as they are given in literature [Ruckenstein, 1971; Doğu, 2003].

4.2.3 Kinetic model for *gel type* adsorbent

In case of an adsorption bed that is filled with a gel type resin, equation 4.1 has to be rewritten according to the morphology of the adsorbent (figure 4.2). In the gel particles, the macropore structure is not present and should be omitted in the set of equations. The diffusion coefficient and the sorbate concentration inside the gel-type particle are then replaced by $D_i = D_a$ and $C_i = C_a$ in equation 4.1.

The set of equations 4.15 through 4.17 simplifies when the adsorption bed is filled with a gel type resin. In this case, the macropore structure is not present in the set of equations. The total flux from the liquid bulk phase is now given by the flux through the gel type – read microparticle – surface. The set of equations now read:

$$\frac{\partial C_b}{\partial t} = u \frac{\partial C_b}{\partial z} - \frac{3(1 - \varepsilon_b)}{\varepsilon_b} \beta \frac{\partial C_i}{\partial \eta} \Big|_{\gamma=1} \quad (4.14)$$

$$\frac{\partial C_i}{\partial t} = \beta \frac{1}{\eta^2} \frac{\partial}{\partial \eta} \left(\gamma^2 \frac{\partial C_i}{\partial \eta} \right) \quad (4.15)$$

With initial and boundary conditions:

$$\begin{aligned} C_b(0, z) &= 0 & C_i(0, z, \eta) &= 0 \\ C_b(t, 0) &= C_{feed} & C_i(t, z, 1) &= K_i f(C_b(t, z)) \\ & & \frac{\partial C_i}{\partial \eta}(t, z, 0) &= 0 \end{aligned}$$

Fitting procedure

The determination of the adsorption parameter β for the gel type particles has been done by fitting the theoretical sorbate concentration to the experimental data over the respective adsorbent particles. Hereby, $K_i f(C_b) = K_{exp} f(C_b)$ takes the form of the Langmuir isotherm as mentioned in chapter 2.

4.3 Experimental

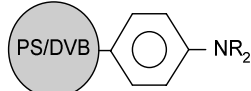
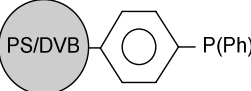
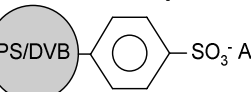
4.3.1 Solutions

CoCl₂ (anhydrous, Fluka) solutions of $0.5 \pm 2 \cdot 10^{-3}$ [mM] in a organic liquid phase were prepared with 1-butanol (p.a., Merck). PPh₃ (99 [%], Sigma-Aldrich) solutions were prepared, containing $0.5 \pm 1 \cdot 10^{-2}$ [mM] of PPh₃. For the liquid organic phase, 1-Butanol (p.a., Sigma-Aldrich) had been selected. The solvents for the PPh₃ solutions were treated with Ar (5.0, Hoekloos) prior to their use to remove oxygen.

4.3.2 Adsorbents

The adsorbents used in this research on their adsorption kinetics are shown in table 4.1. These adsorbents are proven in chapters 2 and 3 to have a high capacity respectively for CoCl₂ or PPh₃.

Table 4.1. Overview of adsorbents used in this research.

Adsorbent type	Structure	Notes
CoCl₂ adsorption		
Amberlyst A21		Macroreticular with $\epsilon_a = 48$ [%] * $R_p = 0.30$ [mm]
Polymer bound PPh ₃		Gel $R_p = 0.024$ [mm] *
PPh₃ adsorption		
Ag ⁺ loaded Amberlyst 15		Macroreticular with $\epsilon_a = 36$ [%] * $R_p = 0.25$ [mm] *

* as given by the manufacturer (Sigma-Aldrich).

Nitrogen functionalized Amberlyst A21 (which needed to be rinsed with dionized water, methanol (p.a., Merck) and 1-butanol (p.a., Merck)) and a phosphor functionalized polymerbound PPh₃ resin (rinsed with methanol and 1-butanol) were commercially available as mentioned in chapter 2. Ag⁺ functionalization of the Amberlyst 15 was done as described in chapter 3. The adsorbent materials thus prepared were used in the adsorption experiments.

4.3.3 Experimental set-up

The experimental set-up that was used to determine the adsorption kinetics of CoCl_2 and PPh_3 over the various adsorbents is shown in figure 4.3.

The complete set-up as shown in figure 4.3 consisted of (in order of flow contact with the pumped liquid phase):

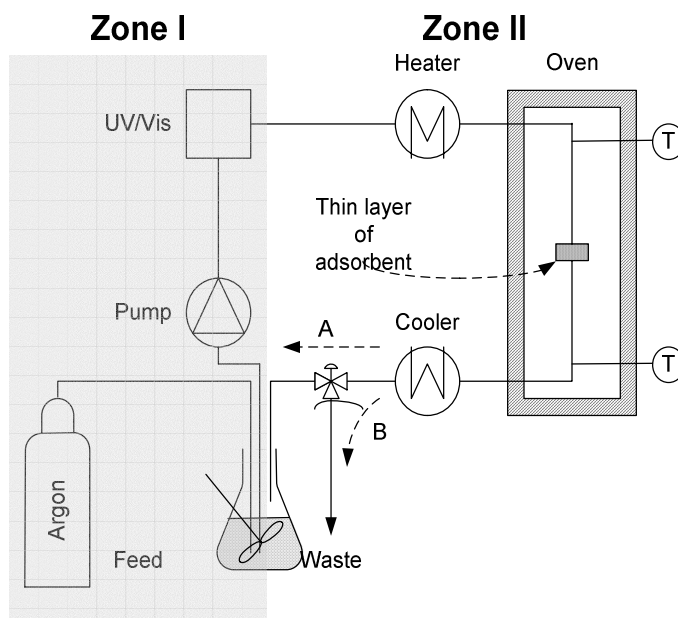


Figure 4.3. Schematic representation of the set-up for the adsorption kinetics measurement (A for recycle mode and B for non-recycle mode).

Glass vessel

As a container of the feed to the set-up, two vessel sizes have been used for the adsorption experiments. For the adsorption kinetic experiments over Amberlyst A21, 25 [ml] of CoCl_2 was placed in a 50 [ml] glass vessel. For the other experiments, 50 [ml] of the respective solution was placed inside a 100 [ml] vessel.

The vessel was placed on top of a magnetic stirrer to enhance the mixing of the recycled liquid flow from the set-up. Optionally, Argon was bubbled through the liquid to avoid the presence of oxygen when experiments with PPh_3 were conducted.

Piston pump and a UV/Vis detector

The pump (Knauer K-1001) was used to deliver the solution from the feed vessel to the set-up with flow rates from 0.01 to 50 [ml/min]. The UV/Vis detector (Knauer K-2600) was equipped with a flow cell for preparative purposes for the high flow rates.

Heater

In this winded heat exchanger, the piping was led through a hot medium, increasing the temperature of the solvent from ambient temperature to 90 [°C]. This option had to be included, as the pump and UV/Vis detector were advised not to be operated at elevated temperatures above 70 [°C].

Adsorbent

A thin layer of one of the selected adsorbents was placed in a column with adjustable end pieces. The layer thickness was chosen to be maximal 2 [mm]. The column was placed inside an oven to maintain a constant temperature of 90 [°C].

Temperature measurement

The temperatures of the liquid phase entering and leaving the column were measured by two thermocouples that were mounted inside the piping of the set-up at both sides of the column. The thermocouples were inserted into the piping by clamping them – with use of a Teflon tubing – into a metal t-piece as shown in figure 4.4.

Cooler

A second winded heat exchanger was placed after the column to cool the liquid phase. Herein, the liquid phase was cooled down to ambient temperature with cooling water.

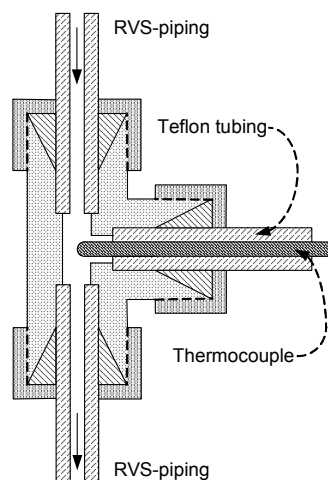


Figure 4.4. T-piece used for fastening thermocouple.

As shown in figure 4.3, the set-up could be operated in a recycle mode or non-recycle mode.

For cleaning purposes and calibration of the cold zone – that is from the feed to UV/Vis detector –, the system was put in non-recycle mode (flow B in figure 4.3). In this mode, the liquid flow was directed through the set-up and directed towards a waste vessel.

For experimental, cleaning and temperature equilibrating purposes and calibration of the complete set-up, the system was operated in a recycle mode (flow A in figure 4.3). Here, the liquid flow was directed back into the feed vessel.

4.3.4 Calibration of the set-up

In this research, the determination of the diffusion coefficients is done by fitting a mathematical model to the results derived from the adsorption experiments that have been conducted in the set-up as described above. The mathematical model thus, should not only be able to describe the adsorption of the sorbate, but also the behavior of the sorbate concentration in the set-up without adsorbent. In order to determine the volumes and mixing behavior of the set-up, various calibration experiments have been performed in the set-up without adsorbent.

First, the set-up was equilibrated with lean solvent in the non-recycling mode (flow B in figure 4.3). The contents of the feed vessel – that originally contained the lean solvent – were then replaced with a 0.5 [mM] CoCl_2 or 0.5 [mM] PPh_3 solution. The UV/Vis detector detected an increase in the sorbate concentration – passing the UV/Vis detector – due to a step change in the feed as shown as the solid line – as an example for 30 [ml/min] – in figure 4.5.

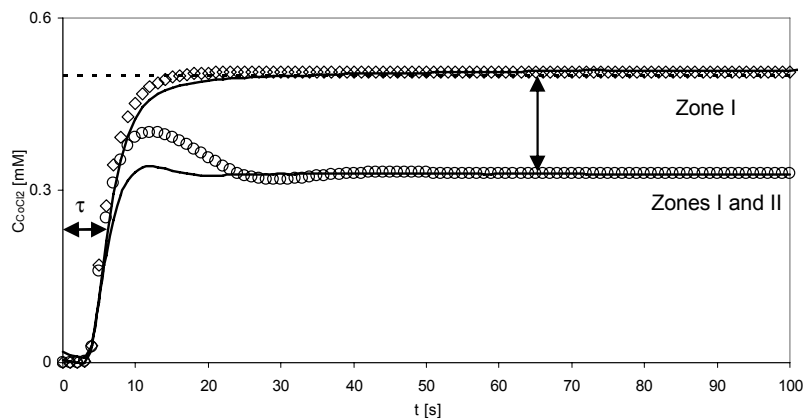


Figure 4.5. Experimental (solid lines) and simulated (\diamond) non-recycle and (\circ) recycled breakthrough concentration profiles at a flow rate of 30 [ml/min].

The volume of the total set-up can then be estimated in the recycle mode (flow A in figure 4.3) after equilibrating the set-up with lean solvent (which was done in the non-recycle mode). The contents of the feed vessel are replaced by a solution of 0.5 [mM] CoCl_2 or 0.5 [mM] PPh_3 , and the liquid phase was directed through the set-up. The resulting concentration of the sorbate passing the UV/Vis detector is shown as the solid line in figure 4.5.

The behavior of the sorbate concentration in zone I can be calibrated from the experimental breakthrough curve without recycle. In figure 4.5, one can recognize a time-lag due to the distance from the feed vessel to the UV/Vis detector. To reckon with the observed time-lag in zone I, the combination of the pump, tubing and detector has been modeled by assuming tubular plug flow. The volume of the time-delay is found to be 1.97 ± 0.06 [ml].

Secondly, it can be seen that mixing with the original lean solvent in the set-up occurs as the breakthrough of the concentration front has widened. The mixing behavior in zone I has been modeled with a Continuous Stirred Cell. The CSC volume was found to be 2.74 ± 0.21 [ml].

Thus, in the simulation of zone I – diamonds in figure 4.5 –, the plug flow relation reckons with the time-lag (τ) and the relation for the stirred cell gives the mixing behavior in zone I as observed from the experimental calibration data.

In the recycled mode, the stationary concentration is lower as observed in the no-recycle mode because of the dilution with the solvent that is initially present in zones I and II. The difference of both stationary concentrations gives the volume of the total set-up. The volume of the zone II is then easily calculated by subtracting the volume of zone I from the total set-up volume.

The whole of zone II – that is from the UV/Vis detector to the exit of the set-up – is symmetrical. Thus, the volumes of the piping before and after the adsorption column may be taken half. The volumes of the two parts of zone II were found to be 3.31 ± 0.32 [ml] individually.

4.3.5 Adsorption experiments

Prior to the adsorption experiments, the set-up – including the adsorbent (0.1 [ml]) – was equilibrated with lean solvent in the non-recycle mode. Then the set-up was switched to the recycle mode and the feed of the set-up (50 [ml] for Amberlyst A21 and 20 [ml] for the remaining adsorbents) was replaced by a fixed concentration (0.5 [mM]) of the selected compound. Inside the adsorption bed, the selected compound – to be adsorbed – diffused towards and into the solid phase. The concentration that left the adsorption bed was lowered

due to the amount that was adsorbed by the adsorbent. The concentration profile over time was recorded by the UV/Vis detector and registered by a computer. From the decrease of concentration, the fluxes could be determined and the various parameters could be estimated by fitting the model to the measurement data.

4.4 Experimental Results

4.4.1 Adsorption of CoCl_2 over macroreticular resins

The concentration profiles of CoCl_2 that passed the UV-detector over time are shown in figure 4.6. The concentration plots are given for various – 5, 10, 20, 30, 40 and 49 [ml/min] – flow rates.

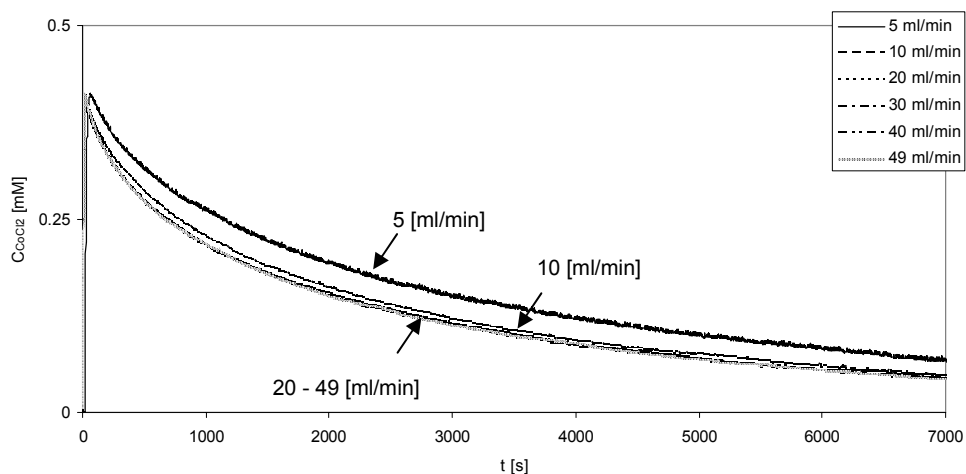


Figure 4.6. CoCl_2 concentration over time during adsorption experiments over Amberlyst A21.

It can be clearly observed from figure 4.6, that the CoCl_2 concentration decreases – due to the fact that it is retained by the Amberlyst A21 – over time for all flow rates. Increasing the flow rate from 5 to 10 [ml/min], leads to an enhanced uptake of CoCl_2 . This is due to the decrease – as mentioned in paragraph 4.2 – of the stagnant layer around the adsorbent particles.

By increasing the flow rates from 20 to 49 [ml/min], no enhancement of the uptake rate is observed. The decrease of the stagnant layer thickness does not effect the mass transfer above the flow rates. Thus, the external mass transfer limitation may be neglected for flow rates above 20 [ml/min].

The experimental data for the higher flow rates – 30, 40 and 49 ml/min – have been used to determine the adsorption rate parameters. As may be concluded from chapter 2, the adsorption isotherm has been taken linear and the respective adsorption constants – K_a and K_i – are given by equations 4.15 and 4.16.

The resulting values for α , β and θ are summarized in the table 4.2. To ensure that external mass transfer limitations may be neglected, the presented results are given as the average of the fits at the highest three measured flow rates of 30, 40 and 49 [ml/min].

Table 4.2. Overview of the calculated kinetic parameters and functional group distributions of CoCl_2 over Amberlyst A21 at flow rates of 30, 40 and 49 [ml/min].

Flow rate [ml/min]	$\alpha = \frac{D_a}{R_p^2}$ [1/s]	$\beta = \frac{D_i}{R_i^2}$ [1/s]	$\theta = \frac{n_{sa}}{n_{sa} + n_i}$ [-]
30	$1.40 \cdot 10^{-3}$	$8.61 \cdot 10^{-6}$	0.03
40	$1.35 \cdot 10^{-3}$	$7.66 \cdot 10^{-6}$	0.04
49	$1.40 \cdot 10^{-3}$	$8.39 \cdot 10^{-6}$	0.03
Average	$1.38 \cdot 10^{-3}$ $\pm 0.03 \cdot 10^{-3}$	$8.22 \cdot 10^{-6}$ $\pm 0.50 \cdot 10^{-6}$	0.03 ± 0.005

As an example of the fitted adsorption rate parameters, in figure 4.7 a comparison is made between the measurement – solid line – and the calculated Co(II) concentration – from the average adsorption rate parameters – in the liquid phase over time. The equilibrium concentration at infinite time is represented by the dotted line.

The simulation is in agreement with the experimental data. Thus, it may be concluded that the CoCl_2 adsorption over Amberlyst A21 can be described by the bi-dispersed model. The results of this simulation, showed that beyond 500 [s], the CoCl_2 concentration profile over the adsorbent layer is constant. All macroreticular Amberlyst A21 particles are thus contacted with a same liquid phase concentration C_i .

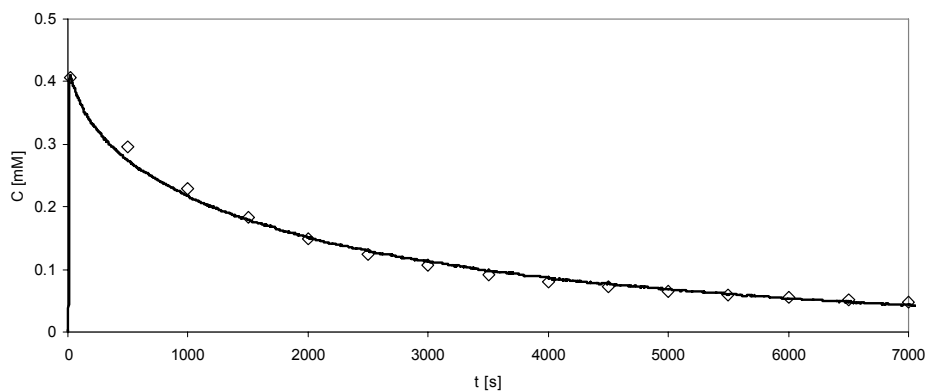


Figure 4.7. experimental (solid line) and predicted (\diamond) CoCl_2 concentrations – at 40 [ml/min] – over Amberlyst A21 in time.

In figure 4.8, the CoCl_2 concentration profiles in the macropores (top) and the microparticles – in the center of the macroreticular particles (left bottom) and at the surface (right bottom) – are shown for times 500, 5,000 and 50,000 [s].

It can be recognized from figure 4.8 (next page), that the CoCl_2 concentration front moves into ($r_a/R_a=0$ is the center of the adsorbent particle) the macropores of the macroreticular adsorbent. The concentration level increases from 0 to 500 [s], due to the increasing bulk concentration. At 5000 [s], the interfacial concentration level is lower as that compared to 500 [s] as the bulk concentration decreases over time.

Analog to the macropore diffusivity, one can recognize the diffusion of CoCl_2 towards the center of the microparticles. This is a slow process – in comparison to the macropore diffusion – as can be noticed in the slow propagation of CoCl_2 into the microparticle structure. The rate of CoCl_2 diffusion into the microparticles at the surface of the macroreticular Amberlyst A21 is faster, compared to the microparticles at the center. Over time, the microparticles at the center of the macroreticular particles are contacted with a lower CoCl_2 , leading to a lower driving force for mass transfer.

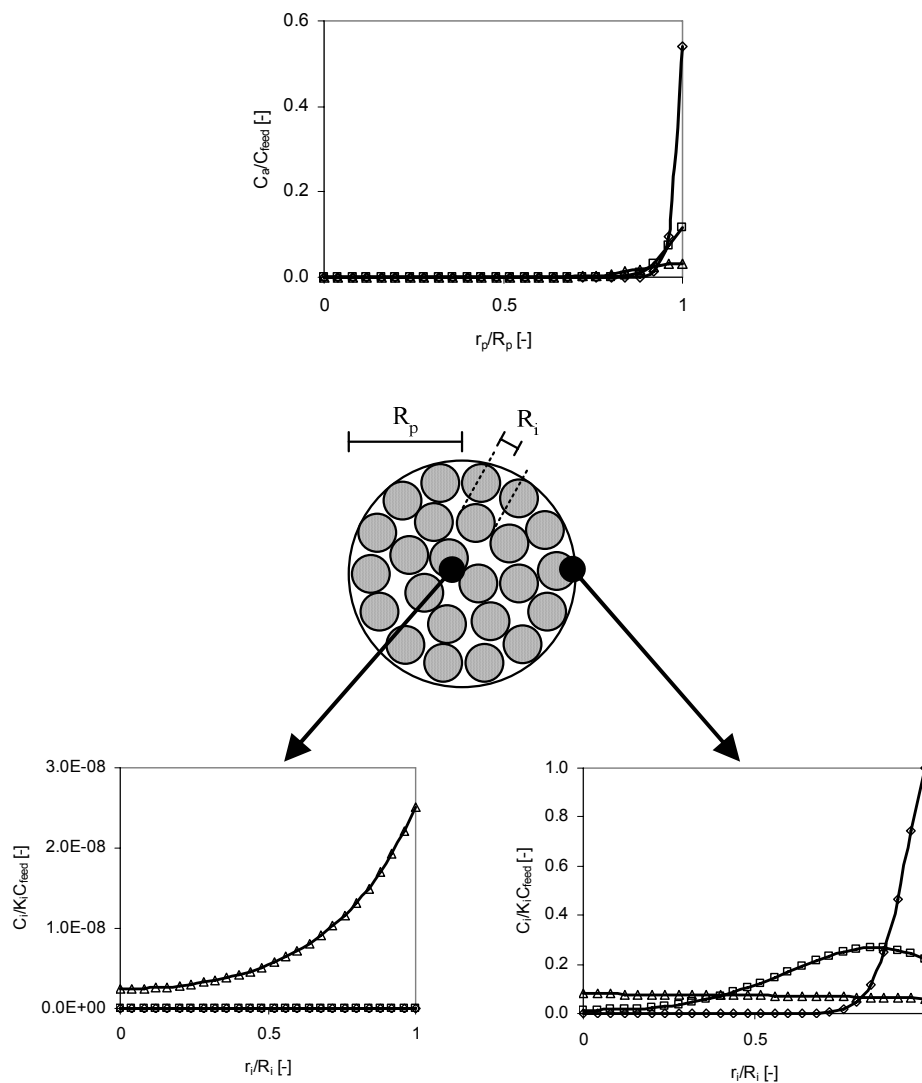


Figure 4.8. CoCl_2 concentration profiles – at 40 [ml/min] – in macropores (top figure), microparticles at the surface of the macroreticular particle (right bottom) and center microparticles (left bottom) of Amberlyst A21. Profiles shown for 500, 5,000 and 50,000 [s] at a flow rate of 40 [ml/min].

4.4.2 Adsorption of PPh_3 over macroreticular resins

Figure 4.9 gives the PPh_3 concentration curves over time during the adsorption experiments over Ag^+ functionalized Amberlyst 15. The resulting curves are given in figure 4.9 for flow rates of 5, 10, 20, 30, 40 and 49 [ml/min].

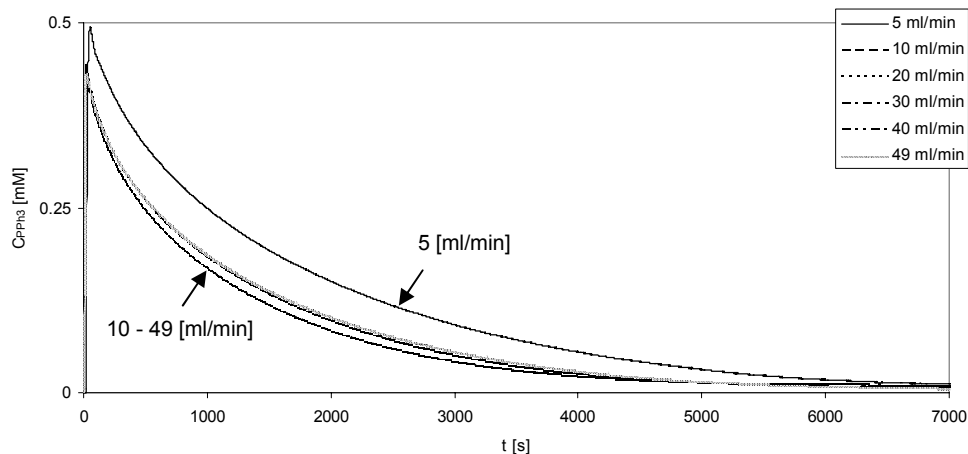


Figure 4.9. PPh_3 concentration over time during adsorption experiments over Ag^+ functionalized Amberlyst 15.

The effect of the decreasing viscous liquid layer with increasing flow rates is again clearly reflected, as the curves start to overlap just above a flow rate of 10 [ml/min]. This gives a sound base to neglect the external mass transfer limitation at flow rates above 10 [ml/min].

The resulting values for α are summarized in the table 4.3. Preliminary calculations on the adsorption results over Ag^+ functionalized Amberlyst 15 showed that for the adsorption of PPh_3 all adsorption sites inside the microparticles did not participate in the adsorption ($\theta=1.00$ [-]).

Table 4.3. Overview of the calculated kinetic parameters and functional group distributions of PPh_3 over Ag^+ functionalized Amberlyst 15 at flow rates of 30, 40 and 49 [ml/min].

Flow rate [ml/min]	$\alpha = \frac{D_a}{R_p^2}$ [1/s]	$\beta = \frac{D_i}{R_i^2}$ [1/s]	$\theta = \frac{n_{sa}}{n_{sa} + n_i}$ [-]
30	$0.78 \cdot 10^{-3}$		
40	$0.80 \cdot 10^{-3}$	micropores are not accessible for PPh_3	
49	$0.80 \cdot 10^{-3}$		
Average	$0.79 \cdot 10^{-3}$ $\pm 0.01 \cdot 10^{-3}$	0	1

As an example of the fitted values, in figure 4.10 a comparison is made between the measurement – solid line – and the calculated PPh_3 concentration – from the average values (table 4.3) – in the liquid phase over time.

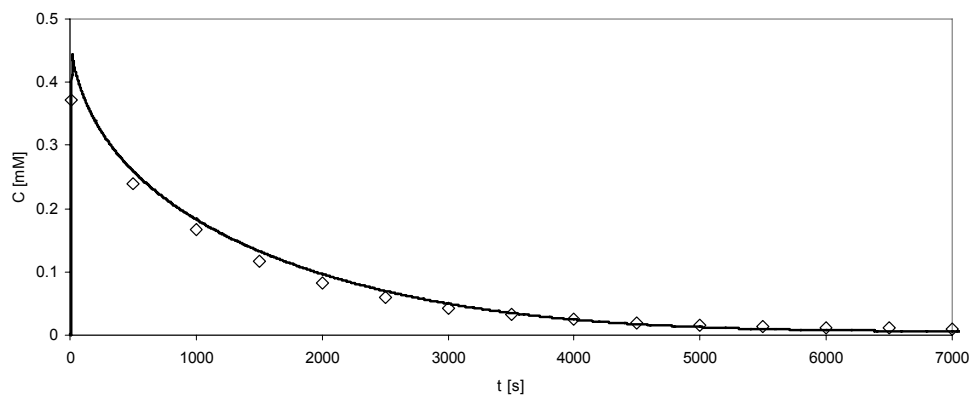


Figure 4.10. experimental (solid line) and predicted PPh_3 concentrations using (□) exponential and (○) Freundlich isotherm – at 40 [ml/min] – over Ag^+ functionalized Amberlyst 15 in time.

At the low PPh_3 concentrations in figures 4.9 and 4.10, the accuracy of the adsorption isotherm measurements as presented in chapter 3, was insufficient to determine K_{exp} . If we use a Freundlich type isotherm – initial slope zero –, figure 4.10 it can be concluded that the model and experiments agree very well. In figure 4.11, the concentration profiles of PPh_3 adsorbed on the macropore walls are shown for 500, 5,000 and 50,000 [s].

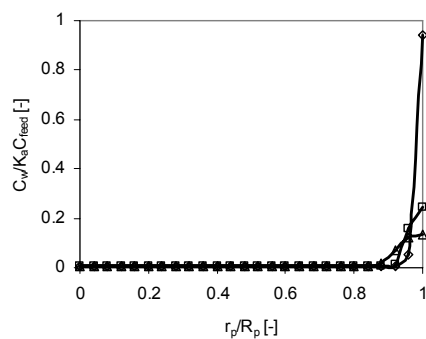


Figure 4.11. concentration profiles of PPh_3 adsorbed on the macropore walls in macroreticular Ag^+ loaded Amberlyst 15 – 40 [ml/min] – at times 500, 5,000 and 50,000 [s].

Due to the large adsorption capacity, PPh_3 is largely retained at the entrance of the macropores at the surface of the Ag^+ loaded Amberlyst 15.

4.4.3 Adsorption of CoCl_2 over gel type resin: polymerbound PPh_3

Figure 4.12 gives the CoCl_2 concentration curves over time during the adsorption experiments over Polymerbound PPh_3 . The resulting curves are given in figure 4.12 for flow rates of 5, 10, 20, 30, 40 and 49 [ml/min].

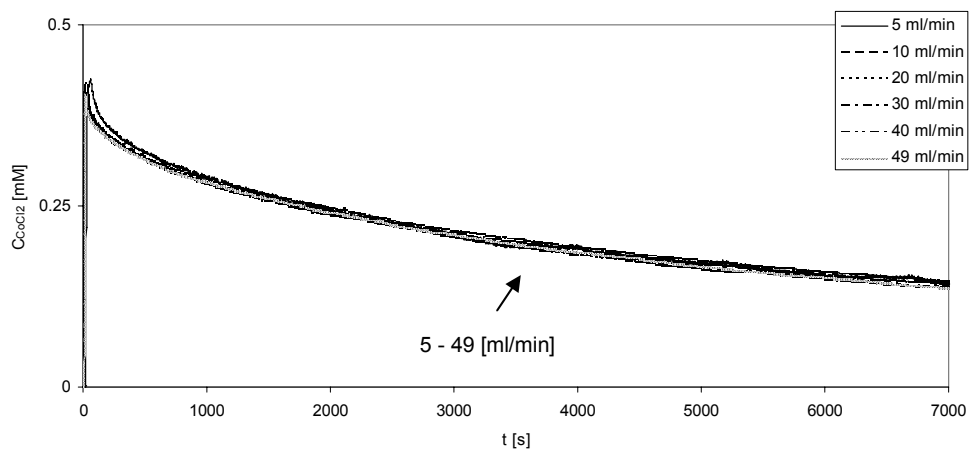


Figure 4.12. CoCl_2 concentration over time during adsorption experiments over Polymerbound PPh_3 .

It can be clearly seen that the curves for all flow rates overlap. This is an indication that all adsorption rates are equal and therefore independent of the external mass transfer limitation. The adsorbent particles are that small in size, that even at a low flow rate of 5 [ml/min], the stagnant layer around the adsorbent particles is small enough to neglect its effect on the adsorption kinetics for all flow rates.

In analogy to the Amberlyst A21, the higher flow rates – 30, 40 and 49 ml/min – have been used to estimate adsorption parameters for the diffusion of CoCl_2 into the gel matrix of polymerbound PPh_3 by using the Langmuir isotherm from chapter 2. The results are summarized in table 4.4

Table 4.4. Overview of calculated kinetic parameters of CoCl_2 over Polymerbound PPh_3 at flow rates of 30, 40 and 49 [ml/min].

Flow rate [ml/min]	$\beta = \frac{D_i}{R_i^2}$ [1/s]
30	$1.21 \cdot 10^{-6}$
40	$1.22 \cdot 10^{-6}$
49	$1.29 \cdot 10^{-6}$
Average	$1.24 \cdot 10^{-6}$ $\pm 0.04 \cdot 10^{-6}$

In figure 4.13, both the experimental – solid line – and the theoretical – diamonds – decrease in the CoCl_2 concentration over time are given. The dotted line represents the equilibrium concentration.

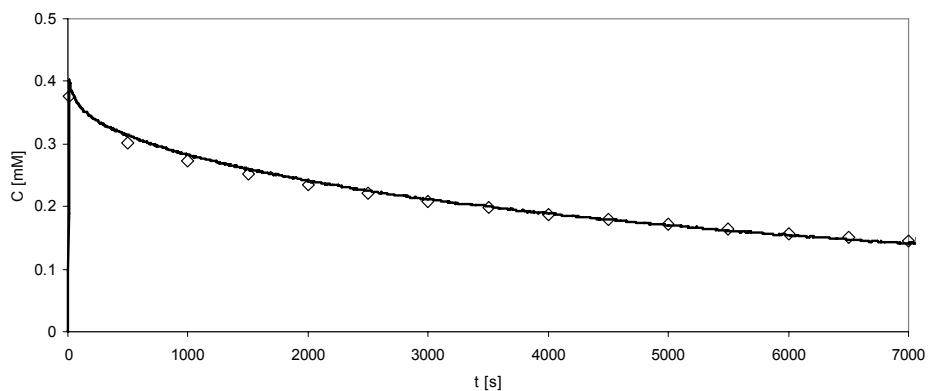


Figure 4.13. experimental (solid line) and predicted (\diamond) CoCl_2 concentrations – at 40 [ml/min] – over Polymerbound PPh_3 in time.

As the experimental data overlaps with the simulated concentration profile, one can conclude that the adsorption kinetics are described by the average diffusivities. In figure 4.14, the CoCl_2 concentration profiles over the adsorbent layer at 500, 5,000 and 50,000 [s]

are shown. The simulation shows that at 500 [s] a constant CoCl_2 concentration level is reached over the adsorption bed.

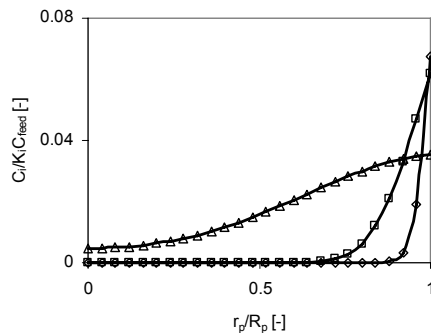


Figure 4.14. CoCl_2 concentration profiles in gel type polymer-bound PPh_3 – 40 [ml/min] – at times 500, 5000 and 50,000 [s].

Figure 4.14 represents the concentration profiles of CoCl_2 inside the matrix of the gel type polymer-bound PPh_2 particles at the entrance of the adsorption bed. Note that, due to the constant CoCl_2 concentration of the adsorbent layer, all particles are contacted with an equal liquid phase concentration. Therefore, figure 4.14 may be extended over all adsorbent particles.

One can recognize the diffusion of the CoCl_2 towards the center of the particles. The CoCl_2 concentration level at the surface initially increases due to the increase in the bulk concentration as the concentrated feed enters the column. After 20 [s], the bulk concentration starts to decrease as a certain amount of CoCl_2 is removed from the liquid phase, leading to a lower surface concentration.

4.5 Discussion

4.5.1 Influence of the liquid flow rate

When comparing the results of the adsorption experiments over Amberlyst A21 and Ag^+ functionalized Amberlyst 15, it can be seen that rates of adsorption increase with increasing flow velocities. This effect is caused by the stagnant film layer around the particles.

Above a flow rate of 20 [ml/min], the overall adsorption rate is not affected by the resistance against mass transfer in the stagnant film layer. The overall mass transfer is completely governed by the internal mass transfer limitation, which does not depend on the liquid flow

rate. This is clearly reflected in figures 4.6 and 4.9, where the adsorption rates are equal at higher flow rates.

For the smaller gel type polymerbound PPh₃ particles it can be seen in figure 4.12 that the adsorption rates are equal for all flow rates. Due to the smaller (see paragraph 4.5.2) internal adsorption rates in this type of adsorbent, the external mass transfer rate already approaches the value for the internal mass transfer at lower flow rates. Figure 4.12 shows that the overall mass transfer is completely governed by the internal mass transfer limitation for all flow rates.

4.5.2 Adsorption rate parameters

With the definitions for the adsorption parameters α (equation 4.4) and β (equation 4.5), the macro- and micropore diffusivities of CoCl₂ or PPh₃ in the respectively used adsorbent can be calculated. The radii of the respective adsorbent particles are summarized in table 4.1 and the resulting calculated diffusivities are summarized in table 4.5.

Table 4.5. Overview of the calculated macro- and micropore diffusivities of CoCl₂ over Amberlyst A21 and polymerbound PPh₃ and PPh₃ over Ag⁺ functionalized Amberlyst 15 at flow rates of 30, 40 and 49 [ml/min].

Flow rate [ml/min]	CoCl ₂		Polymerbound PPh ₃	PPh ₃ Ag ⁺ functionalized Amberlyst 15
	Amberlyst A21			
	$D_a (= \alpha R_p^2)$ [cm ² /s]	$D_i^* (= \beta R_i^2)$ [cm ² /s]	$D_i (= \beta R_p^2)$ [cm ² /s]	$D_a (= \alpha R_p^2)$ [cm ² /s]
30	1.26 · 10 ⁻⁶	8.61 · 10 ⁻¹⁶	6.97 · 10 ⁻¹²	0.50 · 10 ⁻⁶
40	1.22 · 10 ⁻⁶	7.66 · 10 ⁻¹⁶	7.03 · 10 ⁻¹²	0.50 · 10 ⁻⁶
49	1.26 · 10 ⁻⁶	8.39 · 10 ⁻¹⁶	7.43 · 10 ⁻¹²	0.50 · 10 ⁻⁶
Average	1.25 · 10 ⁻⁶ ± 0.03 · 10 ⁻⁶	8.22 · 10 ⁻¹⁶ ± 0.50 · 10 ⁻¹⁶	7.14 · 10 ⁻¹² ± 0.25 · 10 ⁻¹²	0.50 · 10 ⁻⁶ ± 0.07 · 10 ⁻⁶

* Assuming R_i to be 10⁻⁵ [cm].

Amberlyst A21

The macropore diffusivity in a liquid phase – at ambient temperatures – generally range from 10^{-5} to 10^{-7} [cm^2/s] [Ruckenstein, 1971]. In this research, the diffusivity of CoCl_2 from 1-butanol into the macropores of Amberlyst A21 was found to be $1.3 \cdot 10^{-6}$ [cm^2/s]. The sizes of the microparticles are uncertain due to swelling effects [Dogu, 2003], but are in the order of 10^{-5} [cm]. Assuming this equals the size of the microparticles in Amberlyst A21, we have found the diffusivity of the CoCl_2 into the microparticles to be $8.2 \cdot 10^{-16}$ [cm^2/s]. For compounds, diffusing into polymers matrices, the diffusivities range from 10^{-6} to 10^{-15} [cm^2/s] [Ruckenstein, 1971].

Fitting the model parameters to the experimental data reveals that the major – 97 [%] – contribution of the adsorption capacity is located inside the macroparticles. This is in line with the literature data on macroreticular Amberlyst 15 [Ihm, 1996]. Amberlyst 15 is made up of a same polystyrenic carrier which appears to have 95 [%] of its contributing adsorption sites to be located in the microparticles.

Ag^+ loaded Amberlyst 15

θ was found to be equal to 1, which is an indication that all accessible adsorption sites are located at the macropore walls. This is in line with the large dimensions of PPh_3 , which prevented it to penetrate the gel type matrix of the microparticles. This has also been shown in chapter 3 for Co^{2+} functionalized DOWEX 50W-X4, which did not adsorb PPh_3 .

The macropore diffusivity of $0.5 \cdot 10^{-6}$ [cm^2/s] falls well within the range of diffusivities into macropores as mentioned above. Although, compared to the diffusion of CoCl_2 in Amberlyst A21, the macropore diffusion for PPh_3 into Ag^+ loaded Amberlyst 15 is slower; the overall uptake rate of CoCl_2 in Amberlyst A21 is limited by the micropore diffusion. This leads to a higher overall uptake rate for PPh_3 as PPh_3 only has to enter the macropores of the Ag^+ loaded Amberlyst 15.

Polymerbound PPh_3

Diffusivity into polymer matrices, usually range from 10^{-6} to 10^{-15} [cm^2/s] [Ruckenstein, 1971]. The diffusivity of CoCl_2 into polymerbound PPh_3 falls well within this range as it was found to be $7.1 \cdot 10^{-12}$ [cm^2/s].

Compared to the microparticles in Amberlyst A21, the CoCl_2 diffuses faster into the gel matrix of polymerbound PPh_3 . The higher diffusivity of CoCl_2 into the latter matrix reflects the difference in polymer structure. The polymerbound PPh_3 resin is crosslinked by 3 [%] divinylbenzene whereas Amberlyst A21 has a crosslink level of 20 [%] or higher [Corain, 2001]. Less crosslinkage – such as in polymerbound PPh_3 – leads to a looser polymer structure, which in its turn causes a higher accessibility of the solvent in to the matrix.

4.5.3 Comparison with ZLC method

To derive an analytical solution of the diffusivity model for solutes in porous particles measured by the Zero Length Column method, the Zero Length cell is generally taken equivalent to a continuous stirred tank adsorber [Ruthven, 1993; Rodriquez, 1998]. In addition, it is usually assumed for mono-dispersed particles, that there is no limitation in the external mass transfer [Ruthven, 1993; Rodriquez, 1993], no solute holdup in the macropores [Rodriquez, 1993] and the adsorption isotherm is linear [Ruthven, 1993]. On top of these restrictions, for bi-dispersed particles it has to be assumed that no adsorption of the solute onto the surface inside the macropores occurs [Silva, 1996].

The solution of the analytical expression is cumbersome [Loos, 2000] because of the slow converging of the expression to its solution. By relaxing the restriction on the macropore adsorption and allowing a non-linear isotherm, the set of governing equations can be solved numerically.

This way, we were able to determine the combined diffusivities in both the macro- and micropores (Co(II) adsorption onto Amberlyst A21 and polymerbound PPh_3 – see table 4.5 –) or to prove that micropore adsorption does not contribute to the up-take of the solute (PPh_3 in Ag^+ loaded Amerlyst 15 – table 4.5 –). Moreover, the model gives the concentration profile in the shallow bed as a function of time. In all calculations it appeared that $\Delta C < 2$ [%] at times larger than 200 [s] over the shallow bed. Finally, the concentration profiles in the particles can be studied as a function of time and concentration as shown in figures 4.8, 4.11 and 4.14.

4.6 Conclusion

In this research it has been shown that the diffusivities for a non-linear adsorption can be determined by using a generalized Zero Length method. This enables the measurement of diffusivities for adsorption at higher concentrations and extends the adsorption rate measurements to non-ideal interactions.

The internal diffusivity constants for the adsorption kinetics of CoCl_2 into Amberlyst A21 and polymerbound PPh_3 and the adsorption of PPh_3 into Ag^+ functionalized Amberlyst 15 have been determined by fitting a generalized Zero Length model to experimentally determined concentration changes as a function of time. The model was found to be applicable to non-linear isotherms without neglecting the adsorption of the sorbate in at the macropore walls. It was found that:

- CoCl_2 diffuses into the macro- and micropores of the macroreticular Amberlyst A21 with respective diffusion rates of $1.3 \cdot 10^{-6} \text{ [cm}^2/\text{s]}$ and $8.2 \cdot 10^{-16} \text{ [cm}^2/\text{s]}$.
- The adsorption capacity of Amberlyst A21 for CoCl_2 is mainly located in the microparticles.
- CoCl_2 is adsorbed into the gel matrix of polymerbound PPh_3 at a diffusion rate of $7.1 \cdot 10^{-12} \text{ [cm}^2/\text{s]}$. This is faster – due to less crosslinkage –, in comparison to the gel type microparticles of Amberlyst A21.
- The microparticles in Ag^+ functionalized Amberlyst 15 are not accessible for PPh_3 .
- PPh_3 diffuses only into macroporous structure of Ag^+ functionalized Amberlyst 15 at a diffusion rate of $0.5 \cdot 10^{-6} \text{ [cm}^2/\text{s]}$. Although its absolute diffusion rate is lower compared to CoCl_2 macropore diffusion, the overall diffusion is higher when compared to Amberlyst A21 as the latter is limited by the rate of the micropore diffusion.

Thus, adsorbents that show the highest mass transfer rates should not have a microporous structure which limits the adsorption rate. It can be concluded, that adsorbents to be used in Reverse Flow Adsorption, should not only be able to reversibly adsorb homogeneous transition metal complexes. But, should also have particles which are small in size and consisting of a macropore structure.

4.7 Symbols

C_a	= macropore concentration of sorbate	$[\text{mol}/\text{m}^3]$
C_{feed}	= concentration of sorbate in the feed	$[\text{mol}/\text{m}^3]$
C_i	= concentration of sorbate in microparticle	$[\text{mol}/\text{m}^3]$
C_l	= sorbate concentration in the liquid phase between the particles	$[\text{mol}/\text{m}^3]$
C_{sa}	= macropore adsorbed phase of sorbate	$[\text{mol}/\text{m}^2]$
D_a	= macropore diffusivity	$[\text{m}^2/\text{s}]$
D_i	= micropore diffusivity	$[\text{m}^2/\text{s}]$

K_a	= initial slope of the adsorption isotherm for the macropores	[mol/m ²]
$K_{af}(C_a)$	= adsorption isotherm for macropore adsorption	[mol/m ²]
K_{exp}	= initial slope of the experimental adsorption isotherms	[mol/m ³]
K_i	= initial slope of the micropore adsorption	[mol/m ³]
$K_{if}(C_a)$	= adsorption isotherm for microparticle adsorption	[m ³ /m ³]
$K_{if}(C_b)$	= adsorption isotherm	[m ³ /m ³]
n_i	= amount adsorbed in microparticles	[mol]
n_{sa}	= amount adsorbed at the macropore walls	[mol]
r_i	= radial distance in microparticle	[m]
R_i	= radius of microparticle	[m]
r_p	= radial distance in macroreticular particle	[m]
R_p	= radius of adsorbent particle	[m]
t	= time	[s]
u	= interstitial flow rate	[m/s]
z	= axial distance in adsorption bed	[m]
ε_a	= macroporosity	[m ³ /m ³]
ε_b	= bed porosity	[m ³ /m ³]
	= external surface area of microparticles (in macroreticular	
δ_a	matrix: $\delta_a = \frac{3(1-\varepsilon_a)}{R_i}$	[m ² /m ³]
	= external surface area of adsorbent particles: $\delta_b = \frac{3(1-\varepsilon_b)}{R_p}$	
δ_b	= ratio of amounts adsorbed at the macropore walls and inside	[m ² /m ³]
	= ratio of amounts adsorbed at the macropore walls and inside	
θ	the microparticles = $\frac{n_{sa}}{n_{sa} + n_i}$	[-]

4.8 References

Brandani, S. and Ruthven, D., Analysis of ZLC Desorption Curves for Liquid Systems, Chem. Eng. Sci., 50, 2055, 1995

Brandani, S., Analytical Solution for ZLC Desorption Curves with Bi-Porous Adsorbent Particles, Chem. Eng. Sci., 51, 12, 3283, 1996

Study of Adsorption Kinetics of CoCl_2 and PPh_3 over Macroreticular and Gel Type Adsorbents by a Generalized ZLC method

Brandani, S., Effects of Nonlinear Equilibrium on Zero Length Column Experiments, Chem.

Eng. Sci., 53, 15, 2791, 1998

Cavalcante Jr, C., Eic, M., Ruthven, D. M., and Ocelli, M., Diffusion of n-Paraffins in Offretite Type Zeolites, Zeolites, 14, 293, 1995

Corain, B., Zecca, M. and Jeřábek, K., Catalysis and Polymer Networks – the Role of Morphology and Molecular Accessibility, J. Mol. Cat. A: Chem., 177, 3, 2001

Doğu, T., Diffusion and Reaction in Catalyst Pellets with Bidisperse Pore Size Distribution, Ind. Eng. Chem. Res., 37, 2158, 1998

Doğu, T., Aydin, E. and Boz, N., Diffusion Resistances and Contribution of Surface Diffusion in TAME and TAEE Production Using Amberlyst-15, Int. Journ. Chem. React. Eng., 1, 2003

Dunnewijk, J., Bosch, H. and Haan, A.B. de, Reverse flow adsorption: integrating the recovery and recycling of homogeneous catalysts, Sep. Pur. Tech., 40, 3, 317, 2004

Eic, M. and Ruthven, D. M., A New Technique for Measurement of Intracrystalline Diffusivity, Zeolites, 8, 40, 1988

Hufton, J. and Ruthven, D. M., Diffusion of Light Alkanes in Silicalite Studied by the ZLC Method, Ind. Eng. Chem. Res., 32, 2379, 1993

Lee, L. P., The Kinetics of Sorption in a Biporous Adsorbent Particle, AIChE J., 24, 531, 1978

Loos, J. W. P., Verheijen, P. J. T. and Moulijn J. A., Improved Estimation of Zeolite Diffusion Coefficients from Zero-Length Column Experiments, Chem. Eng. Sci., 55, 1, 51, 2000

Perry, R. H. and Green, D. W., Perry's Chemical Engineers' Handbook, 7th edition, Mc Graw Hill, New York, 1998

Rodriguez, J., Valverde, J. and Rodriguez, A., Measurement of Effective Self-Diffusion Coefficients in a Gel-Type Cation Exchanger by the Zero-Length-Column Method, *Ind. Eng. Chem. Res.*, 37, 2020, 1998

Ruckenstein, E., Vaidyanathan A. S., Youngquist, G. R., Sorption by Solids with Bidispersed Pore Structures, *Chem. Eng. Sci.*, 26, 1305, 1971

Ruthven, D. M. and Stapleton, P., Measurement of Liquid Phase Counter-Diffusion in Zeolite Crystals by the ZLC Method, *Chem. Eng. Sci.*, 48, 1, 89, 1993

Rutven, D. M., *Principles of Adsorption and Desorption Processes*, Wiley, New York, 1984

Sanjoz, P., Zhong, G. and Guiochon, G., Influence of the Concentration Dependence of the Mass Transfer Properties on the Chromatographic Band Profiles I. Apparent Axial Dispersion Coefficient in Frontal Analysis, *Journ. Chrom. A*, 728, 15, 1996

Shavit, D., Voogd, P. and Kouwenhoven, H. W., Time-Dependent Non-Steady-State Diffusivities of C6 Paraffins in Silicalite by Zero-Length Column Method, *Collect. Czech. Chem. Commun.*, 57, 698, 1992

Silva, J. A. and Rodrigues, A. E., Analysis of ZLC Technique for Diffusivity Measurements in Bidisperse Porous Adsorbent Pellets, *Gas. Sep. Purif.*, 10, 4, 207, 1996

Silva, J. and Rodrigues, A., Sorption and Diffusion of n-Pentane in Pellets of 5-A Zeolite, *Ind. Eng. Chem. Res.*, 36, 493, 1997

Son-Ki Ihm, Jou-Hyeon Ahn and Young-Do Jo, Interaction of Reaction and Mass Transfer in Ion-Exchange Resin Catalysts, *Ind. Eng. Chem. Res.*, 35, 2946, 1996

Valverde, J. L., De Lucas, A., Carmona, M., González, M. and Rodríguez, J. F., A Generalized Model for the Measurement of Effective Diffusion Coefficients of Heterovalent Ions in Ion Exchangers by the Zero-Length Column Method, 59, 71, 2004

Study of Adsorption Kinetics of CoCl_2 and PPh_3 over Macroreticular and Gel Type Adsorbents by a Generalized ZLC method

Voogd, P., Bekkum, H., Shavit, D. and Kouwenhoven, W. H., Effect of Zeolite Structure and Morphology on Intracrystalline n-Hexane Diffusion in Pentasil Zeolites Studied by the Zero-Length Column Method, J. Chem. Soc. Faraday Trans., 87, 21, 3575, 1991

Westerterp, K. R., van Swaaij, W. M. P., Beenackers and A. A. C. M., Chemical Reactor Design and Operation, Wiley, New York, 1995

5

Simulation of Reverse Flow Adsorption

5.1 Introduction

In chapter 1, the advantages of using homogeneous catalysts in comparison to heterogeneous catalysts have been discussed. As pointed out there, homogeneous catalysts are still not as common in use as heterogeneous catalysts due to the difficult recovery of the homogeneous catalysts. Usual methods to recover homogeneous catalysts are for example distillation and extraction. All the recovery methods have draw-backs, such as: decomposition, leaching and/or the use of additional solvents. To overcome these draw-backs, we have proposed [Dunnewijk et al, 2001, 2004] a novel homogeneous catalyst recovery method which combines an adsorptive separation with the reverse flow technology: Reverse Flow Adsorption.

The concept of Reverse Flow technology was first proposed and patented by Cottrell (1938) for the removal of pollutants from a gas phase in a Reverse Flow Reactor. Frank-Kamenetskii (1955) described the use of a Reverse Flow Reactor for the oxidation of isopropyl-alcohol to acetone. In 1975 a patent for the reduction of SO₂ in a Reverse Flow Reactor was issued to Watson (1975). The application of SO₂ oxidation in Russia [Boreskov et al., 1979; Boreskov and Matros, 1983; Matros, 1989] then led to a more extensive study on Reverse Flow Reactors.

Other investigations include the removal of NO_x [Bobrova et al., 1988], syngas-production [Blanks et al., 1990], methanol synthesis [Neophytides and Froment, 1992], the catalytic destruction of VOCs [Nieken et al., 1994; Van de Beld, 1995] and catalytic oxidation of CO [Züfle and Turek, 1997]. An extensive review on the applications and studies of the Reverse Flow Reactor was presented by Matros and Bunimovich [Matros and Bunimovich, 1996].

The main advantage of the Reverse Flow concept in the above mentioned processes is to keep the heat of reaction inside a fixed bed. In 1988, a shift in focus from heat entrapment to mass trapping was proposed by Agar and Ruppel (1988). Agar, Ruppel and others [Noskov et al., 1996; Snyder and Subramanian, 1998] proposed to maintain a zone of adsorbed ammonia inside the reactor for the catalytic reduction of NO_x. Extending the Reverse Flow technology for mass entrapment to non-reactants was suggested by Beckmann and Keil

(2003). They suggested entrap a solvent, evaporating from a SLP-catalyst inside a fixed bed reactor, by periodically changing the flow direction.

All the references mentioned above, apply to flow reversal in a gas phase. For the recovery of homogeneous catalysts though, the Reverse Flow concept should be applied in the liquid phase. The combination of reversible adsorption with Reverse Flow technology is a potential method for a semi-continuous integrated recovery and recycling of homogeneous catalysts which takes place in a liquid phase. Only a limited number of papers are devoted to flow reversal of a liquid phase. To our knowledge only one research group at the KTH in Sweden has proposed to apply Reverse Flow for mass-entrapment in a liquid phase. Bjornbohm and Hung undertook a theoretical study [Bjornbohm et al, 2001a; 2001b; 2003; Hung et al., 2000; 2003] to use flow reversal for the catalyst-mass entrapment to avoid leaching of an imperfectly immobilized catalyst. This study was done for non-specified reactants and products and focused on the mass transfer limitations of a system in which both reaction and recovery occur in a batch reactor. Moreover, they expected that de-complexation of the catalyst – equilibrium between the transition metal center and its ligands – would not occur and assumed only one adsorbent would be needed.

Here, we propose a method to recover homogeneous catalysts by adsorption externally from the reactor. Thereby, the homogeneous catalyst system – that is the equilibrium between the ligands and the transition metal center – will remain unaffected inside the reactor. De-complexation of the homogeneous catalyst can be avoided by recovering the individual species of the catalyst.

In our proposal, the catalyst is recovered at process conditions and recycled to the reactor after desorption from the adsorption beds located up-stream the reactor (Flow A in figure 5.1).

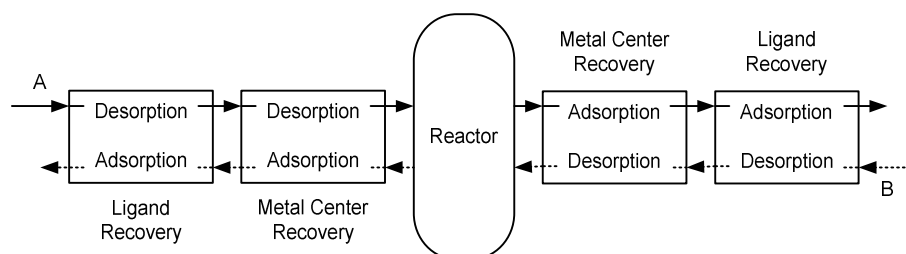


Figure 5.1. Homogeneous catalyst recycling by a four bed set-up of Reverse Flow Adsorption (feed alternates between A and B).

The catalyst leaving the reactor with the product stream is then recovered at process conditions by adsorption in the adsorption beds up-stream of the reactor. In the subsequent

step, the direction of the process flow is reversed (Flow B in figure 5.1) and the recovery and recycling modes of the adsorption beds are interchanged.

In chapters 2 and 3 we studied the adsorption and subsequent desorption of a transition metal based homogeneous catalyst complex from a liquid phase. We showed that the adsorption of the individual components – the transition metal and its ligands – of bischlorodiphenylphosphinecobalt(II) – $(PPh_3)_2CoCl_2$ – was reversible for the selected adsorbents.

As the adsorbents were selected for the recovery of one of its components, four adsorption beds have to be implemented in the Reverse Flow Adsorption process for the recovery and recycling of the homogeneous catalyst (as shown in chapter 1 in figure 1.5). For our testing purposes – to find out if a stable process can be achieved – described in this chapter, we are only interested in the adsorption of $CoCl_2$ in the first adsorption beds on the left and right hand side of the reactor (figure 5.1). This is because the adsorption of the ligands of the homogeneous catalyst is completely analog to the adsorption of the transition metal center.

In this chapter we present a model describing the concentration profiles in the adsorption beds during adsorption and desorption. We use this model to demonstrate the feasibility of the Reverse Flow Adsorption concept by studying the influence of following process parameters: strength of the adsorption (initial slope of adsorption isotherm), adsorption capacity, effective internal diffusion, velocity of the liquid phase and the dimensionless cycle time. The model parameters concerning the adsorption isotherm and kinetics are taken from previous chapters.

Finally, this model will be applied to an industrial scale OXO-synthesis process to illustrate the implementation of Reverse Flow Adsorption in a real scale processes.

5.2 Dynamic model for concentration gradients in adsorption beds

In chapter 4, we derived two generalized models for the ZLC method to describe the adsorption kinetics of the transition metal and its ligands. The first model was derived for the adsorption in bi-dispersed particles and the second for adsorption in mono-dispersed particles. In both models, a shallow adsorption bed has been modeled as a plug-flow reactor. In order to apply these models to the Reverse Flow Adsorption processes, the model for the plug-flow reactor is extended to larger adsorption beds by including the effects of intra-particle mixing and external mass transfer on the concentration gradients.

As it was shown that the degree of utilization of the adsorbent particles was low, we will use the Linear Driving Force [Glueckauf, 1947] model to describe the mass transfer between the liquid and solid phases. This gives us the advantage that both types of adsorbents – mono-

and bi-dispersed – are described by just one dimensionless model. As a further simplification we neglect adsorption of components other than the metal center and ligands of the catalyst.

Differential molar balance over adsorption bed

For a single adsorption bed, the dimensionless plug-flow model reads (for the definitions of the dimensionless parameters – Ψ , Γ , τ and γ – see nomenclature section):

$$\frac{\partial \Psi}{\partial \tau} + \frac{(1-\varepsilon)}{\varepsilon} \alpha \frac{\partial \langle \Gamma \rangle}{\partial \tau} = -\frac{1}{\varepsilon} \frac{\partial \Psi}{\partial \gamma} + \frac{1}{Bo} \frac{\partial^2 \Psi}{\partial \gamma^2} \quad (5.1)$$

with the ratio of the solid and liquid phase capacities:

$$\alpha = \frac{\rho_s q_m}{C_{reactor}}$$

For the estimation of the Bodenstein number (Bo), the correlation of Chung and Wen (1968) was used:

$$Bo \equiv \frac{u_{sup} L}{D_{ax}} = N \left(0.20 + 0.011 Re^{0.48} \right)$$

with the number of particles along the axial position:

$$N = \frac{L}{d_p}$$

External mass transfer

The external mass transfer rate is assumed to be given by the liquid film Linear Driving Force (LDF) model:

$$\frac{\partial \langle \Gamma \rangle}{\partial \tau} = \frac{6}{\alpha} St_m N (\Psi - \Psi_i) \quad (5.2)$$

The Stanton number for mass transfer (St_m) is estimated from the Sherwood (Sh) correlation for packed beds [Wilson and Geankopolis, 1966]:

$$St = \frac{k_{ext}}{u_{sup}} = \frac{Sh}{ReSc} = \left(\frac{1.09}{\varepsilon} \right) Re^{-2/3} Sc^{-2/3}$$

Internal mass transfer

The internal rate of mass transfer in the particles is given by the dimensionless equation of the solid film LDF model:

$$\frac{\partial \langle \Gamma \rangle}{\partial \tau} = \frac{60}{\beta} N(\Gamma_i - \langle \Gamma \rangle) \quad (5.3)$$

with the ratio of amounts of catalyst that passes the particles versus the transport inside the particles:

$$\beta = \frac{u_{sup} d_p}{D_{eff}}$$

Adsorption equilibrium at interface of adsorbent particles

$$\Gamma_i = \frac{\chi \Psi_i}{1 + \chi \Psi_i} \quad (5.4)$$

where the dimensionless adsorption strength is given by:

$$\chi = bC_{reactor}$$

This model for a single adsorption bed – equations 5.1 through 5.4 –, has been verified on basis of the experimental breakthrough behavior of hIlgG over PG700 and PG1000 [McCue et al., 2003]. The effective diffusion coefficient (D_{eff}), has been taken from Özdural (2004) for Reynold numbers of 0.07 and 0.14 [-].

The model has been programmed in the g-Proms (PSE, London, UK) programming language to calculate the changes in the concentration profiles of *hlgG* as a function of time. This verification showed that our LDF model describes the experimental data as well as their pore diffusion model.

In Reverse Flow Adsorption, multiple adsorption beds are coupled up and down-stream a reactor (as shown in figure 5.1) to recover both the metal center and the ligands of a homogeneous catalyst. But, as the models for the adsorption beds for the ligand recovery are analog to the models for the transition metal center adsorption, here a simplified 2 bed form of Reverse Flow Adsorption of CoCl_2 will be discussed. The two bed system for CoCl_2 recovery and recycling by Reverse Flow Adsorption is shown in figure 5.2.

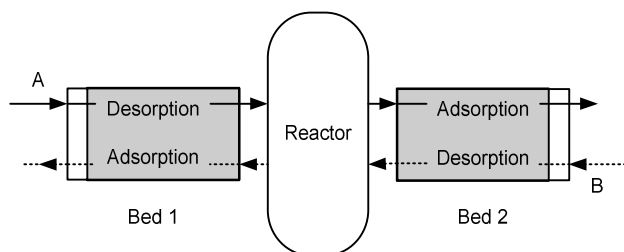


Figure 5.2. CoCl_2 recycling by a two bed set-up of Reverse Flow Adsorption (shaded areas indicate initial loading).

The shaded areas in beds 1 and 2 indicate the initially saturated fractions of bed volumes of the adsorbent beds. The initially unused parts have been introduced to accommodate for broadening of the CoCl_2 concentration gradients.

From the start of a cycle, a liquid flow (A in figure 5.2) – containing nothing but the solvent and reactants – is continuously fed to adsorption bed 1. During the first half of a cycle – the half cycle time ($\tau_{1/2}$) of the Reverse Flow Adsorption process –, CoCl_2 desorbs from the saturated part of adsorption bed 1 into the liquid flow that is fed to the reactor. In its turn, the CoCl_2 leaving the reactor is recovered from the product flow by adsorption in the unused fraction of adsorption bed 2.

Then, to complete the cycle, the flow direction is reversed. Now adsorption bed 2 is being fed with a liquid flow (B in figure 5.2). During the second half of a cycle, CoCl_2 is desorbing from the adsorbent in adsorption bed 2. The liquid flow leaving adsorption bed 2 is fed to the reactor. The CoCl_2 leaving the reactor is adsorbed in adsorption bed 1.

The concentration of the catalysts inside the reactor is constant. Thus, the choice of reactor type will not influence the simulation results. For simulation purposes, a continuous ideal stirred tank reactor is selected:

$$\frac{\partial \Psi_{out}}{\partial \tau} = \frac{1}{\tau_R} (\Psi_{in} - \Psi_{out}) \quad (5.5)$$

In equation 5.5, τ_R , Ψ_{in} and Ψ_{out} respectively represent the dimensionless residence time, the concentration fed and concentration leaving the reactor. To describe the changes in the concentration gradients over time, the set of equations has been programmed in the g-Proms (PSE, London, UK) programming language. As it has been found in chapter 4, external mass transfer did not limit the metal center uptake rate for Reynold numbers exceeding 0.1 [-]. To neglect the effect of external mass transfer limitation, the Reynold number has been taken at least 0.2 [-]. The simplified two bed model will be used in this chapter to:

- Show that Reverse Flow Adsorption leads to a stable process for the integrated recovery and recycling of homogeneous catalysts.
- Show the effects of the process and adsorbent specific parameters – that can be used for optimization purposes – on the behavior of the catalyst concentration gradients in the adsorption beds.
- Indicate the advantage of implementation of Reverse Flow Adsorption in an OXO-synthesis process.

5.3 Simulation Results and Discussion

5.3.1 Process Stability

To show that Reverse Flow Adsorption converges to a stable process, a reference simulation has been done. The values of the dimensionless parameters used for the reference simulation are summarized in table 5.1.

The values for the adsorbent specific parameters have been derived from the experimental data given in chapter 2. Here, the values for α and χ have been taken from the Langmuir isotherm for Rb^+ functionalized Amberlyst 15.

As mentioned above, for reasons to justify the neglecting of external mass transfer, Re has been taken 0.2 [-]. Then, setting the half cycle time determines the bed length (L) and number of particles along the axial position (N) of the adsorption bed. Successively, the

value for Bo is then to be derived from Re and N . The effective diffusion coefficient for calculating β has been taken from chapter 4.

The half cycle time has been taken such that the $CoCl_2$ concentrations at both sides of the adsorption beds remain constant during the first 500 complete cycles. Thus, the concentration inside the reactor remaining constant over time and the dimensionless reactor residence time (τ_R) is of no importance in the reference simulation of the Reverse Flow Adsorption process.

Table 5.1: Dimensionless input parameters for Reverse Flow Adsorption simulation.

Variable	Value for $CoCl_2$ adsorption
<i>Adsorbent specific parameters</i>	
$\alpha = \frac{\rho_s q_m}{C_{reactor}}$	$1.2 \cdot 10^3$
$\chi = bC_{reactor}$	5.4
<i>Process related parameters</i>	
$Re = \frac{u_{sup} d_p}{\nu}$	0.2
$\tau_{1/2} = \frac{u_{sup}}{L} t_{1/2}$	10.0
$N = \frac{L}{d_p}$	$3.0 \cdot 10^4$
$\beta = \frac{u_{sup} d_p}{D_{eff}}$	$2.4 \cdot 10^3$
$Bo \equiv \frac{u_{sup} L}{D_{ax}} = N(0.20 + 0.011Re^{0.48})$	$4.1 \cdot 10^3$

In figure 5.3, besides the initial concentration profile (0), the calculated concentration gradients are shown as a function of the dimensionless axial position in adsorption bed 1 (bed position defined in figure 5.2) respectively after the desorption steps of the 1st, 100th, 200th, 300th, 400th and 500th cycles. In addition, the concentration gradients in adsorption bed 1 at the end of the adsorption steps of respectively the 1st, 100th, 200th, 300th, 400th and 500th cycles are shown in figure 5.4.

During the first half cycle, the concentration gradient migrates through the adsorption bed from the initial straight gradient to its end position at the end of the desorption step of cycle 1 (see figure 5.3). Then, the second half of the first cycle is started by reversing the flow direction. Now, CoCl_2 is being adsorbed during the remaining cycle time. Eventually, the concentration gradient migrates backwards to the end position of the first cycle which is represented as gradient 1 in figure 5.4.

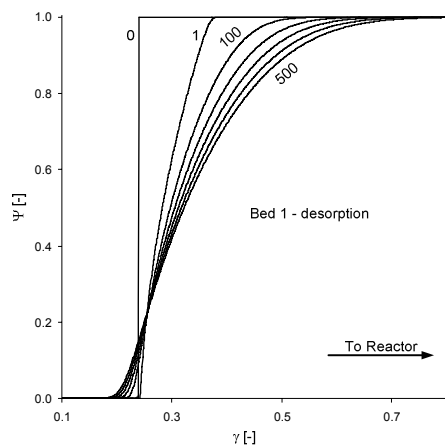


Figure 5.3. Concentration gradients in bed 1 at the initial state (0) and after desorption for a selected number of cycles.

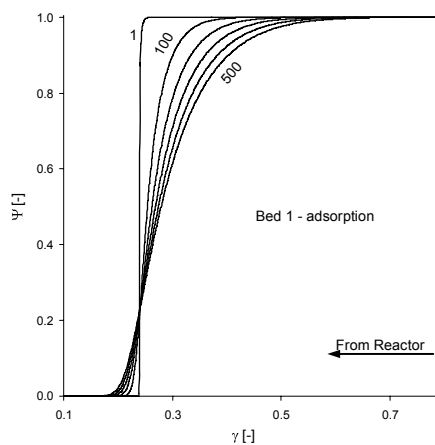


Figure 5.4. Concentration gradients in bed 1 after adsorption for a selected number of cycles.

After a number of selected cycles (1, 100, 200, 300, 400 and 500), the end positions of the concentration profiles after desorption are shown in figure 5.3. The end positions of the concentration gradients after adsorption are shown in figure 5.4 for the selected cycle numbers mentioned above.

From figure 5.3 it can be observed that the concentration gradient at the end of the desorption step broadens with increasing the number of cycles. This is caused by two mechanisms: an equilibrium effect and a limitation in internal mass transfer rate.

During desorption, due to the favorable isotherm, low concentrations fall behind higher concentrations. Thus, leading to a broadening of the concentration gradients during desorption. The broadening of the concentration gradient is then amplified by the limitation in the mass transfer rate of the catalyst from inside of the particles to the surface.

In the second half of a cycle, the flow direction is reversed and CoCl_2 is being adsorbed. Now during the adsorption, due to the favorable isotherm higher concentrations move faster

through the adsorption bed as lower concentrations. As a result, the high feed concentration – originating from the reactor – catches up with the lower concentrations, resulting in a straighter concentration gradient. In contrast to the desorption, here the straightening of the concentration gradients is enhanced by the limitation in the uptake rate. The higher concentrations slip over the adsorption particles to catch up with lower concentrations, but also leads to a slip of CoCl_2 into the initially unused volume. The latter is shown on the left hand side of gradient 1 – at low concentrations – in figure 5.4.

Another aspect of the results shown in figures 5.3 and 5.4, relates to the change in end positions of the concentration gradients at the end of the desorption and adsorption steps after an increasing number of cycles. The difference in the end position of the concentration gradients at the end of each cycle decreases. After approximately 500 cycles, the end positions of the concentration gradients – after desorption and adsorption – hardly change anymore. Thus, it can be concluded that with increasing the number of cycles the concentration fronts stabilize. This stabilization means that, independent of the number of cycles the whole desorption and adsorption process is confined in a limited volume so that no leaching of catalyst can occur.

The effect in adsorption bed 2 is similar, except the fact that here the process is started with adsorption.

5.3.2 Influence Adsorbent Parameters

Next, the effects of the adsorbent specific parameters on the CoCl_2 concentration gradients are to be investigated by comparing the results for different input parameters with the reference simulation. By changing the adsorbent, the strength of adsorption, the adsorption capacity can be influenced. The effects of these parameters will be discussed in this paragraph.

Effect of adsorption strength on concentration profiles

In figure 5.5, the concentration gradients at the end of the desorption step at the stable situation (after 500 cycles) are shown for three different adsorption strengths (χ). Besides the adsorption strength used in the reference simulation ($\chi = 5.4$ [-]), both an increased ($3\chi = 16.2$ [-]) and decreased ($\frac{1}{3}\chi = 1.8$ [-]) are shown in figure 5.5.

Decreasing the strength of adsorption, results in a faster mass transport from inside of the solid phase into the liquid phase. This is clearly reflected in figure 5.5, where the concentration gradient for $\frac{1}{3}\chi$ is less broad as the gradient from the reference simulation.

The difference ($\Delta\gamma$) between the axial position where Ψ starts to increase from 0 [-] to the position where Ψ becomes equal to 1 [-], is in proportion to the ratio of the required bed length versus the bed length used in the reference simulation. From figure 5.5 it can then be calculated that lowering the adsorption strength by a factor 3, results in a change in the required bed length that is 18 [%] smaller compared to the required bed length for the reference simulation. On the other hand, increase of the adsorption strength by a factor 3 results in a required change in bed length that is at least 58 [%] – because the width of the gradient passes $\gamma = 1$ – larger in comparison to the reference case.

From this, it is clear that the increase in adsorption strength is certainly not linear proportional to the factor at which the adsorption strength is increased. In conclusion it may be stated that a decrease in adsorption strength is more preferable than an increase.

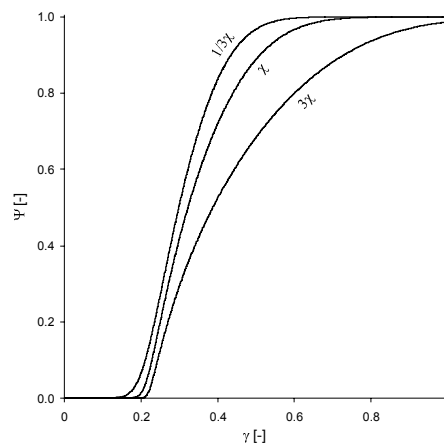


Figure 5.5. Concentration gradients in adsorption bed 1 at the end of the first half of the 500th cycle at three different adsorption strengths.

Effect of adsorption capacity on concentration profiles

In figure 5.6, the concentration gradients at the end of the first half of cycle 500 are shown for three different adsorption capacities (α). Besides the adsorption capacity used in the reference simulation ($\alpha = 1.2 \cdot 10^2$ [-]), both an increased ($2\alpha = 2.4 \cdot 10^2$ [-]) and a decreased ($\frac{1}{2}\alpha = 0.6 \cdot 10^2$ [-]) adsorption capacities are shown in figure 5.6.

Increasing the adsorption capacity leads to a higher internal mass transport as the maximal concentration difference between the internals and the surface of the solid phase – and thus

the driving force – becomes larger. As a consequence, the concentration gradient becomes less broad (as shown in figure 5.6) and the required adsorption bed length decreases.

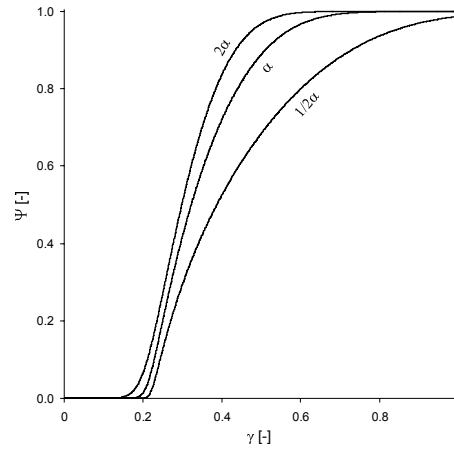


Figure 5.6. Concentration gradients in adsorption bed 1 at the end of the first half of the 500th cycle at three different adsorption capacities.

Concluding from figure 5.6, it may be stated that an increase in the adsorption capacity is preferred as this will lead to a smaller required length of the adsorption bed.

5.3.3 Influence Process Parameters

Decreasing the cycle time

Besides changing the adsorbent specific parameters, another possibility to ensure no breakthrough at either side of the adsorption beds occurs, is to vary the process parameters. This can be done by changing the dimensionless half cycle time by varying the time of one half cycle ($t_{1/2}$) or the liquid phase velocity, as these parameters influence the dimensionless cycle time as: $\tau_{1/2} = \frac{u_{sup}}{L} t_{1/2}$. By changing the dimensionless cycle time, the penetration of the concentration gradients into the adsorption bed can be influenced.

The effect of a half cycle time, lowered by a factor 2 ($1/2\tau_{1/2} = 5$) by respectively changing ($t_{1/2}$) and u_{sup} on the concentration profiles at the end of the first half of the 500th cycle is shown in figure 5.7 in comparison to the reference case ($\tau_{1/2} = 10$).

The concentration gradients for $\frac{1}{2}\tau_{1/2}$ (shown in figure 5.7) overlap and the curve is valid for the changes in both $t_{1/2}$ and u_{sup} . It can be seen that during the desorption mode of adsorption bed 1 the concentration profile does not penetrate the adsorption bed as far as in comparison to the reference case. In conclusion, by lowering the dimensionless cycle time, a smaller part of the adsorption bed is used.

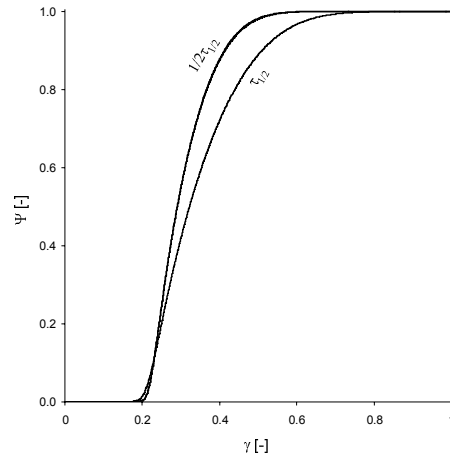


Figure 5.7. Concentration gradients in the first adsorption bed at the end of the first half of the 500th cycle compared to the reference case.

Effect of the internal diffusion rate on the concentration profiles

Lowering the internal diffusion coefficient influences the variable β by increasing the latter. The effect of lowering the internal diffusivity on the concentration profiles is shown in figure 5.8 for three different β values, namely: the value used in the reference simulation ($\beta = 2.4 \cdot 10^3$), increased by a factor 10 ($\beta = 2.4 \cdot 10^2$), and 100 ($\beta = 2.4 \cdot 10^1$). In figure 5.8, the concentration gradients at the end of the first half of cycle 500 are shown for three different internal diffusivities.

Lowering the internal diffusion by a factor 10 gives a process that still stabilizes within the chosen bed length. On the other hand, lowering the internal diffusion by a factor of 100 leads to an instable process as can be seen in figure 5.8.

In the latter case, the internal diffusion becomes too slow for Reverse Flow Adsorption to release and entrap the adsorbed species in the given adsorption bed. At the exit of the adsorption bed leaching of CoCl_2 occurs as shown in figure 5.8 and a longer adsorption bed

will be required for an internal diffusion that is a factor 100 or lower compared to the reference value.

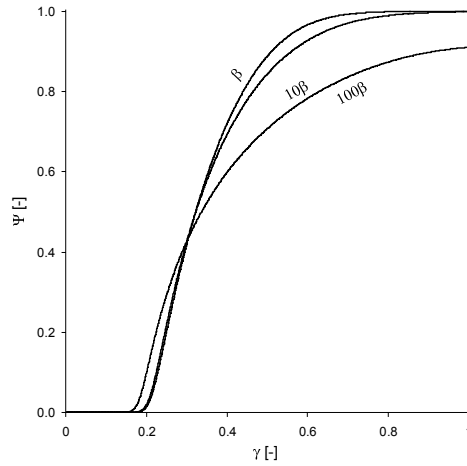


Figure 5.8. Concentration gradients in the first adsorption bed at the first half of the 500th cycle by decreasing the effective diffusion rate (by a factor 10 and 100) compared to the adsorption strength of the reference simulation.

5.3.4. OXO-synthesis process

In this paragraph, the implementation of Reverse Flow Adsorption will be discussed on basis of a theoretical study by connecting 4 adsorption beds – 2 for CoCl_2 and 2 for the PPh_3 recovery – to an OXO-synthesis reactor. The process parameters have been taken from Bhaduri [2001] and summarized in table 5.2.

Table 5.2: Process conditions for the OXO-synthesis process.

Variable	Description	Value	Notes
V_R	Reactor volume	90 [m ³]	Taken from Bhaduri
Φ	Flow rate	$5.0 \cdot 10^{-3}$ [m ³ /s]	Taken from Bhaduri
C_{reactor}	Catalyst concentration	0.3 [mol/m ³]	Taken from Bhaduri
$\tau_R = \frac{u_{\text{sup}}}{L} \frac{V_R}{\Phi}$	See equation 5.5	21.6 [-]	See text

In the reference simulation, the dimensionless half cycle time ($\tau_{1/2}$) was set to 10 [-], which is approximately half the dimensionless residence time of the reactor. The choice of this dimensionless half cycle time determines the required bed length for the CoCl_2 recovery. It has been shown that in the reference simulation approximately 50 [%] of the total bed volume was effectively in use. Thus, the set number of particles along the axial position can be reduced from $N = 3.0 \cdot 10^4$ [-] to approximately $N = 1.5 \cdot 10^4$ [-].

The particle diameter should be sufficiently small to facilitate internal mass transport and sufficiently large to minimize pressure drop. Here d_p has been chosen to be $1.0 \cdot 10^{-4}$ [m]. From $N = 1.5 \cdot 10^4$ [-] and the selected value for d_p , it follows that the required absolute length of the adsorption bed measures 1.50 [m]. Secondly, from the selected d_p and $\text{Re} = 0.2$ [-], the superficial velocity of (u_{sup}) can be calculated. In combination with the given flow rate, u_{sup} gives the required diameter of the adsorption bed. For the reference simulation, this diameter measures 1.8 [m].

The total volume of the adsorption bed that is required for the recovery of CoCl_2 , thus values $3.8 \text{ [m}^3\text{]}$. This is equal to approximately 4 [%] of the reactor volume. The pressure drop over this volume has been estimated to value 0.6 [bar] from the Ergun equation for fixed bed columns:

$$\frac{\Delta P}{L} = 150 \frac{\rho v (1 - \varepsilon)^2 u_{\text{sup}}}{\varepsilon^3 d_p^3} + 1.75 \frac{(1 - \varepsilon) \rho u_{\text{sup}}^2}{\varepsilon^3 d_p}$$

The two adsorption beds required for the CoCl_2 recovery, thus have a total volume of 8 [%] of the reactor volume. The total pressure drop over these two beds measures 1.2 [bar].

As discussed in chapter 3, a wide range of adsorbents can reversibly recover the PPh_3 ligands of the homogeneous catalyst. These adsorbents differ in their adsorption capacity and strength of adsorption of PPh_3 . With the choice of adsorbent, the values for α and χ can be selected so that the PPh_3 can be carried out in adsorption beds of the same dimensions as the CoCl_2 recovery. Therefore, the required volumes of the adsorption beds for the recovery PPh_3 are at least equal to the volumes required for the CoCl_2 recovery.

Concluding it can be stated, that even for the un-optimized case presented here, Reverse Flow Adsorption can be carried out in a total volume for 4 adsorption beds that is less than 16 [%] in comparison to the volume of the reactor. The pressure drop over these 4 beds measures 2.4 [bar], which is less than 5 [%] of the process pressure – 50-100 [bar] – for a cobalt/phosphine catalyzed OXO-process [Hagen, 1999]

5.4 Conclusion

The model for the ZLC method as described in chapter 4, has been extended to larger adsorption beds by including axial dispersion and external mass transfer effects. The resulting model was verified by comparing the calculation results to experimental breakthrough data of *hlgG* over PG700 and PG1000 [McCue, 2003].

Reverse Flow Adsorption was modeled for a CSTR with an adsorption bed upstream and another downstream the reactor. It was found that the concentration fronts after adsorption and desorption eventually reach a fixed position, even if internal mass transfer is a limiting factor: no leaching of catalyst will occur.

From the discussion on the adsorbent specific parameters, it was concluded that the required adsorption bed volumes can be minimized if the adsorbents – to be used in Reverse |Flow Adsorption – have:

- A low adsorption strength.
- A high adsorption capacity.
- Fast effective diffusivity from inside the particles to the liquid phase.

Implementation of the Reverse Flow Adsorption process in an OXO-synthesis process is possible with adsorption beds with a relative volume less than 16 [%] of the reactor volume.

The total pressure drop is then approximately 5 [%] of the process pressure.

We conclude that Reverse Flow Adsorption concept proved to be a technical feasible.

5.5 Symbols

b	= Initial slope Langmuir isotherm	$[m^3/mol]$
Bo	= Bodenstein number = $\frac{u_{sup}L}{D_{ax}}$	$[-]$
D_{ax}	= Axial dispersion coefficient	$[m^2/s]$
D_{eff}	= Effective internal diffusion coefficient	$[m^2/s]$
D_m	= Free molecular diffusion coefficient	$[m^2/s]$
d_p	= Particle diameter	$[m]$
C_i	= Liquid phase concentration at particle surface	$[mol/m^3]$
$C_{reactor}$	= Feed concentration	$[mol/m^3]$
k_{ext}	= External mass transfer coefficient	
L	= Column length	$[s]$

N	= Number of adsorbent particles over axial direction = $\frac{L}{d_p}$	[-]
$\langle q \rangle$	= Average solid phase concentration	[mol/kg]
q_m	= Monolayer solid phase concentration	[mol/kg]
q_i	= Solid phase loading at particle surface	[mol/kg]
Re	= Reynolds number = $\frac{u_{sup} d_p}{\nu}$	[-]
Sc	= Schmidt number = $\frac{\nu}{D_{mol}}$	[-]
Sh	= Sherwood number = $\frac{k_{ext} d_p}{D_{mol}}$	[-]
St_m	= Stanton number for mass transfer = $\frac{k_{ext}}{u_{sup}} = \frac{Sh}{ReSc}$	[-]
u_{sup}	= Superficial velocity	[m/s]
V_R	= Reactor volume	[m ³]
z	= Axial position	[m]
α	= Ratio of catalyst adsorbed in solid/liquid phase = $\rho_s \left(\frac{q_m}{C_{reactor}} \right)$	[-]
β	= Peclet number = $\frac{u_{sup} d_p}{D_{eff}}$	[-]
γ	= Dimensionless axial distance = $\frac{z}{L}$	[-]
ϵ	= Bed porosity	[-]
χ	= Variable for dimensionless Langmuir isotherm = $bC_{reactor}$	[-]
Φ	= Volumetric liquid flow rate	[m ³ /s]
ρ_s	= Density of solid phase	[kg/m ³]
ρ_l	= Density of liquid phase	[kg/m ³]
τ	= Dimensionless time = $\frac{u_{sup}}{L} t$	[-]
τ_R	= Dimensionless residence time of reactor = $\frac{u_{sup}}{L} \frac{V_R}{\Phi}$	[-]
ν	= Viscosity of liquid phase	[Pa·s]

$$\begin{aligned}\langle \Gamma \rangle &= \text{Dimensionless average solid phase loading} = \frac{\langle q \rangle}{q_m} & [-] \\ &= \text{Dimensionless average solid phase loading at particle interface} \\ \Gamma_i &= \frac{q_i}{q_m} & [-] \\ \Psi &= \text{Dimensionless liquid phase concentration} = \frac{C}{C_{reactor}} & [-] \\ &= \text{Dimensionless liquid phase concentration at particle interface} \\ \Psi_i &= \frac{C_i}{C_{reactor}} & [-] \\ &= \text{Dimensionless liquid phase concentration entering reactor} \\ \Psi_{in} &= \frac{C_{in}}{C_{reactor}} & [-] \\ \Psi_{out} &= \text{Dimensionless liquid phase concentration out of reactor} = \frac{C_{out}}{C_{reactor}} & [-]\end{aligned}$$

5.6 References

Agar, D. and Ruppel, W., Multifunctionale Reaktoren für die Heterogene Katalyse, Chem. Ing. Tech., 60, 731, 1988

Beckmann, A. and Keil, F.J., Increasing Yield and Operating Time of SLP-Catalyst Processes by Flow Reversal and Instationary Operation, Chem. Eng. Sci., 58, 841, 2003

Bhaduri, S., Mukesh, D. (2001), Homogeneous Catalysis; Mechanisms and Industrial Applications, Wiley-Interscience

Björnbohm, P. and Åkermark, B., A Catalytic Process in a Reverse Flow Reactor, PCT Patent Application WO 01/28674, to KTH Holding AB, April 26, 2001

Björnbohm, P., Hung, K.G.W., Anderlund, M. and Åkermark, B., Reverse Flow Operation for Catalyst Trapping, AIChE Meeting, Reno, NV, 2001

Blanks, R.F., Wittrig, T.S., Peterson, D.A., Bidirectional adiabatic synthesis gas reactor, Chem. Eng. Sci. 45, 2407, 1990

Bobrova, L.N., Slavinskaya, E.M., Noskov, A.S., Matros, Y.S., Unsteady-state performance of NO_x catalytic reduction by NH₃, *React. Kinet. Catal. Lett.* 37, 267, 1988

Boreskov G.K, Matros Yu. Sh., Kiselev O.V., Catalytic Processes Carried Out Under Nonstationary Conditions: Thermal Front in a Fixed Bed of Catalyst, *Kinet. Catal.*, 20(3), 773, 1979

Boreskov, G.K, Matros Yu. Sh., Unsteady-state Performance of Heterogeneous Catalytic Reactions, *Catal. Rev.-Sci. Eng.*, 25, 4, 551, 1983

Cotrell, F.G., Purifying Gases and Apparatus Therefore, U.S. Patent 2,171,733, June 21, 1938

Dunnewijk, j., Bosch, H. and de Haan, A. b., Reverse Flow Adsorption: Integrating the Recovery and Recycling of Homogeneous Catalysts, *Sep. Pur. Techn.*, 40, 3, 317, 2004

Dunnewijk, j., Bosch, H. and de Haan, A. b., Reverse Flow Adsorption Concept for the Recovery of Homogeneous Catalysts: A Technical Feasibility Study, AIChE Meeting, Reno, NV, 2001

Glueckauf, E. and Coates, J. I., *J. Chem. Soc.*, 1315, 1947

Hagen, J., *Industrial Catalysis, A Practical Approach*, Wiley-VCH, New York, 1999

Hung, K.G.W., Anderlund, M., Åkermark, B. and Björnbohm, P., A Reverse Flow Reactor for Homogeneous/Heterogeneous Catalysis, AIChE Meeting, Los Angeles, CA, 2001

Hung, K.G.W., Papadias, D. and Björnbohm, P., Reverse-Flow Operation for Application of Imperfectly Immobilized Catalysts, *AIChE Journ.*, 49, 1, 151, 2003

Matros, Yu. Sh., *Catalytic Processes under Unsteady State Conditions*, Elsevier Amsterdam, 1989

Matros, Yu.Sh. and Bunimovich, G.A., Reverse-Flow Operation in Fixed Bed Catalytic Reactors, *Cat. Rev. Sci. Eng.* 38, 1, 1996

McCue, J.T., Kemp, G., Low, D. and Quinones-Garcia, J. *Chromatogr. A*, 989, 139, 2003

ÖZDURAL, A.R., Alkan, A. and Kerkhof, P.J.A.M., Modeling Chromatographic Columns Non-Equilibrium Packed-Bed Adsorption with Non-Linear Adsorption Isotherms, *J. Chromatogr. A*, 1041, 77, 2004

Neophytides, S.G. and G.G. Froment, A bench scale study of reversed flow methanol synthesis, *Ind. Eng. Chem. Res.* 31, 1583, 1992

Nieken, U., Kolios, G. and Eigenberger, G., Fixed-Bed reactors with periodic flow reversal: experimental results for catalytic combustion, *Cat. Today* 20, 355, 1994

Noskov A.S. and Chumachenko V.A., New Processes and Reactors for the Catalytic Gas Purification under Unsteady-State Conditions, *Khim. Prom.*, 4, 215, 1996

Snyder, J.D. and Subramanian, B., Numerical Simulation of a Reverse-Flow NO_x-SCR Reactor with Side-Stream Ammonia Addition, *Chem. Eng. Sci.*, 53, 727, 1998

van de Beld, B., Air purification by catalytic oxidation in an adiabatic packed bed reactor with periodic flow reversal, PhD Thesis, University of Twente, Enschede, NL, 1995

Watson, E.W., Method and Apparatus for Reacting for Sulfur Dioxide and Natural Gas, U.S. Patent 3,865,927, 1975

Züfle, H. and Turek, T., Catalytic combustion in a reactor with periodic flow reversal. Part 1. Experimental results, *Chem. Eng. Proc.* 36, 327, 1997

6

Conclusions and Recommendations

6.1 Conclusions

The goal of this thesis is to prove the technical feasibility of the Reverse Flow Adsorption concept for the integrated recovery and recycling of homogeneous catalysts. By exploiting an adsorptive separation at temperatures below the decomposition temperature of the homogeneous catalyst, this concept overcomes the common drawbacks of the common recovery processes, for example: decomposition during distillation, need for additional solvents during extraction or leaching of catalyst compounds in membrane filtration.

To prove the technical feasibility of the Reverse Flow Adsorption concept, this research was splitted into three parts:

1. Selection and testing of potential adsorbents that can reversibly recover the homogeneous catalyst in its individual components.
2. Determination of the kinetics of the mass transfer from the liquid phase to the internals of the solid adsorbent particles.
3. Development of a mathematical model to describe the behavior of the concentration fronts in the adsorption beds over time.

Finally, this model has been applied to an industrial scale OXO-synthesis process to illustrate the implementation of Reverse Flow Adsorption in a real scale processes.

6.1.1 Adsorbents

To make the Reverse Flow Adsorption concept technically feasible, the availability of adsorbents that can selectively and reversible recover the homogeneous catalyst from the product flow is crucial.

From the literature it is known that transition metal complexes are always in equilibrium with its individual components: the ligands and transition metal center. In chapters 2 and 3, three adsorption mechanisms have been experimentally tested – for the homogeneous model catalyst $(PPh_3)_2Co(II)Cl_2$ – that can be exploited to recover the individual compounds: ion exchange, acid/base equilibrium and σ/π interactions.

It was found that the transition metal center – Co(II)Cl₂ – can be recovered by ion exchange or σ/π interactions. From the experimental results it could be concluded that:

- Ion exchange over the higher group I elements was found to reversibly adsorb Co(II) from 1-butanol according to: $\text{Cs}^+ \approx \text{Rb}^+ > \text{K}^+ > \text{Na}^+$.
- Reversible adsorption has been observed for the adsorbents that use σ -donation and π -back-donation for the recovery of Co(II). The observed trend was: Group IV (N and P) > Group V (O and S) > Group IV (Cl and Br)

The ligands can be recovered by an acid/base equilibrium or σ/π interactions. From the experimental results it could be concluded that:

- Adsorption of the PPh₃ ligands by an acid/base equilibrium was found to be reversible.
- PPh₃ prefers Ag⁺ functionalized Amberlyst 15 above the other types of selected metals. The trend in the adsorption capacity for the recovery by σ/π -interactions follows: $\text{Ag}^+ \gg \text{Ni}^{2+} \approx \text{Co}^{2+} > \text{Fe}^{2+} > \text{Mn}^{2+} > \text{Na}^+ \approx \text{K}^+ \approx \text{Rb}^+ \approx \text{Cs}^+$.

6.1.2 Kinetics

Besides the adsorption capacity of the adsorbents, the dimensions of the adsorption beds are also determined to a significant extent by the adsorption kinetics. These latter causes a broadening of the concentration fronts.

In this research it has been shown that the diffusivities for a non-linear adsorption can be determined by using a generalized Zero Length method. This enables the measurement of diffusivities for adsorption at higher concentrations and extends the adsorption rate measurements to non-ideal interactions.

In chapter 4, the internal diffusivity constants of CoCl₂ and PPh₃ during adsorption have been determined by fitting a generalized Zero Length model to experimentally determined concentration changes as a function of time.

It was found for the transition metal center of the homogeneous catalyst that:

- Although CoCl₂ diffuses both into the macro- and micropores of the macroreticular Amberlyst A21, the main adsorption capacity is located in the microparticles.
- CoCl₂ is adsorbed into the gel matrix of polymerbound PPh₃ at a faster diffusion rate compared to the gel type microparticles of Amberlyst A21 due to the lower crosslinkage.

For the ligand it was found that:

- The microparticles in Ag^+ functionalized Amberlyst 15 are not accessible for PPh_3 .

6.1.3 Simulation

In chapter 5, all experimental data from chapter 2, 3 and 4 have been combined to demonstrate the principle of the Reverse Flow Adsorption concept. For this purpose a mathematical model has been developed to describe the concentration fronts in the adsorption beds.

Reverse Flow Adsorption was modeled for a CSTR with an Co(II)Cl_2 adsorption bed upstream and another downstream the reactor. It was found that the concentration fronts after 1500 adsorption and desorption steps eventually reach a fixed position. Even if internal mass transfer is a limiting factor: no leaching of catalyst will occur.

From the discussion on the adsorbent specific parameters, it was concluded that the required adsorption bed volumes can be minimized if the adsorbents – to be used in Reverse Flow Adsorption – have:

- A low adsorption strength.
- A high adsorption capacity.
- Fast effective diffusivity from inside the particles to the liquid phase.

6.1.4 Implementation into an OXO-synthesis process

For a complete recovery of the homogeneous catalyst, Reverse Flow Adsorption requires 4 adsorption beds to be installed: two adsorption beds – up and down stream of the reactor – for the transition metal recovery and two for the ligand recovery.

From the mathematical model it can be concluded that implementation of the Reverse Flow Adsorption process in an OXO-synthesis process is possible with adsorption beds with a relative volume less than 16 [%] of the reactor volume. The total pressure drop is estimated to be approximately 5 [%] of the process pressure.

6.1.5 Overall conclusion

From the existence of potential adsorbents, fast adsorption kinetics, reaching of a fixed position of the concentration front and the small adsorption bed volumes, it is concluded that

Reverse Flow Adsorption concept can become technical feasible for the integrated recovery and recycling of homogeneous catalysts.

However, before Reverse Flow Adsorption can be applied in real processes, some subjects presented in this thesis still need a more detailed study.

6.2 Recommendations

The matrices of the adsorbents used in this research were all made up from a polymeric network. From literature [Dorfner 1991; Helfferich, 1995] it is known that these type of matrices swell under influence of a solvent and the amount of sorbate present in the solid phase.

The effect of swelling and shrinking of the adsorbent particles on the mass transfer and adsorption capacity was not determined in this research, but may negatively affect the latter two. Therefore, it is recommended to use adsorbents which do not show this swelling behavior such as silica's.

Co(II)Cl₂ penetrates both into the macropores as well as the microparticles of the polymeric adsorbents (see chapter 4). The mass transfer rate of smaller molecules into the microparticles does form an extra limitation on the overall adsorption kinetics. It is therefore recommended to use mono-dispersed – to ensure one type of diffusion – but macroporous – to achieve the highest possible mass transfer rate – adsorbents in which this extra limitation in mass transfer absent.

The PPh₃ ligands influence the capacity of the Co(II)Cl₂ recovery. Although this has been shortly discussed in chapter 2, the real mechanism behind this is still unknown. A more detailed study into the equilibrium mechanisms of the homogeneous catalyst complex has to give a better understanding in the real mechanism: is it caused by co-adsorption of PPh₃ – steric hindrance – during the Co(II)Cl₂ recovery or does the latter stay behind due to the equilibrium with the soluble PPh₃?

In a real application of the Reverse Flow Adsorption concept, a multiple of adsorption/desorption cycles will be applied in a reactive system. In this research, reaction was neglected and only one adsorption/desorption cycle has been experimentally studied. It is therefore crucial to study if:

- The activity and selectivity of the homogeneous catalyst is affected by continuously alternating functions – adsorption or desorption – of the adsorption beds.
- Possible co-adsorption of reactants and products with the homogeneous catalyst affect the overall adsorption capacity.

The theoretical study performed in chapter 5, showed that a large number of parameters can be varied. This fact can be used to optimize the Reverse Flow Adsorption concept by optimizing:

- The choice of adsorbent, which influences the adsorption strength and capacity.
- The process parameters, such as adsorption bed length, liquid phase velocity and cycle times.

Finally it is recommended to broaden this research to more types of homogeneous catalysts, solvents, reactants and products. All of these affect the adsorption and need a more detailed study for the Reverse Flow Adsorption concept to grow with the increasing degree of diversity of the fine chemistry.

6.3 References

Dorfner K., Ion Exchangers, Walter de Gruyter, 1991

Helfferich F., Ion Exchange, Dover Publications Inc., 1995